

Analysis of Whitianga, Tararu and Kawhia sea-level records to 2014

Prepared for Waikato Regional Council

June 2015

Prepared by:
Scott Stephens
Ben Robinson
Rob Bell

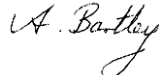
For any information regarding this report please contact:

Scott Stephens
Coastal Scientist
Coastal and Estuarine Processes Group
+64-7-856 7026
scott.stephens@niwa.co.nz

National Institute of Water & Atmospheric Research Ltd
PO Box 11115
Hamilton 3251

Phone +64 7 856 7026

NIWA CLIENT REPORT No: HAM2015-046
Report date: June 2015
NIWA Project: EVW15214

Quality Assurance Statement		
	Reviewed by:	Michael Allis
	Formatting checked by:	Alison Bartley
	Approved for release by:	Andrew Swales

© All rights reserved. This publication may not be reproduced or copied in any form without the permission of the copyright owner(s). Such permission is only to be given in accordance with the terms of the client's contract with NIWA. This copyright extends to all forms of copying and any storage of material in any kind of information retrieval system.

Whilst NIWA has used all reasonable endeavours to ensure that the information contained in this document is accurate, NIWA does not give any express or implied warranty as to the completeness of the information contained herein, or that it will be suitable for any purpose(s) other than those specifically contemplated during the Project or agreed by NIWA and the Client.

Contents

- Executive summary 8**

- 1 Introduction 11**
 - 1.1 Background 11
 - 1.2 Scope of the project..... 12

- 2 Sea level variability and decomposition..... 14**
 - 2.1 Processes contributing to sea-level variability and extreme sea levels 14
 - 2.2 Sea-level data used in the study 16
 - 2.3 Decomposition of sea level data..... 17
 - 2.4 Quality assurance..... 18

- 3 Drift in the Whitianga gauge 19**

- 4 Mean sea level and local vertical datum 21**

- 5 Tide exceedance curves..... 25**
 - 5.1 Mean high-water springs in the Waikato region 27
 - 5.2 Nodal tidal cycles 29

- 6 Storm surge 33**
 - 6.1 Extreme storm-surge analysis..... 33
 - 6.2 Descriptive analysis of the largest storm surge events 35

- 7 Storm tide extreme-value analysis..... 68**
 - 7.1 Monte Carlo joint-probability analysis 68
 - 7.2 Breakdown of the largest storm-tide events..... 71
 - 7.3 Seasonality of storm tides 75
 - 7.4 Maximum values of tide and surge 77

- 8 Sea level anomaly 79**

- 9 Wave measurements at Tararu 82**

- 10 Review of sea-level gauge network 84**

- 11 Conclusions 86**

- 12 Acknowledgements 88**

- 13 Glossary of abbreviations and terms 89**

14	References.....	92
Appendix A	Quality assurance of tide-gauge data	94
Appendix B	MHWS elevations.....	96

Tables

Table 2-1:	Sea level gauges analysed in this project showing the periods where quality assurance was undertaken.	17
Table 4-1:	Sea-level gauge-zero offsets to local vertical datum.	21
Table 4-2:	MSL offsets to MVD-53 datum at Auckland, Moturiki, Whitianga, Tararu and Kawhia.	22
Table 5-1:	Analysis of high waters at Whitianga, Kawhia and Tararu relative to MSL = 0.	27
Table 5-2:	Tidal analysis for Mercury Bay covering the 90-day deployment period in 2002, with amplitudes for the main twice-daily tidal constituents and the sum.	29
Table 6-1:	Frequency–magnitude distribution of extreme storm surges.	35
Table 6-2:	Source of meteorological data used for storm surge descriptive analysis.	36
Table 6-3:	The top five storm surges on record at Whitianga.	36
Table 6-4:	The top five storm surges on record at Tararu.	49
Table 6-5:	The top three storm surges on record at Kawhia.	59
Table 7-1:	Extreme storm-tide distribution at Whitianga.	68
Table 7-2:	Extreme storm-tide distribution at Kawhia.	69
Table 7-3:	Extreme storm-tide distribution at Tararu.	70
Table 7-4:	The top 20 storm tide events and list of contributing components elevations for Kawhia.	72
Table 7-5:	The top 20 storm tide events and list of contributing components elevations for Tararu.	72
Table 7-6:	The top 20 storm tide events and list of contributing components elevations for Whitianga.	73
Table 7-7:	Maximum measured sea-level components.	78
Table 8-1:	Mean, maximum and minimum SLA for each month of the year at Whitianga.	80
Table 8-2:	Mean, maximum and minimum SLA for each month of the year at Tararu.	80
Table 8-3:	Mean, maximum and minimum SLA for each month of the year at Kawhia.	81

Figures

Figure 1-1:	Location of sea-level gauges at Whitianga, Tararu and Kawhia.	12
Figure 2-1:	Decomposed sea level at Kawhia for November 2012.	18
Figure 3-1:	Annual mean sea level at Whitianga.	20
Figure 4-1:	Relationships and conversions between the three LVDs: Moturiki (MVD-53), Auckland (AVD-46) and Tararu (TVD-52).	22
Figure 4-2:	A comparison between the annual mean sea level of five tide gauges.	23
Figure 4-3:	One-month and six-month running average of non-tidal sea level and wind speed at Kawhia.	24

Figure 5-1:	High-tide markers at Whitianga relative to MSL=0.	26
Figure 5-2:	High-tide markers at Kawhia relative to MSL=0.	26
Figure 5-3:	High-tide markers at Tararu relative to MSL=0.	27
Figure 5-4:	Locations of two NIWA water level gauge moorings in October–November 2002, one at Pandora Rock off Shakespeare Cliff, the other at Motukorure (Centre).	28
Figure 5-5:	Annual standard deviation of predicted tide at Auckland.	30
Figure 5-6:	Annual standard deviation of predicted tide at Tararu, Whitianga and Kawhia.	31
Figure 5-7:	Monthly analysis of M2 tidal amplitude at Whitianga.	32
Figure 6-1:	Extreme value analysis of storm surges using a GPD fitted to storm surges over a high threshold.	34
Figure 6-2:	Extreme value analysis of storm surges using a GEV fitted to annual maxima storm surges.	34
Figure 6-3:	Storm surge (red line) and inverted barometer (blue line) at Whitianga for 2008, in mm above gauge zero.	37
Figure 6-4:	Variability of storm surge height relative to the inverted barometer (IB) height for Whitianga.	38
Figure 6-5:	Mean sea level pressure map at 1200 hrs, 26 July 2008 around the time of the largest measured storm surge (502 mm) at Whitianga.	39
Figure 6-6:	Measured sea level and its components during 26 July 2008 storm surge at Whitianga.	40
Figure 6-7:	Measured sea level and its components during 25 September 2013 storm surge at Whitianga.	41
Figure 6-8:	Mean sea level pressure at 0000 hours, 25 September 2013 around the time of the second largest measured storm surge (494 mm) at Whitianga.	42
Figure 6-9:	Measured sea level and its components during 29 Jan 2011 storm surge at Whitianga.	43
Figure 6-10:	Mean sea level pressure map at 0600 hrs, 29 January 2011 around the time of the third largest measured storm surge (468 mm) at Whitianga.	43
Figure 6-11:	Measured sea level and its components during 21 Aug 2003 storm surge at Whitianga.	44
Figure 6-12:	Mean sea level pressure at 0300 hours, 21 August 2003 around the time of the fourth largest measured storm surge (416 mm) at Whitianga.	45
Figure 6-13:	Measured sea level and its components during 20 Jun 2002 storm surge at Whitianga.	46
Figure 6-14:	Monthly boxplot of the 5 largest storm surge events per year at Whitianga.	47
Figure 6-15:	Sea level at Whitianga during Cyclone Pam.	48
Figure 6-16:	Storm surge (red line) and inverted barometer (blue line) at Tararu for 1995, in mm above gauge zero. Records are divided into 3 month periods with Jan-Mar (top), Apr-Jun (2nd from top), Jul-Sep (2nd from bottom) and Oct-Dec (bottom). Largest storm-surge for this year observed as spike in September.	49
Figure 6-17:	Variability of storm surge height relative to the inverted barometer (IB) height for Tararu.	50
Figure 6-18:	Measured sea level and its components during 12 Jun 2006 storm surge at Tararu.	51

Figure 6-19:	Mean sea level pressure map at 0900 hrs, 12 June 2006 around the time of the largest measured storm surge (970 mm) at Tararu.	52
Figure 6-20:	Measured sea level and its components during 6 Sep 1995 storm surge at Tararu.	53
Figure 6-21:	Measured sea level and its components during 31 Aug 2009 storm surge at Tararu.	54
Figure 6-22:	Mean sea level pressure map at midnight, 31 August 2009 around the time of the third largest measured storm surge (640 mm) at Tararu.	55
Figure 6-23:	Measured sea level and its components during 21 Oct 1998 storm surge at Tararu.	56
Figure 6-24:	Measured sea level and its components during 21 Aug 2003 storm surge at Tararu.	57
Figure 6-25:	Monthly boxplot of the 5 largest storm surge events per year at Tararu.	58
Figure 6-26:	Storm surge (red line) and inverted barometer (blue line) at Kawhia for 2013, in mm above gauge zero.	59
Figure 6-27:	Variability of storm surge height relative to the inverted barometer (IB) height for Kawhia.	60
Figure 6-28:	Measured sea level and its components during 6 May 2008 storm surge at Kawhia.	61
Figure 6-29:	Mean sea level pressure at 1200 hours, 6 May 2013 around the time of the largest measured storm surge (889 mm) at Kawhia.	62
Figure 6-30:	Measured sea level and its components during 26 May 2010 storm surge at Kawhia.	63
Figure 6-31:	Mean sea level pressure at midnight, 26 May 2010 around the time of the second largest measured storm surge (815 mm) at Kawhia.	64
Figure 6-32:	Measured sea level and its components during 11 September 2008 storm surge at Kawhia.	65
Figure 6-33:	Mean sea level pressure at 1200 hours, 11 September 2008 around the time of the third largest measured storm surge (707 mm) at Kawhia.	66
Figure 7-1:	Extreme storm tide prediction levels, and annual maximum sea levels for Whitianga.	69
Figure 7-2:	Extreme storm tide prediction levels, and annual maximum sea levels for Kawhia.	70
Figure 7-3:	Extreme storm tide prediction levels, and annual maximum sea levels for Tararu.	71
Figure 7-4:	Breakdown of the sea-level components contributing to the largest 20 storm tides observed at Kawhia (2008-2014).	74
Figure 7-5:	Breakdown of the sea-level components contributing to the largest 20 storm tides observed at Tararu (1990-2014).	74
Figure 7-6:	Breakdown of the sea-level components contributing to the largest 20 storm tides observed at Whitianga (1999-2014).	75
Figure 7-7:	Monthly boxplot of the five largest storm tide events per year at Whitianga.	76
Figure 7-8:	Frequency of the five largest storm-tides each year sorted by month at Whitianga.	76
Figure 7-9:	Monthly boxplot of the five largest storm tide events per year at Tararu.	77
Figure 7-10:	Frequency of the five largest storm-tides each year sorted by month at Tararu.	77

Figure 8-1:	Mean, minimum and maximum monthly sea-level anomaly.	79
Figure 9-1:	Wave height measured at Tararu in August 2008.	82
Figure 9-2:	Thames wave data - change of sampling resolution in June 2011.	83
Figure 14-1:	Raw and quality assured Kawhia sea level data.	94
Figure 14-2:	Tararu sea level data.	95

Executive summary

Waikato Regional Council (WRC) operates sea-level gauges at Tararu, Whitianga and Kawhia. Digital sea-level records at Tararu, Whitianga and Kawhia began in 1990, 1999 and 2008 respectively. WRC engaged NIWA to analyse the sea-level records. Of particular interest was the analysis of extremes in the sea-level records to understand the local anatomy of storm-tides in terms of sea-level response to tide, weather and wave action. This report presents a variety of sea-level analyses useful for coastal planning and regulation and hazard assessment, for the three gauge locations. The report accompanies electronic tables in excel format.

The gauges are delivering data of sufficient quality to confidently extract the various sea-level components, determine mean sea-level, and calculate extreme sea levels. Discrepancies with the Whitianga data reported by NIWA in 2012 and 2014 have been resolved. The discrepancies arose from datum offsets that were not being recorded in the data received by NIWA as part of the live data feed, and were not related to the sea-level gauge itself nor the quality of the data being collected by the gauge. In this study we used a high-quality sea-level record held by WRC, which included the correct datum offsets to the local vertical datum. The live feed that NIWA continues to receive now has the correct datum offset applied.

Mean sea levels of 0.16, 0.12, 0.14, 0.18 and 0.13 m relative to Moturiki vertical datum were calculated for Auckland, Moturiki, Whitianga, Tararu and Kawhia respectively, for the 2008–2014 period.

Mean high-water springs (MHWS) elevations were calculated from the three gauge records using several MHWS definitions. MHWS elevations are also presented at other locations around the coastline of the Waikato region. Considerable tidal dissipation occurs over the ebb-tidal delta of Whitianga Harbour, so MHWS elevations measured at the gauge location inside the harbour are about 10 cm lower than outside. It is likely that a similar effect occurs at the Kawhia gauge, which is also located inside a harbour. MHWS elevations measured by the gauge at Tararu are representative of MHWS along the nearby coastline. A substantial change in the tidal amplitudes was measured in the Whitianga estuary in February–March 2006, which is probably related to morphological change in the estuary entrance channel.

The frequency–magnitude distribution of storm surge was calculated at each gauge. 1% Annual Exceedance Probability (AEP) storm surges of 0.69, 0.97 and 1.36 m estimated for Whitianga, Tararu and Kawhia respectively. There is considerable uncertainty in these extreme storm surge estimates, particularly for the estimate at Kawhia which has higher uncertainty due to the short 6-year length record. We observed a different storm-surge climate between the east (Whitianga) and west (Kawhia) coasts of New Zealand. Storm surges at Whitianga were dominated by the drop in barometric pressure associated with tight, fast-moving, low-pressure weather systems. Onshore wind speeds are not sustained for long enough to produce surges much larger than 0.5 m at Whitianga. Conversely, storm surges at Kawhia were dominated by wind stress associated with persistently strong north-westerly winds from weather fronts blowing over several hours to days; they drive surges almost double those experienced at Whitianga with likely maximum storm surges of over 1 m. Likewise, wind fronts that align with the Firth of Thames are the dominant cause of the largest storm surges occurring at Tararu, and again these surges are larger than those experienced at Whitianga, and likely to reach over 1 m at times.

The frequency–magnitude distribution of storm tide was calculated at each gauge. 1% AEP storm tides of 1.46, 2.44 and 2.63 m were estimated for Whitianga, Tararu and Kawhia respectively. The tide formed the dominant component of storm-tide in all cases. Large storm-tides occasionally consisted almost exclusively of tide, compounded by sea-level anomaly. However, the great majority of storm tides have some positive storm surge component, but often it is relatively small, especially at Tararu and Kawhia. Only one of the storm-surge annual maxima were observed in the top 20 storm-tides at Tararu and Kawhia; storm tides at these sites were generally dominated by the tide, despite large surges being observed. The large storm tides that did include an annual maximum storm surge were still not the largest storm tides at these sites, because peak storm-surge did not coincide with the peak of high-tide. Given the large size of some storm surge events at Tararu and Kawhia, there is potential for storm tides to occur that are very much larger than those observed in the existing gauge records, should they peak at the same time as a high spring tide. Four storm-surge annual maxima were observed in the top-20 storm tides at Whitianga. Whitianga is more storm dominated despite its smaller storm-surge climate, because it has a smaller tidal range.

A clear seasonal sea-level trend is apparent at all three gauge locations, with the sea-level anomaly peaking in May and being at its lowest during October/November. The seasonality of storm surges and storm tides was examined for Whitianga and Tararu, but not for Kawhia, which is too short to indicate patterns reliably. At both sites there were a greater number of large storm surges occurring in winter, but Whitianga also had a noticeable peak of large storm surges in summer due to its exposure to ex-tropical cyclones. There was no clear seasonal trend in the *magnitude* of storm tides, but greater *number* of large storm tides occurred in the winter months, reflecting the greater number of large storm surges occurring then.

There is a positive relationship between wave height and storm surge at Tararu because the same weather events that drive storm surge in the Firth of Thames also create sea waves, although there is considerable variability/scatter in the relationship. The wave data at Tararu could be used to undertake a joint-probability analysis between storm tide and wave height in future, which can be used for hazard assessments. Wave setup raises the sea level at the shore due to wave breaking, and could contribute up to about 0.1 m to the elevation of storm surge measured at Tararu.

Overall, the tidal gauges are collecting sound data and with continued gauge maintenance the records will be suitable for future analysis of sea-level trends, storm-surge and storm-tide anomalies. The sea-level records at Tararu (25 years long) and Whitianga (16 years long) are valuable historical sea-level records that should be maintained and extended to improve extreme sea level estimates and measure changing mean sea level and rates of sea-level rise. The Kawhia gauge record is still relatively short, and has less value for mean sea level or extreme sea-level analyses at this stage, but will prove valuable in the long term if maintained.

The sea-level network could be improved by adding gauges at open-coast locations on both the east and west coasts of the Waikato region to meet future sea-level record requirements. This is because small estuaries can be prone to large morphological changes that affect the tides within them. For example, the aforementioned change in tidal amplitude at Whitianga, which was probably related to a morphological change in the estuary. It was also shown that sea level in Kawhia Harbour is responding strongly to seasonal wind setup, which is causing higher annual mean sea level variability than is usually observed in New Zealand gauge records. For the purpose of measuring tides and mean sea level, sea-level gauges would ideally be located in an open-water location where tidal and storm surge amplitudes represent the adjacent coastline well, and outside of the wave breaking zone, since waves are known to degrade the quality of “still-water” sea level measurements. Good locations

would be on the lee side of small offshore islands, or on the lee side of a peninsula with relatively deep water adjacent, away from breaking waves and outside of estuaries. A good location on the east of the Coromandel Peninsula would be at or northward of Mercury Bay, as this is approximately halfway between the Tararu gauge and the Moturiki Island gauge operated by NIWA.

Land vertical tectonic movements should be recorded at all sea-level gauge locations to enable absolute MSL to be determined in future.

1 Introduction

1.1 Background

Waikato Regional Council (WRC) operates sea-level gauges at Tararu, Whitianga and Kawhia (Figure 1-1). Digital sea-level records at Tararu, Whitianga and Kawhia began in 1990, 1999 and 2008 respectively.

Goodhue (2012) produced tidal exceedance curves and high-water tide marks for the Tararu and Whitianga gauges relative to the relevant local vertical datum. The annual mean sea level (MSL) for both gauges shows the relative sea level at each location was mostly tracking in tandem with each other from year to year and also in tandem with the longer term (1974-onward) sea-level record of Moturiki Island at Mt. Maunganui. However, Goodhue (2012) observed that the Whitianga record changed in the calendar years of 2006-2009, during which the annual MSL dipped significantly compared to the Moturiki and Tararu MSL values. Subsequent analysis by NIWA in August 2014 suggested that the Whitianga gauge had exhibited a spurious upward drift since 2012. The source of that drift is explained within this report.

Sea-level records provide information to:

- Calculate tide heights and mean high-water springs (MHWS) elevations that define the legal boundary between land and sea.
- Calculate present-day MSL that forms a datum for extreme sea-level analyses and MHWS.
- Track sea-level rise over the long term.
- Compare relative MSL between sites around the coastline.
- Understand the sea-level response to tide, weather and climate.
- Undertake extreme sea-level analyses to inform coastal inundation hazard assessments.
- Calibrate or provide boundary information for coastal hydrodynamic models.
- Check the quality of sea-level information being collected.

WRC requires an updated analysis of the sea-level records from their gauges at Tararu, Whitianga and Kawhia, to provide information such as described in the bullet points above. Of particular interest is the analysis of extremes in the sea-level records to understand the local anatomy of storm-tides in terms of sea-level response to tide, weather and wave action.

This report presents a variety of sea-level analyses useful for coastal planning, regulation and hazard assessment, for the three gauge locations. The report accompanies electronic tables in excel format.

The report uses technical language for which a glossary has been included in Section 13.

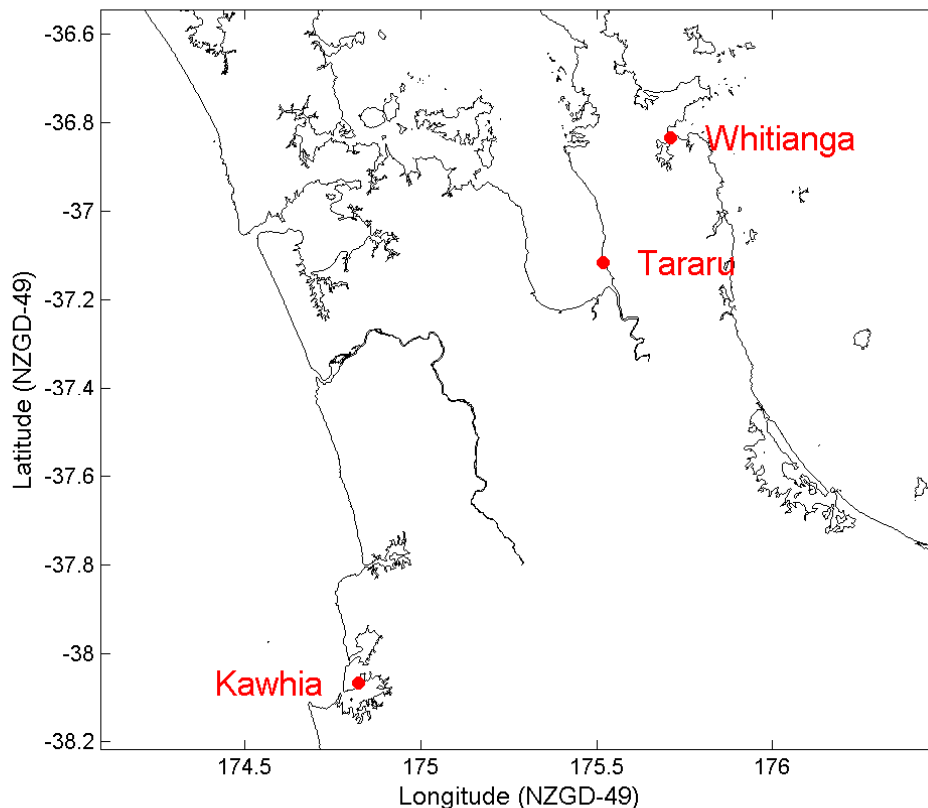


Figure 1-1: Location of sea-level gauges at Whitianga, Tararu and Kawhia.

1.2 Scope of the project

The following analyses were undertaken for each of WRC's Tararu, Whitianga and Kawhia sea-level records:

1. Undertake quality assurance, tidal harmonic analysis, wavelet decomposition and detrending as required for subsequent analyses. This splits the sea-level record into components of astronomical tide, sea-level anomaly (SLA), storm surge (SS), and remaining high-frequency energy (HF). Quality assurance and tidal harmonic analysis of the Tararu and Whitianga records was already partly completed by Goodhue (2012) and as part of MSL analysis pre-emptively supplied to WRC.
2. Investigate Whitianga Tide Gauge 'drifts' (see background). NIWA has compared the live feed that it was receiving from the gauge with sea-level data supplied WRC. Differences between the datasets are explained in Section 3. The WRC dataset is robust, and was used in this study.
3. We undertook tidal harmonic analysis and have included tidal exceedance curves and tables with tide marks relative to datums. The seasonal tides were omitted as the seasonal cycle was treated as part of the non-tidal residual (described in bullet 10 of this list).

4. We calculated annual MSL and undertook inter-gauge MSL comparison, including Moturiki and Auckland to the limits of available data. A MSL datum was calculated for three different epochs, which included the duration of the sea-level gauge records.
5. A description of the effect of the nodal tidal cycle at the gauge sites is included.
6. Extreme storm-surge analysis was undertaken to determining the storm surge frequency–magnitude distribution. The extreme storm surge and maxima data were plotted and are supplied in tables.
7. Extreme storm-tide (total sea-level) analysis was undertaken to determine the storm tide frequency–magnitude distribution using the Monte Carlo joint-probability technique. The extreme storm tide and maxima data were plotted and are supplied in tables.
8. A table is presented of the highest 20 storm-tide events and the contributing sea-level component elevations (SLA, tide, storm-surge, remaining high-frequency oscillations).
9. A monthly boxplot of the largest 5 storm-tide and storm-surge events per year is presented. The boxplots highlight seasonality in storm-tide and storm-surge hazard.
10. The mean seasonal sea-level cycle was determined for each gauge, and is plotted and presented within tables, including the mean, minimum and maximum SLA per month of the year.
11. The inverse barometer (IB) correlation to storm surge was determined. A partial series time-series plot and a lagged cross-correlation analysis with scatter plot and linear regression was produced along with a discussion of outliers and the degree of predictability provided by IB.
12. A descriptive analysis is presented of the largest 3–5 storm surges at Tararu and Whitianga gauge and 1–3 events in shorter Kawhia record. Those events were identified as large outliers from the earlier extreme sea-level analyses. The descriptive analyses include synoptic weather maps, situational weather analysis, and IB response.
13. A preliminary assessment of our ability to identify wave-driven sea-level setup at Tararu gauge has been undertaken.
14. Recommendations to assist the long-term usefulness of the sea-level gauge network are made.

2 Sea level variability and decomposition

We begin Section 2 with a summary of the various components of sea-level variability and a description of the “drivers” of those components. This provides some background, since the remainder of the report breaks the gauge data down and describes several of these sea-level components. We then address how the various sea level components are determined, and how we dealt with errors in the data.

2.1 Processes contributing to sea-level variability and extreme sea levels

There are a number of meteorological and astronomical phenomena that cause the sea level to change. On rare occasions these sea-level components can combine to inundate low-lying coastal margins. The processes involved are:

- Astronomical tide (tide).
- Storm surge (SS).
- Sea-level anomaly (SLA).
- Changes in mean sea level (MSL), as a result of sea-level rise.
- Tsunami – not considered in this study.
- Wave setup and runup.

The tides are caused by the gravitational attraction of solar-system bodies, primarily the Sun and the Earth’s moon, which then propagate as forced long waves in the ocean interacting in a complex way with continental shelves. In New Zealand the astronomical tides have by far the largest influence on sea level, followed by storm surge (in most locations).

Low-pressure weather systems and/or adverse winds cause a rise in water level known as storm surge. Storm surge results from two processes: 1) low-atmospheric pressure relaxes the pressure on the ocean surface causing a temporary rise in sea-level, and 2) wind stress on the ocean surface pushes water down-wind, or alternatively, to the left of an alongshore wind (in the southern hemisphere) from a persistent wind field, piling up against any adjacent coast e.g., for the Whitianga gauge located on New Zealand’s east coast, this would occur for onshore winds (from NE quadrant) and alongshore winds from SE respectively, and for Kawhia on the west coast, onshore winds from south-west and alongshore winds from north-west. Wind setup within harbours varies according to the fetch present at various tide states, but at high tide can be several decimetres.

SLA describes the variation of the non-tidal sea level on longer time scales ranging from a monthly basis, through an annual sea-level cycle, up to decades due to climate variability, including the effects of El Niño–Southern Oscillation (ENSO) and the Interdecadal Pacific Oscillation (IPO) patterns on sea level, winds and sea temperatures, and seasonal effects.

Storm tide is defined as the sea-level peak reached during a storm event, from a combination of SLA + tide + SS. It is the storm-tide that is measured by sea-level gauges. Storm-tide is the sea-level quantity relevant to coastal inundation.

MSL is obtained by averaging sea level over a defined time period (usually several years). New Zealand’s local vertical datums were obtained in this way. For example, Auckland Vertical Datum

1946 (AVD-46) was established as the MSL at Port of Auckland (Waitemata) from 7 years of sea level measurements collected in 1909, 1917–1919 and 1921–1923. Moturiki Vertical Datum 1953 (MVD-53) was established as the MSL at Moturiki Island, from 4 years of sea level measurements from 1949-1952. Thus, for the purposes of this report, MSL is the average sea level over a defined time period. MSL changes in time, due to climate variability and long-term sea-level rise. Therefore the MSL offset to the local vertical datums changes depending on the sea-level averaging epoch used.

Climate change will also cause acceleration in long-term trends of sea-level rise (MfE 2008) and could cause minor increases in the drivers (winds, barometric pressure) that produce storm surges (Mullan et al. 2011).

Waves also raise the effective sea level at the coastline. Wave setup describes an average raised elevation of sea level when breaking waves are present. Wave runup is the maximum vertical extent of wave “up-rush” on a beach or structure above the instantaneous still water level (that would occur without waves), and thus constitutes only a short-term fluctuation in water level relative to wave setup, tidal and storm-surge time scales. Wave runup includes the wave setup component. When offshore waves are large, wave setup and runup can raise the water level at the beach substantially.

2.1.1 Tides – what are they?

Ocean tides are the rise and fall of sea levels caused by the combined effects of the gravitational forces exerted by the Moon and the Sun and the rotation of the Earth.

The times and amplitude of the tides at a given location are influenced by the alignment of the Sun and Moon, by the pattern of tides in the deep ocean and by the shape of the coastline and near-shore bathymetry that substantially modifies the tidal wave.

The Equilibrium Tide has three coefficients that characterise the main *species* of lunar tides (Pugh 2004):

- the *long-period species*, with tidal changes over a month and longer; these are due to changes in the lunar distance and declination
- the *diurnal species* at a frequency of around one cycle per day, controlled by the lunar declination and the earth’s rotation
- the *semidiurnal species* at two cycles per day, controlled by the earth’s rotation.

Tidal constituents are the individual components which comprise the tides. Each constituent arises either from a specific astronomical feature or from the interaction between two or more constituents. Semi-diurnal or “twice-daily” tidal constituents dominate New Zealand tides (Walters et al. 2001) with tidal periods between 12–13 hours, e.g., the solar semi-diurnal constituent S_2 (12 hour period); the lunar semi-diurnal constituent M_2 (12.42 hour period); the elliptic semi-diurnal constituent N_2 (12.66 hour period) that covers the elliptical nature of the Moon’s orbit around Earth each month.

In the Waikato Region there are two high tides most days with different heights (and two low tides also of different heights), a pattern resulting from the interaction of the M_2 , S_2 and N_2 harmonic constituents, and known as a mixed semi-diurnal tide.

In New Zealand, the largest constituent is the “principal lunar semi-diurnal”, also known as the M_2 tidal constituent, which results directly from the Moon’s gravitational pull on the oceans (M stands

for “Moon”). Its period is about 12 hours and 25.2 minutes, which is half the “lunar day” (24 hours 50 minutes) required for the Earth to rotate once relative to the Moon. The M_2 tidal constituent alone represents approximately an average tide range (between spring and neap). The two other most dominant harmonics are the S_2 and N_2 constituents.

S_2 , the solar semi-diurnal constituent has a period of exactly 12 hours and this arises because the Sun passes over the same spot on Earth every 24 hours. Spring/neap tides occur every fortnight (14.765 days to be exact) in conjunction with Moon’s phase in relation to alignment with the Sun: spring tides occur just after New and Full Moon; neap tides occur just after First and Last Quarter. Spring tides have a larger tidal range than neap tides because at New and Full Moon, the Moon and Sun are lined up and they pull together upon Earth’s waters; whereas at First and Last Quarter the Moon and Sun are opposed and the pull is less. Another equivalent definition is that spring and neap tides are the result of M_2 (the lunar semi-diurnal constituent) beating in and out of phase with the S_2 (the solar semi-diurnal constituent). The S_2 tide is quite small on the east coast of New Zealand (Walters et al. 2001) compared to the west coast, which makes the fortnightly spring/neap cycle less pronounced on the eastern coasts (especially in the central regions).

N_2 , the elliptic semi-diurnal constituent, arises from the elliptic orbit of the Moon around Earth. Each constituent has a unique tidal period. Perigean/Apogean tides occur every month (27.555 days to be exact) in conjunction with the position of the Moon in its elliptical orbit around Earth. When the Moon is closest to Earth, it is in its perigee and larger than normal Perigean tides occur. When the Moon is farthest from Earth, it is in its apogee and smaller than normal Apogean tides occurs. Another equivalent definition is that Perigean and Apogean tides are the result of M_2 (the lunar semi-diurnal constituent) beating in and out of phase with N_2 (the elliptic semi-diurnal constituent). Because the N_2 tide doesn’t decrease on the east coast of New Zealand as much as the S_2 tide does, the main variation in tides on the east coast arises from a monthly Perigean/Apogean cycle superimposed on a smaller spring/neap cycle. This explains why the tides every second spring-tide period are higher than the previous set a fortnight earlier.

Perigean-spring combination tides peak about every 7 months (206.6 days to be exact) when New or Full Moon occurs at the same time as the Moon is in its perigee. Usually, these are the tides with the largest tidal range often referred to as “king tides”. NIWA publishes annually a red-alert tide calendar¹ which covers the dates in New Zealand when higher Perigean-spring tides will occur and if they combine with storms, can have the potential to cause coastal inundation of low-lying areas.

While M_2 , S_2 and N_2 are the major harmonic constituents in the Waikato Region, there are 62 tidal constituents (albeit mostly small) resolved in most harmonic analysis techniques, depending on the sea-level record length and quality.

2.2 Sea-level data used in the study

Details of the sea-level data records are presented in Table 2-1.

¹ <http://www.niwa.co.nz/natural-hazards/physical-hazards-affecting-coastal-margins-and-the-continental-shelf/storm-tide-red-alert-days-2014>

Table 2-1: Sea level gauges analysed in this project showing the periods where quality assurance was undertaken.

Sea Level Gauge	Site Number	Start Date	End Date	Sampling Interval
Whitianga	11599	31 st July 1999	12 th August 2014	1 to 5 minutes
Kawhia	41799	29 th August 2008	30 th October 2014	1 to 2 minutes
Tararu	9415	25 th May 1990	18 th August 2014	1 to 7.5 minutes

2.3 Decomposition of sea level data

The sea-level records at Whitianga, Kawhia and Tararu were decomposed into sea-level components as follows:

- Tide was resolved using tidal harmonic analysis UniTide; Foreman et al. (2009). The tide was then subtracted to produce a non-tidal residual (NTR).
- SLA was obtained by low-pass filtering NTR, using a wavelet filter (Goring 2008), to remove sea-level motion with periods of less than 1 month. The remaining SLA time-series contained only sea-level variations with periods of motion of one month or greater. Another method to obtain SLA is to average NTR on a monthly basis.
- The long-term trend in MSL can be calculated from NTR, but was not done so for the Whitianga, Kawhia and Tararu records, which are still relatively short for such purposes. For extreme sea-level analyses it is important to remove any non-stationary long-term MSL trend. This is accounted for in the Monte-Carlo joint-probability extreme sea-level method (Section 7).
- SS was obtained by band-pass wavelet filtering NTR, to obtain sea-level with periods of motion between 24 hours and 1 month.
- After removing the tide, SS and SLA from the NTR, some high-frequency (<24 hour period) sea-level motion remains. This remaining high-frequency energy (HF) is primarily due to “leaked” tidal energy that was not resolved by the harmonic analysis, but can also include seiche within enclosed basins. HF is not a large component of sea level, but it contributes to the total sea level so was included in extreme sea-level analyses.
- The sea-level gauges do not measure wave runup. Sea-level gauges located inshore of breaking waves can record a component of wave setup; where possible gauges are located to avoid this. Wave setup has similar periods of motion to SS, so if wave setup is present then it will contribute to the SS signal, and cannot be separated from SS using digital filters. An attempt is made to investigate wave setup at Tararu (Section 9).
- All sea-level components and extreme sea-level analyses were calculated relative to a zero MSL. Thus a MSL offset is subsequently required to relate the results to a known datum.

2.4 Quality assurance

Examination of the various sea-level components can highlight erroneous sea-level data:

1. Spikes in the non-tidal components can indicate errors in the original data.
2. An oscillating non-tidal residual indicates that tide data may be out of phase with the raw data, indicating a spurious time shift in the recordings.
3. Jumps in the non-tidal residual for certain periods can indicate datum shifts in the measured data.

For example, analysis of the non-tidal residual at Kawhia revealed a spike around 22 November 2012 (Figure 2-1) requiring correction.

Data from the Whitianga, Tararu and Kawhia gauges were quality-assured (QA) and prepared for extreme-value analysis.

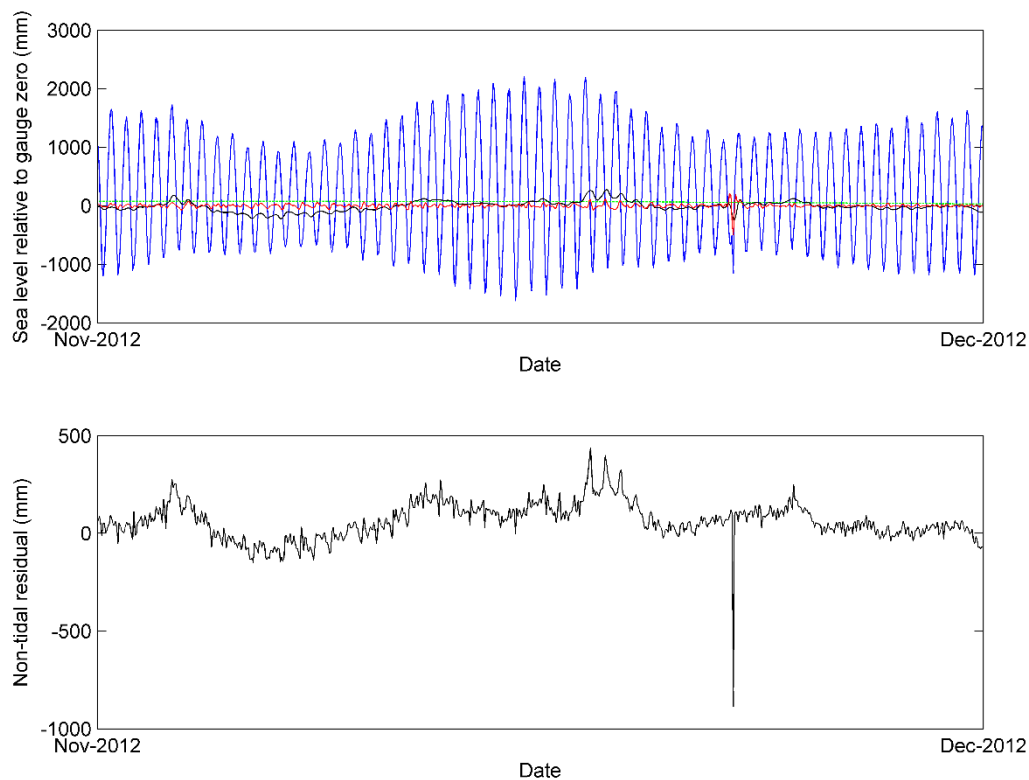


Figure 2-1: Decomposed sea level at Kawhia for November 2012. Top: Measured sea level data (blue), SS (black), SLA (green), HF (red). Bottom: NTR.

3 Drift in the Whitianga gauge

Goodhue (2012) compared annual MSL at Moturiki, Tararu and Whitianga up until the end of 2011. He reported that “The annual MSL for both gauges shows the relative sea level at Tararu and Whitianga is mostly tracking in tandem with each other from year to year and with the longer term sea-level record of Moturiki Island. The notable deviation is the Whitianga record for the calendar years of 2006-2009 in which the annual MSL record dipped significantly compared to the Moturiki and Tararu MSL values. This deviation may be due to gauge or datum issues and warrants further investigation.”

Figure 3-1 shows annual MSL at Whitianga, using two datasets. The first dataset (plotted in blue) is that used by Goodhue (2012), which is the same as the live feed that NIWA was receiving from the gauge until August 2014. The second dataset (plotted in black) was received from WRC in November 2014. Finally, a vertical offset was applied to the live-feed data so that MSL matched the WRC dataset for the 1999–2005 epoch (plotted in red). Figure 3-1 shows two notable features:

1. There is a vertical offset between the live feed of data that NIWA was receiving direct from the gauge, and the data supplied by WRC. The live feed has a mean of approximately zero, whereas the WRC dataset has a mean of 115 mm over the 1999–2014 epoch.
2. There was a downward vertical shift in the live feed data beginning in 2006.
3. There was an upward jump in MSL in 2013.

These features are explained as follows:

1. WRC has clarified that there is a constant adjustment made to the raw data, which ensures the Whitianga data is presented relative to MVD-53. It appears that a different (lower) offset was applied to the data recorded by NIWA compared with that recorded by WRC.
2. Between 10 February 2006 15:40 and 04 August 2013 12:15 there was an error in the offset applied (due to an error in surveying when the gauge was moved). Accordingly WRC has now corrected the data (offset + 0.118m from original raw data) over this time period.
3. The live feed NIWA was receiving from the gauge changed at 12:15 on 4 August 2013, at the time the survey offset was corrected. The live feed after that date included the correct offset, but before that date it did not. This affected (raised) the MSL calculation for 2013.

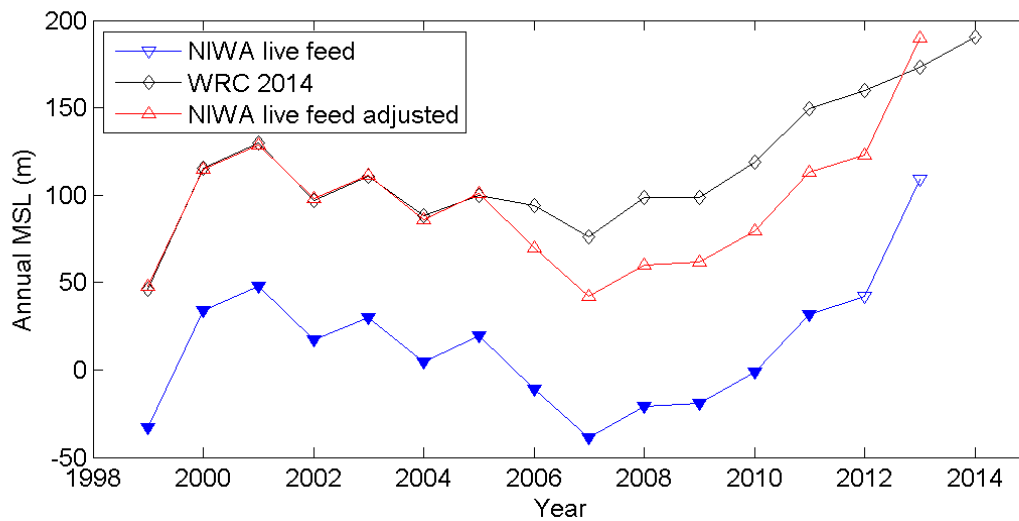


Figure 3-1: Annual mean sea level at Whitianga. Black line = WRC (2014) dataset; blue = live data feed received directly by NIWA (Goodhue (2012) data is marked by solid triangles); red = live data feed received directly by NIWA, for MSL has been adjusted to match MSL from the WRC dataset for the 1999–2005 epoch.

In summary: the downward shift in MSL at Whitianga observed by Goodhue (2012) from 2006-2009 was the result of a vertical offset error that has now been corrected. The “spurious drift” after 2012 resulted from the change in the datum of the live feed which occurred on 4 August 2013. The data recently supplied by WRC is robust and is presented relative to MVD-53, and suitable for the analyses presented in this report. The sea-level data that has been collected from the live feed subsequent to November 2014 is consistent with the dataset supplied by WRC prior to that date, so we are confident that the tide gauge is continuing to supply high-quality data correctly referenced to MVD-53, and NIWA is now receiving that data correctly.

4 Mean sea level and local vertical datum

Before the introduction of New Zealand Vertical Datum 2009 (NZVD2009) in September 2009, land heights in New Zealand were referred to one of 13 local vertical datums (LVD), two of which are applicable to the Waikato region, being Moturiki Vertical Datum 1953 and Tararu Vertical Datum 1952 (TVD-52).² The Auckland Vertical Datum 1946 (AVD-46) is a nearby LVD, which can be used for reference.

These local datums were established historically by determining MSL at a tide-gauge and then transferring this level by precise levelling to benchmarks in the surrounding hinterland.

Sea level is known to vary around the coast of New Zealand and the LVDs were set at different times during last century. This means that the level of MSL determined at each LVD's tide-gauge are different and that offsets occur between adjacent datums. Also, in most cases the level of MSL for the vertical datums was determined many decades ago and has not been officially updated since then to include the effect of sea level rise. Recent MSL values relative to these local vertical datums have been reported by Hannah and Bell (2012).

MVD-53 was established as MSL at Moturiki Island from sea-level measurements between 7 February 1949 and 15 December 1952 (Hannah and Bell 2012).

TVD-52 was established as MSL at Tararu Point from sea-level measurements in 1922–1923 (Hannah & Bell 2012).

AVD-46 was established as MSL at Port of Auckland from 7 years of sea level measurements collected in 1909, 1917–1919 and 1921–1923 (Hannah & Bell 2012). Based on these historical measurements, the MSL for Auckland Vertical Datum-1946 (AVD-46) was set in 1946 to +1.743 m relative to the present tide gauge zero at Port of Auckland, which equals Chart Datum.³

For navigation purposes, depths on nautical charts are specified relative to Chart Datum (CD). The CD adopted usually approximates Lowest Astronomical Tide (LAT) which is the lowest tide predicted to occur under normal meteorological conditions. CD is defined with reference to permanent benchmarks ashore and the zero of the tide gauge. It is common to set the zero of the tide gauge to CD, and thus there is a local offset from CD to LVD, as shown for Auckland and Moturiki in Table 4-1. The convention adopted for the three gauges in the Waikato region is for gauge zero = 0 m LVD (Table 4-1).

Table 4-1: Sea-level gauge-zero offsets to local vertical datum.

Sea-level gauge location	Local vertical datum	Gauge zero
Auckland	AVD-46	-1.743 m (AVD-46)
Moturiki	MVD-53	-1.487 m (MVD-53)
Whitianga	MVD-53	+0 m (MVD-53)
Tararu	TVD-52	+0 m (TVD-52) +0.118 m (MVD-53)
Kawhia	MVD-53	+0 m (MVD-53)

² <http://www.linz.govt.nz/geodetic/datums-projections-heights/vertical-datums/mean-sea-level-datums>

³ Note: prior to the present Chart Datum set in 1 Jan 1973, the old Auckland Harbour Board Chart Datum was 0.15 m lower.

Figure 4-1 shows the vertical offset between the three LVDs: Moturiki (MVD-53), Auckland (AVD-46) and Tararu (TVD-52), which can be used to convert the data to an alternative local vertical datum.

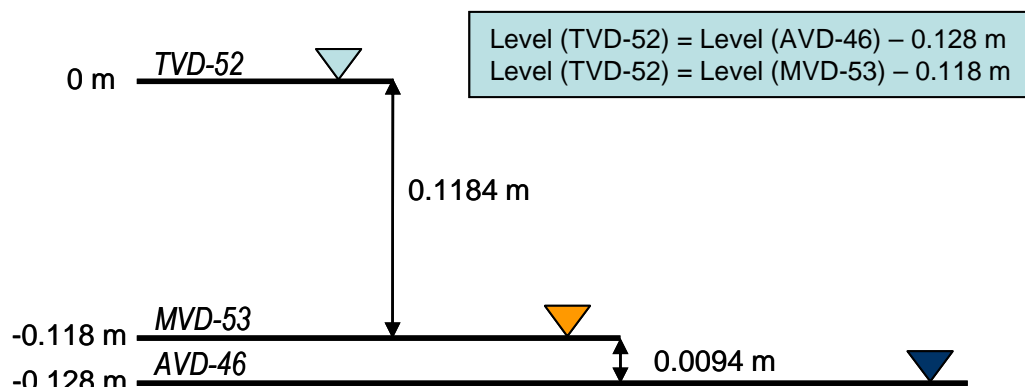


Figure 4-1: Relationships and conversions between the three LVDs: Moturiki (MVD-53), Auckland (AVD-46) and Tararu (TVD-52).

MSL has been calculated for Auckland and for the WRC tide gauges relative to MVD-53, both for 1999–2014 (a full tidal epoch), and 2008–2014 (length of the Kawhia record), and the recent decade 2005–2014 (Table 4-2). MSL at Tararu was corrected for a known land subsidence rate of -2.7 mm per year (Denys 2014). We calculated MSL over the respective epochs from annual MSL, which are plotted in (Figure 4-2). MSL appears to be tracking similarly at all locations.

Table 4-2: MSL offsets to MVD-53 datum at Auckland, Moturiki, Whitianga, Tararu and Kawhia. MSL epoch averages were calculated from annual means.

Location	Mean sea-level offset relative to MVD-53	MSL averaging period	Description
Auckland	+0.16 m	2008–2014	Kawhia record duration
Moturiki	+0.12 m	2008–2014	Kawhia record duration
Whitianga	+0.14 m	2008–2014	Kawhia record duration
Tararu	+0.18 m	2008–2014	Kawhia record duration
Kawhia	+0.13 m	2008–2014	Kawhia record duration
Auckland	+0.14 m	1999–2014	Whitianga record duration
Moturiki	+0.11 m	1999–2014	Whitianga record duration
Whitianga	+0.11 m	1999–2014	Whitianga record duration
Tararu	+0.19 m	1999–2014	Whitianga record duration
Auckland	+0.15 m	2005–2014	Recent decade
Moturiki	+0.11 m	2005–2014	Recent decade
Whitianga	+0.13 m	2005–2014	Recent decade
Tararu	+0.18 m	2005–2014	Recent decade

MSL and SLA at annual or longer timescales is continually changing in response to large-scale weather patterns such as El Niño–Southern Oscillation (ENSO) at 2–4 year timescales and Inter-decadal Pacific Oscillation (IPO) at longer 20–30 year timescales, as well as long-term sea-level rise. Figure 4-2 shows the annual MSL for five tide gauges. The Waikato tide gauges are still too short to ascertain long-term sea level rise, but a recent rising sea-level trend can be seen in all the gauge records. A long-term linear rate of SLR of 0.15 m/century was measured at Auckland since 1903 (Hannah and Bell 2012). Even for that long record it is not possible to statistically distinguish any recent acceleration in SLR from climate variability effects.

Annual MSL at Auckland and Moturiki have exhibited similar behaviour since 1974. Annual MSL at Tararu since 1990 and at Whitianga since 1999 are consistent with the Auckland and Moturiki records.

Annual MSL at Kawhia shows a high degree of variability – larger than would be expected due to the influence of climate variability on water temperature. Sea-level at the Kawhia gauge seems to be highly influenced by wind, with periods of prevailing northerly winds inducing higher sea-levels in Kawhia Harbour (Figure 4-3). The Coriolis force causes wind setup against the coast when the coast is to the left of the prevailing wind direction. As shown in 6.2.3, Kawhia Harbour is also highly-responsive to strong north-west winds, which produce large storm surges in the Harbour. This analysis suggests that Kawhia is not ideal for monitoring long-term MSL changes for the open west coast, because background MSL change will be masked by wind-driven response to climate variability. Notwithstanding this, over many decades the wind-driven variability will tend to average out. It is unclear how much an open-coast gauge may also be influenced by wind setup, but it is likely to be considerably less than inside Kawhia Harbour.

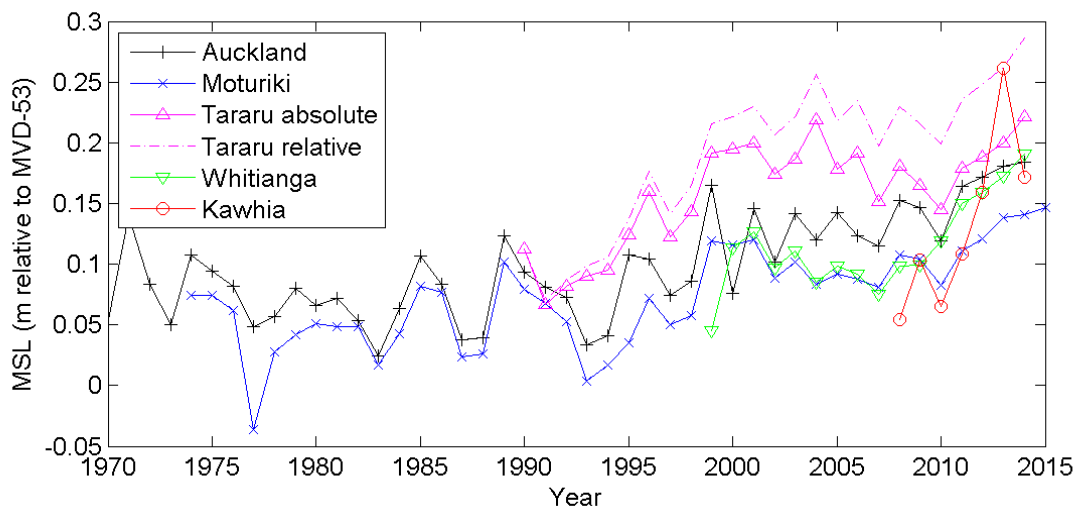


Figure 4-2: A comparison between the annual mean sea level of five tide gauges. Tararu for 1990-2014, Whitianga for 1999-2014, Kawhia for 2008-2014, Moturiki for 1974-2012, Auckland for 1970-2014. All sites show relative MSL, which is the elevation relative to the local land elevation. Absolute MSL is also shown for Tararu, after correcting for a measured land subsidence rate of -2.7 mm/year.

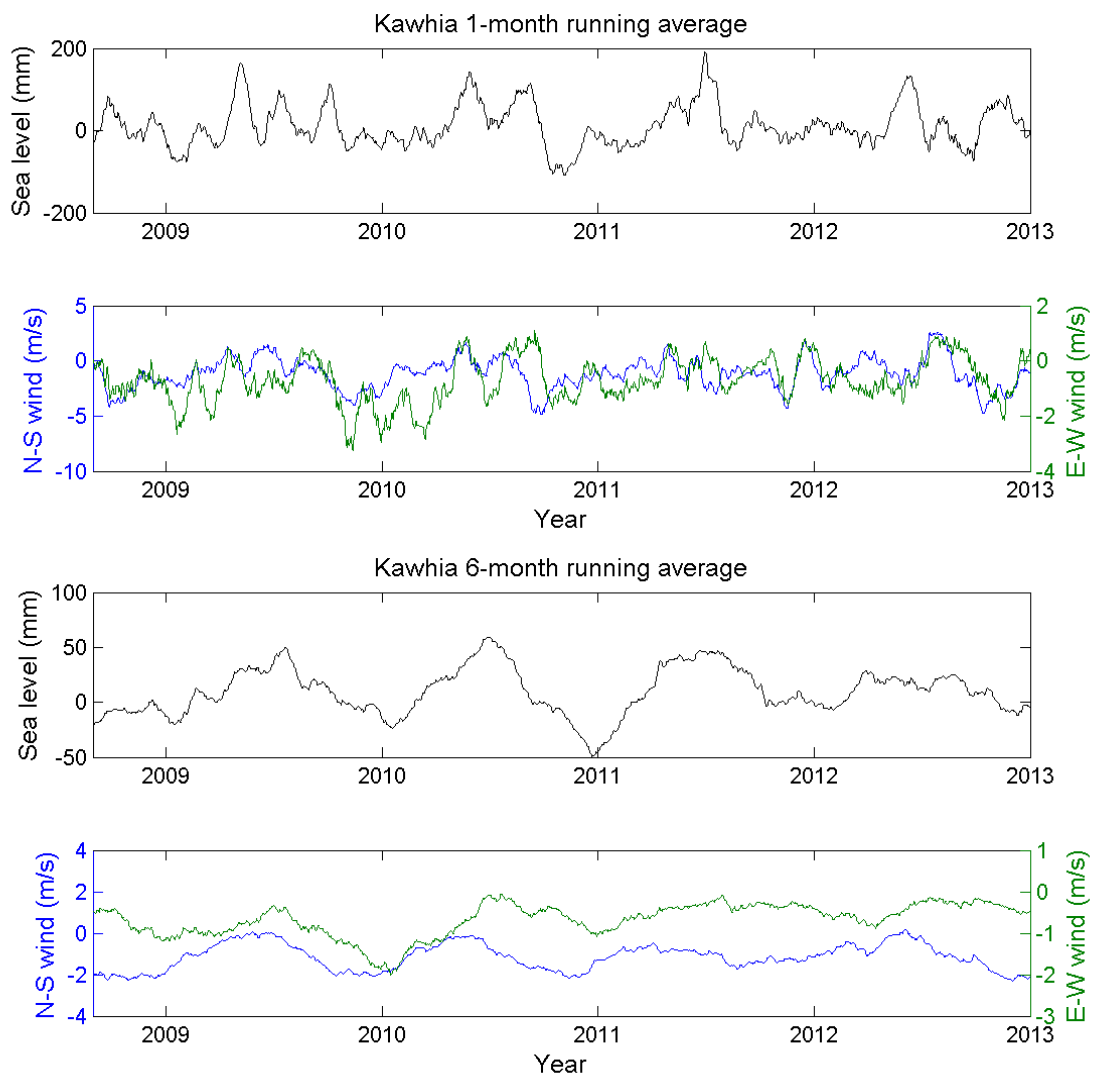


Figure 4-3: One-month and six-month running average of non-tidal sea level and wind speed at Kawhia. N-S = wind speed in the north–south. E-W = wind speed in the east–west direction. Data are shown only for the period during which wind at Taharoa was available.

5 Tide exceedance curves

We undertook a tidal harmonic analysis on the quality assured sea-level gauge records from Whitianga, Kawhia and Tararu. Tide exceedance curves were then generated by predicting 100 years of high tides and plotting the cumulative exceedance of the high tides. These curves exclude weather (SS) and climate-related (SLA) effects. High-tide exceedance curves, based on the cumulative distribution function (CDF) of long-term tide predictions, allow MHWS to be consistently defined based on a common exceedance threshold that is independent of tide regime (Bell 2010; Stephens et al. 2014).

To forecast the high tides, tidal harmonics were calculated on an annual basis, and then vector averaged. Years with more than 31 days missing data were excluded. Tidal predictions excluded the gravitational solstice tides S_a and S_{sa} , as these were instead included in the seasonal sea-level cycle. The reason for this is that the solstice tides for most practical purposes would be too small to worry about except that they aren't just produced by solar gravity; they get a boost from other effects that follow the sun's seasonal cycles such as solar heating of the oceans and changes in circulation in the atmosphere (Boon 2013). Therefore they are best included in the SLA component of sea level.

Figure 5-1, Figure 5-2 and Figure 5-3 show the tide exceedance curves for Whitianga, Kawhia and Tararu relative to MSL=0, and the data for these plots is summarised in Table 5-1. To adjust from MSL=0 to LVD, add a datum offset such as provided in Table 4-2. These plots show that Kawhia has the largest tidal range, followed by Tararu and Whitianga. The plots and table show the elevation of mean high-water springs (MHWS) calculated in several ways.

In New Zealand, the intersection of the mean high-water springs (MHWS) elevation with the land defines the landward jurisdictional boundary of the coastal marine area, yet MHWS can be defined in different ways, such as the nautical definition $MHWS_n = M_2 + S_2$ for example (Pugh 1987). Alternatively, NIWA's red-alert tide calendar⁴ alerts a user to times when high-tide peaks equal or exceed the sum of the amplitudes of the three largest tidal harmonics, otherwise known as mean high-water perigean springs (MHWPS), M_2 (principal lunar semi-diurnal) + S_2 (principal solar semi-diurnal) + N_2 (larger lunar elliptic semi-diurnal). Despite New Zealand's tidal regime being semi-diurnal (with small diurnal constituents) there is a contrast between the west and east coasts. The west coast tides are dominated by $M_2 + S_2$, leading to fortnightly spring and neap tides of approximately equal amplitude, whereas on the east coast the tidal regime is dominated by the 27.5-day cycle of perigean and apogean tides and a single dominant spring tide per month, because the S_2 solar tide degenerates to low amplitudes (Walters et al. 2001). Because of the variability in tide regimes, definitions of MHWS (or red-alert elevations) can be inconsistent when tide characteristics vary substantially around the New Zealand coast (Stephens et al. 2014). Bell (2010) showed that high-tide exceedance curves, based on the cumulative distribution function (CDF) of long-term tide predictions, allow MHWS to be consistently defined based on a common exceedance threshold that is independent of tide regime. This leads to the definition of MHWS-10, for example, as the elevation equalled or exceeded only by the largest 10% of all high tides. Likewise, MHWS-6 is equalled or exceeded by the largest 6% of all high tides.

⁴ <https://www.niwa.co.nz/natural-hazards/physical-hazards-affecting-coastal-margins-and-the-continental-shelf/storm-tide-red-alert-days-2014>

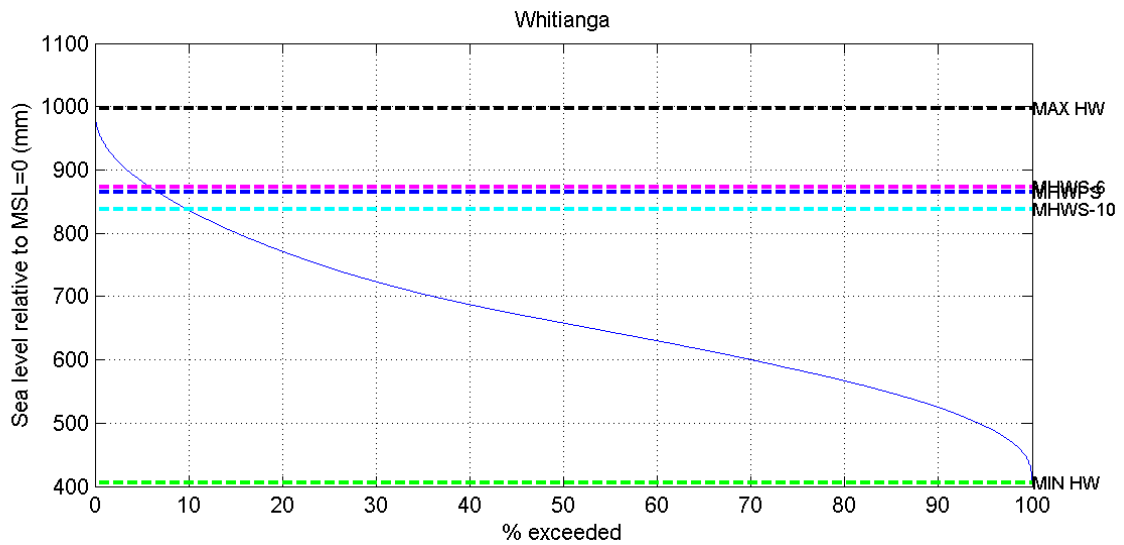


Figure 5-1: High-tide markers at Whitianga relative to MSL=0. MAX/MIN HW = maximum and minimum high waters from predicting 100 years of high tides; MHWS-6 = tide height exceeded by 6% of all tides; MHWS-10 = tide height exceeded by 10% of all tides; MHWPS = mean high water perigean springs ($M_2 + N_2 + S_2$).

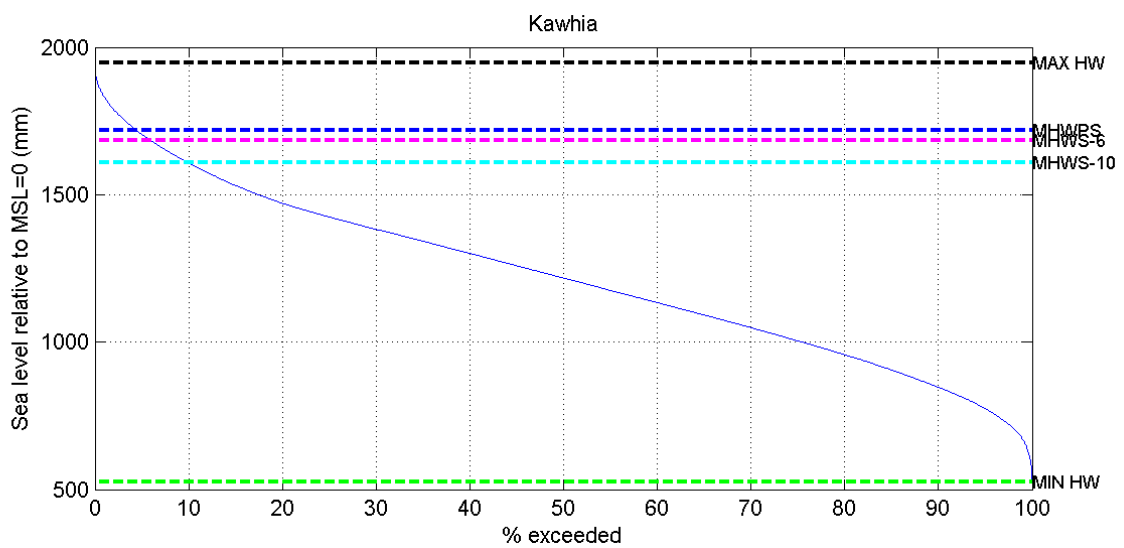


Figure 5-2: High-tide markers at Kawhia relative to MSL=0. MAX/MIN HW = maximum and minimum high waters from predicting 100 years of high tides; MHWS-6 = tide height exceeded by 6% of all tides; MHWS-10 = tide height exceeded by 10% of all tides; MHWPS = mean high water perigean springs ($M_2 + N_2 + S_2$).

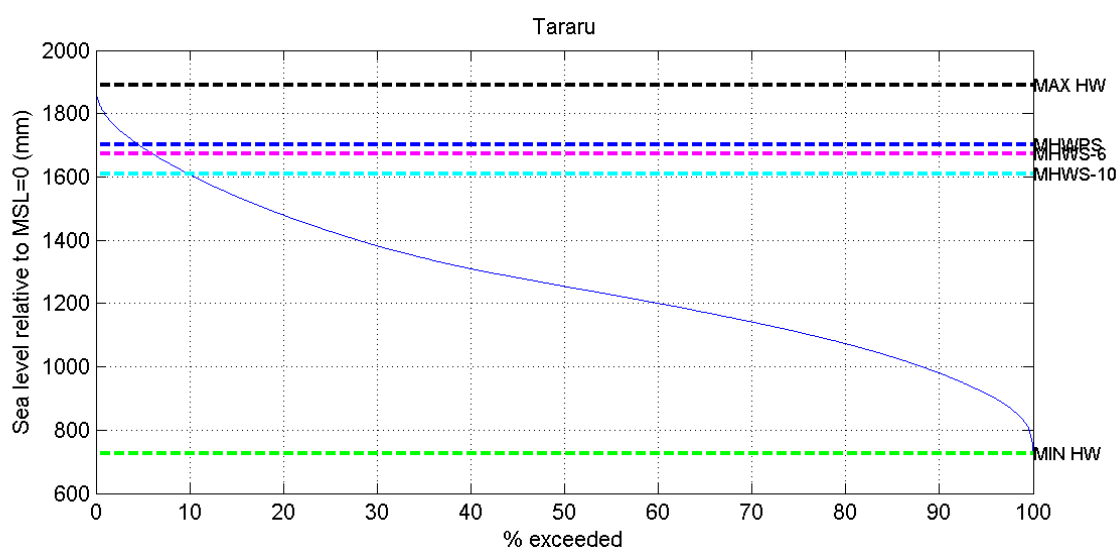


Figure 5-3: High-tide markers at Tararu relative to MSL=0. MAX/MIN HW = maximum and minimum high waters from predicting 100 years of high tides; MHWS-6 = tide height exceeded by 6% of all tides; MHWS-10 = tide height exceeded by 10% of all tides; MHWPS = mean high water perigean springs ($M_2 + N_2 + S_2$).

Table 5-1: Analysis of high waters at Whitianga, Kawhia and Tararu relative to MSL = 0. MHWS-6 = mean high water spring height exceeded by 6% of all tides, MHWS-10 = mean high water spring height exceeded by 10% of all tides, MHWPS = mean high water perigean spring ($M_2 + S_2 + N_2$). The MHWS elevations presented here are given relative to a zero MSL. To calculate the elevations relative to MVD-53, add the present-day MSL datum offsets in Table 4-2.

MHWS marker	Whitianga	Kawhia	Tararu
Minimum high water (mm)	376	564	733
MHWPS (mm)	864	1717	1701
MHWS-6 (mm)	872	1684	1674
MHWS-10 (mm)	837	1608	1609
Maximum high water (mm)	1053	1939	1919

5.1 Mean high-water springs in the Waikato region

This section includes data from a memo to WRC by Dr Rob Bell, dated 8 January 2015. We note that the Whitianga tide gauge record does not represent tidal amplitudes outside of the Whitianga Harbour well. This is due to tidal shoaling over the ebb-tidal delta, which reduces the amplitude of the tidal wave inside the harbour.

NIWA used the EEZ tide model to generate tidal predictions for high tides over a 100-year period and analysed the exceedance distribution curve to evaluate the 10% exceedance value known as MHWS-10. The baseline for this analysis was a MSL = 0 (i.e., the tide rides on the back of a still water level set to zero). A MSL offset from the relevant local vertical datum is then required to situate MHWS-10 locally with respect to the required datum (see below).

MHWS-10 values for the Waikato west coast from the EEZ tide model compare well with the values from the Kawhia and Port Taranaki gauges, so no adjustments were needed for the Waikato west coast.

Comparisons of the EEZ tidal model results with gauge data on the east coasts showed:

- MHWS-10 in the Firth of Thames was overestimated by the EEZ tide model by up to 10 cm at the southern end at Thames (probably due to the tide wave shoaling with no mean tide set-up included in ocean tide model). The value at Thames was adjusted based on MHWS-10 derived from the Tararu gauge, and then proportionately interpolated throughout the Firth up to Port Jackson and Waiheke Island where the tide model values agree with spring-tide ranges from other data sources (e.g., Secondary Port data from the LINZ Nautical Almanac).
- On the east Coromandel coast, most gauge data records (e.g., Port Charles, Whangamata, Tairua) indicated the model-derived MHWS-10 or alternative Mean HW Perigean Spring (MHWPS) values were in close alignment – the only exception being for Whitianga, which appeared to be overestimated by ~10 cm.

The apparent discrepancy for Whitianga was investigated further, using two previous gauge deployments NIWA undertook in 2002 within Mercury Bay (Figure 5-4) and comparing with the concurrent data from the WRC gauge at Whitianga Wharf. The overlapping 90-day period for all records was from 1800 hrs 22 August to 2200 hrs 20 November 2002.

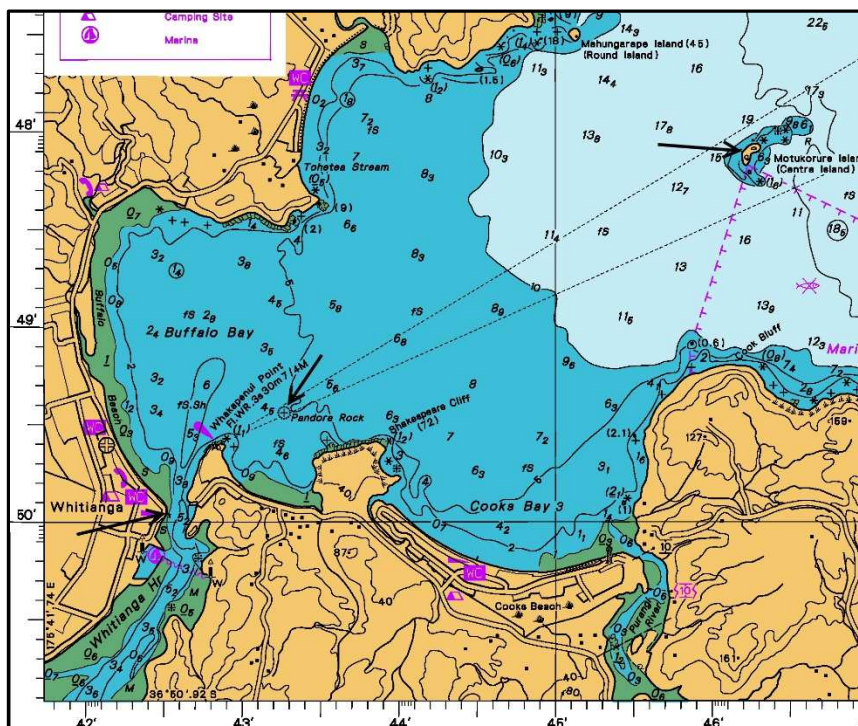


Figure 5-4: Locations of two NIWA water level gauge moorings in October–November 2002, one at Pandora Rock off Shakespeare Cliff, the other at Motukorure (Centre).

A tidal analysis on all three overlapping gauge records was undertaken. To compare the relative MHWS values at all three sites and with the EEZ tidal model, the MHWPS values, generated from the M2, N2, and S2 twice-daily tidal constituents at each site, are shown in Table 5-2.

The tides out in Mercury Bay (Pandora Rock and Motukorure Island) are similar in tide range but the tidal range at Whitianga Wharf (black time series) is noticeably attenuated – presumably damped by the constricted and shallow entrance to Whitianga Harbour.

Table 5-2: Tidal analysis for Mercury Bay covering the 90-day deployment period in 2002, with amplitudes for the main twice-daily tidal constituents and the sum. The tidal elevations presented here are given relative to a zero MSL. To calculate the elevations relative to MVD-53, add the present-day MSL datum offsets in Table 4-2.

	Motukorure Is.	Pandora Rock	Whitianga Wharf	EEZ tide model
M2 (M)	0.747	0.755	0.625	
N2 (M)	0.151	0.152	0.122	
S2 (M)	0.108	0.108	0.083	
MHWPS (M)	1.006	1.015	0.830	0.99

The MHWPS results in Table 5-2 show the EEZ tidal model results are indeed consistent for the open coast of Mercury Bay (within 1-2 cm), as are values for the rest of the east coast of the Coromandel Peninsula. This consistency also applies to the model-derived MHWS-10 values, which for the rest of Mercury Bay is 0.96 m (3 cm less than MHWPS). What has become apparent is the substantial attenuation in tidal range that occurs across the ebb-delta system of Whitianga Harbour inlet, with an 18 cm drop in MHWPS levels across the inlet delta for this 2002 period. The recent multi-year analysis of the Whitianga Wharf record by NIWA for WRC shows that MHWS-10 is ~0.84 m, and 0.87 m for MHWPS. The latter is slightly higher than the 0.83 for the 3-month deployment in 2002 (Table 5-2), but is also likely to fluctuate somewhat over time depending on bathymetric/geomorphic changes around the entrance to Whitianga Harbour.

Tidal damping of the main tidal constituents was also noted by Goring (1999) and the presence of overtides, generated in shallow environments by seabed friction, demonstrates the attenuation through the harbour entrance.

Consequently, the MHWS-10 value of 0.96 m, as derived from the EEZ-tidal model, should apply to the open coast of Mercury Bay (including Cooks Beach, Maramaratotara Bay, Ohuka Bay and Buffalo Beach away from the Entrance). However, GIS map analyses derived from LiDAR should include the lower MHWS-10 value of 0.84 m for evaluating the inundation potential within the environs of Whitianga Harbour and Entrance.

The final set of MHWS-10 estimates from the EEZ tidal model, adjusted where needed as described above, are shown for the Waikato regional coastlines in Table B-1.

Note: On open-coast beaches, a purely-tidally derived MHWS-10 will be an under-estimate of the height of the upper part of the natural beach, due to wave set-up from persistent background wave conditions. This was locally implemented on open-coast beaches for the Auckland Council in a 2012 NIWA report on defining a MHWS boundary for the Auckland region (Stephens et al. 2012).

5.2 Nodal tidal cycles

As explained in Section 2.1.1, the *diurnal* tides arise because the angle (or declination) of the moon's orbit around the earth changes, relative to the equatorial plane. The lunar declination north and south of the equator varies over a 27.21-day period. The maximum diurnal tidal ranges occur when

the lunar declination is greatest, and the ranges become very small when the declination is zero (Boon 2013; Pugh 2004). The effect of declination is to produce an asymmetry between the two high and the two low water levels observed as a point rotates on the earth; in other words it creates an inequality in the *semidiurnal* tide (Pugh 2004).

The nodal cycle arises from variations in the lunar declination (and strength of the *diurnal* tides) over an 18.6-year period, as explained by (Pugh 2004): The earth’s equatorial plane is inclined at 23° 27’ to the plane in which the earth orbits the sun (called the ecliptic). This inclination causes the seasonal changes in our climate, and the regular seasonal movements of the sun north and south of the equator. The plane in which the moon orbits the earth is inclined at 5° 09’ to the plane of the ecliptic; this plane rotates slowly over a period of 18.61 years. As a result, over this 18.61-year *nodal* period the amplitude of the lunar declination increases and decreases slowly. The maximum declination north and south of the equator varies between 18° 18’ and 28° 36’. There are maximum values of lunar declination in 1969, 1987, 2006 and 2025, and minimum values in 1978, 1997, 2015 and 2034. In the southern hemisphere the nodal cycle is therefore presently near its peak amplitude.

The nodal cycle affects all tides. It affects M_2 by about 3.7%, O_1 by 18.7%, K_1 by 11.5% and K_2 by 28.6%. This means that the nodal effect “beats” due to the interaction of the various tidal components, and so it can’t be isolated as a unique harmonic. The effect of the nodal cycle is most easily examined by looking at the standard deviation of the predicted tide; Figure 5-5 shows an example for Auckland. Auckland is a long record and it shows the signature of several nodal cycles – it also shows an apparent decrease in tidal range which could be related to sea-level rise or to gradual siltation of the harbour in which the gauge is located.

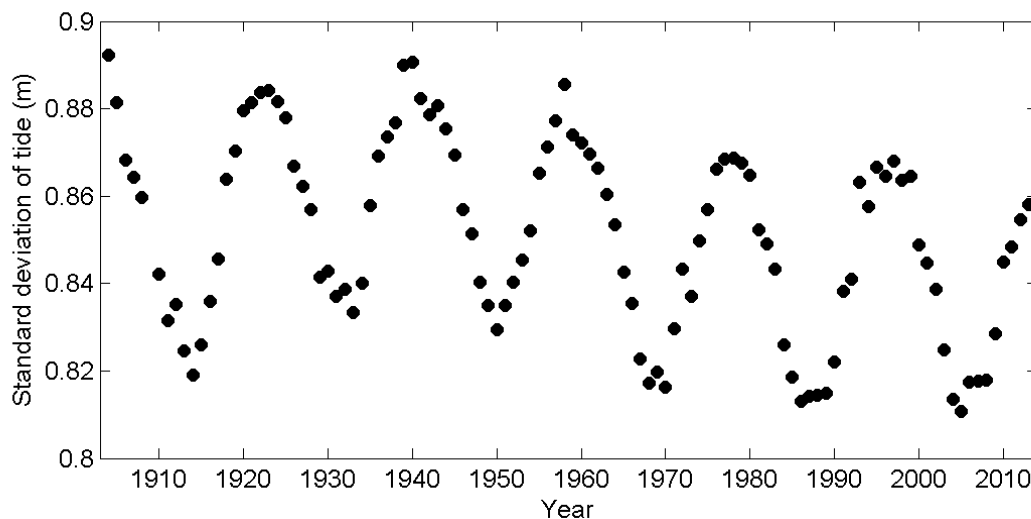


Figure 5-5: Annual standard deviation of predicted tide at Auckland.

The annual standard deviation of predicted tides are shown for Tararu, Whitianga and Kawhia (Figure 5-6). Of these, only the Tararu record is long enough to include a full nodal cycle, but the effects of the nodal cycle are visible in the standard deviations from all the gauge records.

At Whitianga there is an obvious jump (increase) in the standard deviation that occurred in 2006. This relates to a change in the tidal regime within the harbour. As noted in Section 5.1, the mean high-water spring elevation also increased. Figure 5-7 shows that this is linked to an increase in the amplitude of the M_2 tide in February–March 2006, which is probably driven by a change in

morphology of the harbour entrance. This could be related to a storm when the entrance morphology deepened, change in sand pulses which periodically switch from east to west, or engineering works such as extension of a seawall, dredging, or construction of a canal in the harbour. There was also a decrease in the M2 tidal amplitude in January 2000 (Figure 5-7).

This is a good example of why small estuaries are not ideal locations for tide gauges, because there is a strong link between the estuary morphology and its effect on the tidal wave, and small estuaries can be prone to rapid morphological change. Note that the MSL record was not affected by the tidal regime change (Figure 4-2).

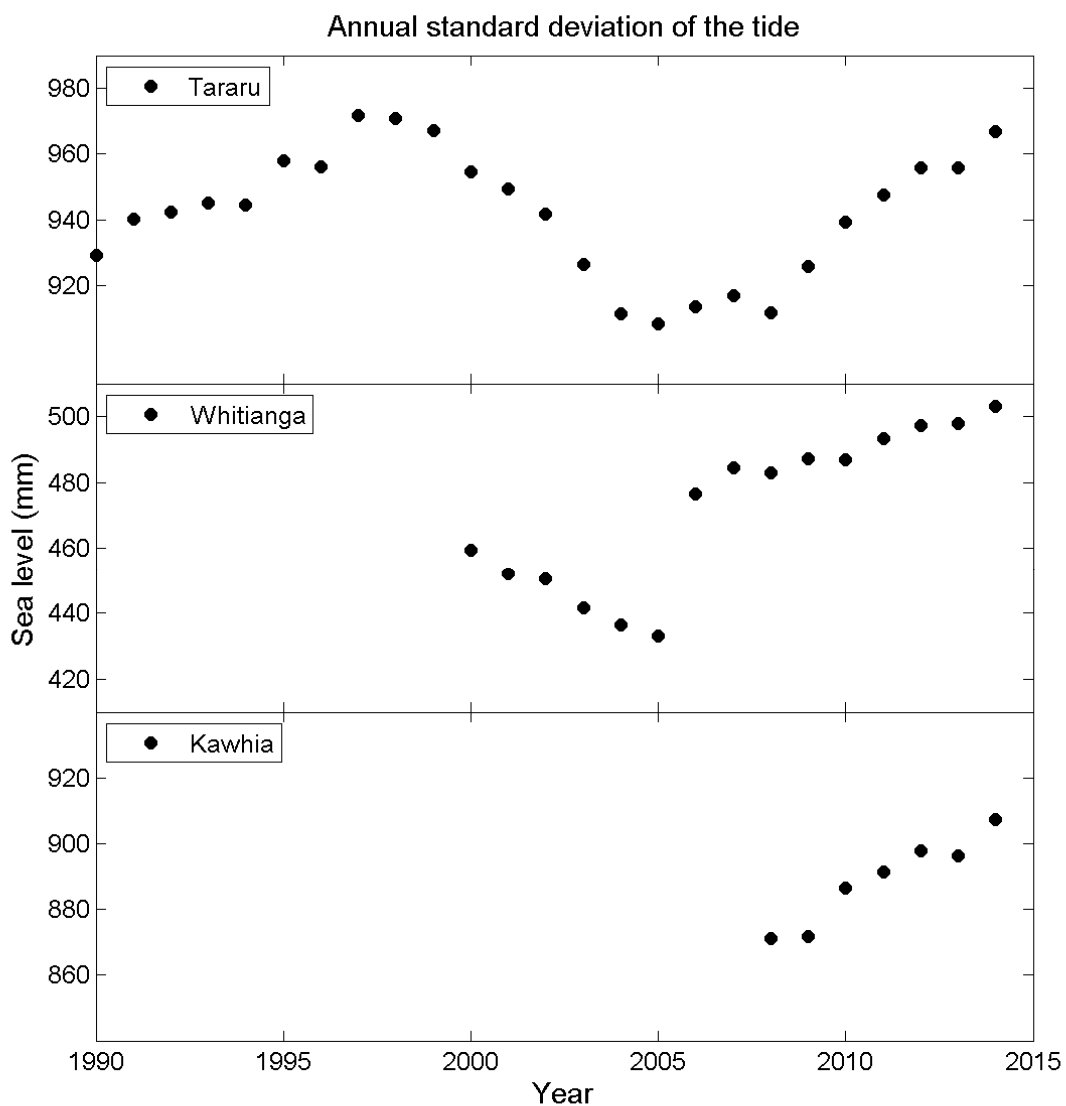


Figure 5-6: Annual standard deviation of predicted tide at Tararu, Whitianga and Kawhia. The three plots have the same vertical axis scale so can be directly compared.

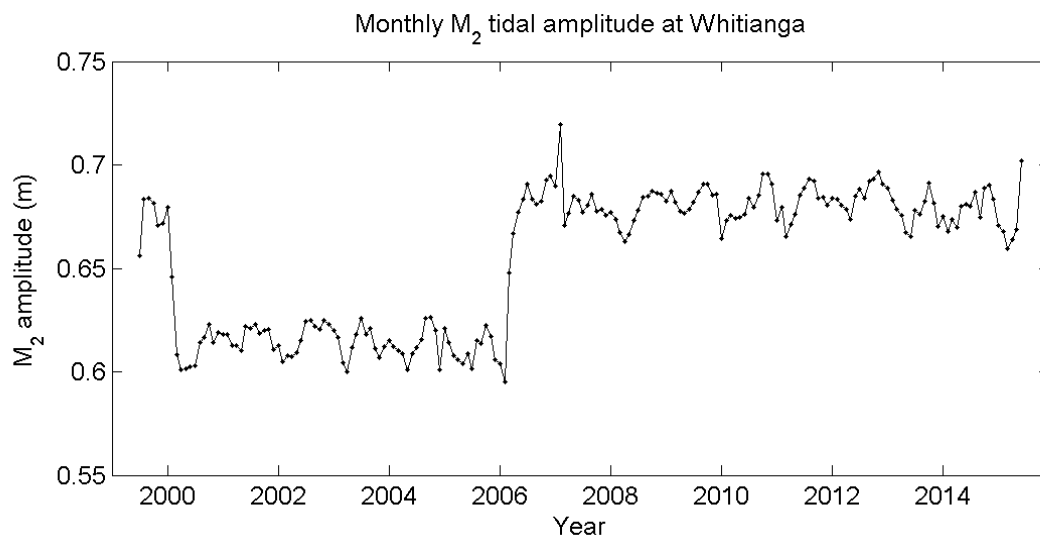


Figure 5-7: Monthly analysis of M2 tidal amplitude at Whitianga.

6 Storm surge

6.1 Extreme storm-surge analysis

Storm surge is the response of the ocean to changing atmospheric pressure and wind. Tide can be forecast many years into the future, but our knowledge of the storm-surge distribution is restricted to the sea-level gauge measurement period. However it is possible that more extreme storm surges have occurred historically, or could occur in future. Extreme-value models predict the likelihood and magnitude of extreme storm surges, based on measured data.

The term annual exceedance probability (AEP) describes the probability of a given (usually high) sea level being equalled or exceeded in elevation, in any given calendar year. AEP can be specified as a fraction (e.g., 0.01) or a percentage (e.g., 1%). The term average recurrence interval (ARI) describes the average time interval (averaged over a very long time period and many “events”) that is expected to elapse between recurrences of an infrequent event of a given large magnitude (or larger). A large infrequent event would be expected to be equalled or exceeded in elevation, once, on average, every “ARI” years, but with considerable variability. AEP can be related to ARI as follows:

- Over an L -year period, the risk (R) of a sea-level elevation with a specified AEP occurring is $R = 1 - (1 - \text{AEP})^L$
- Over an L -year period, the risk of a sea-level elevation with a specified ARI occurring is $R = 1 - \exp(-L/\text{ARI})$, so
- When $R = \text{AEP}$, $L = 1$, so $\text{AEP} = 1 - \exp(-1/\text{ARI})$, and $\text{ARI} = -1/\log(1 - \text{AEP})$.

There are two extreme value models commonly-applied to analyse storm surge: 1. the generalised extreme-value (GEV) model fitted to block maxima (such as annual maxima) and 2. the generalised Pareto distribution (GPD) fitted to independent data peaks that exceed a given high threshold, known as peaks over threshold (POT). The GPD/POT method is often preferred because it uses more of the available data, but the choice of threshold is subjective and can influence the result.

A GEV model fitted to annual maxima data is generally only reliable for predicting magnitudes with ARI out to 3–5 times the record length (18–30 years for Kawhia and up to 120 years for Tararu). However, our experience with the much longer (> 100 years) Auckland record has shown that even 33-year records can be unstable using GEV fits to annual maxima, and at least 50-years of data is generally required for a robust analysis using this technique (Haigh et al. 2010). We found that the maximum-likelihood estimates of extreme storm surge were similar when using either the GEV or GPD techniques (Table 6-1), but that the GPD gave tighter confidence intervals.

While the GPD/POT method is more efficient, no method can make up for lack of data, which may have been collected during a particularly energetic or quiescent period. For example, the storm surge of 929 mm at Tararu appears to be an outlier for the given record length relative to the fitted frequency–magnitude distribution (Figure 6-1), but presumably it would lie closer to the curve in a longer record, as either more events of this size or larger occurred, or the record duration pushed its plotting position further out. The storm-surge frequency–magnitude distribution at Kawhia cannot be reliably estimated yet due to its short gauge record.

We note that there is considerable statistical uncertainty in the extreme storm surge models at all three sites (Figure 6-1, Figure 6-2), but the Kawhia extreme storm surge distributions have particularly high uncertainty due to the short record there. One reason for uncertainty in the

extreme-value models is that the storms which drive the surges have different meteorology, and so the models are an imperfect fit to the inhomogeneous surge population. There are different populations of storms and surges, certain types of storm drive the largest surges. For a very long record, the surges could be separated into populations and extreme-value modelling could be done for unique storm types. But for records the length of these, all surges must be used to reduce statistical uncertainty as much as possible.

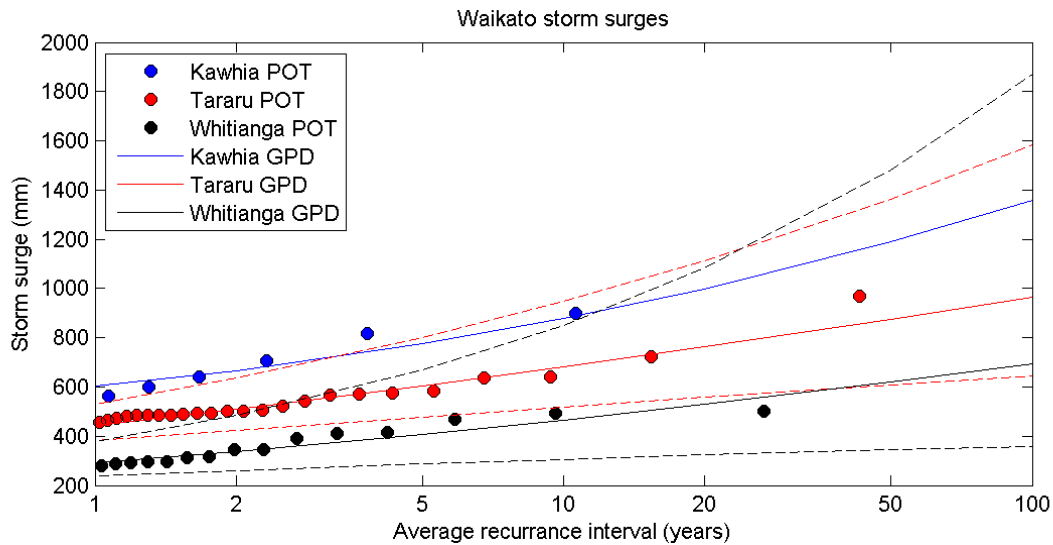


Figure 6-1: Extreme value analysis of storm surges using a GPD fitted to storm surges over a high threshold. POT = peaks over threshold, GPD = generalised Pareto distribution fitted to storm surge peaks. Only peaks with an ARI ≥ 1 year are shown. Dashed lines represent 95% confidence intervals, these are omitted for Kawhia as they skew the plot and are unreliable.

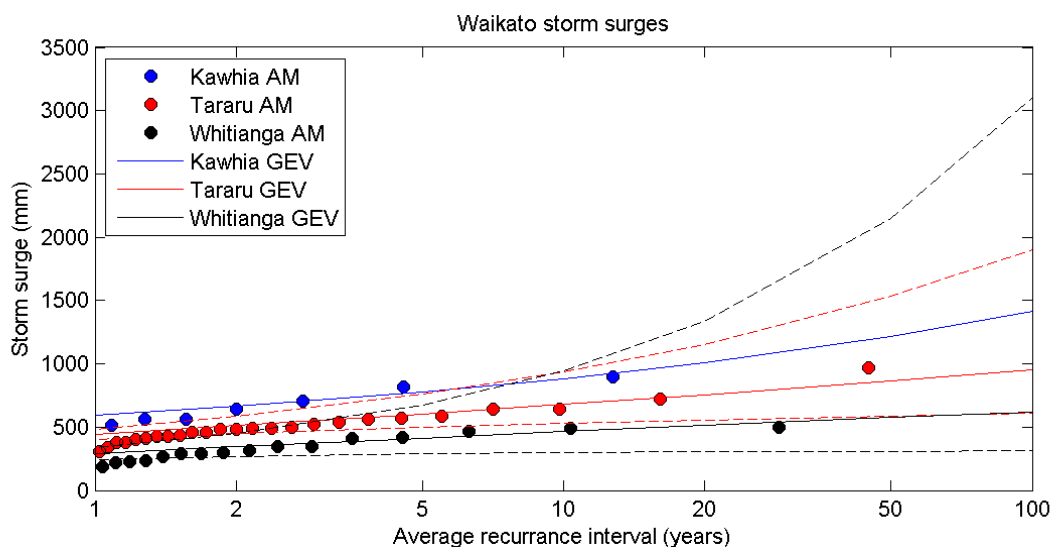


Figure 6-2: Extreme value analysis of storm surges using a GEV fitted to annual maxima storm surges. AM= annual maximum storm surges, GEV = generalised extreme value distributions fitted to the annual maxima. Dashed lines represent 95% confidence intervals; these are omitted for Kawhia as they are so wide due to the very short AM record, which makes the GEV fit unreliable.

Table 6-1: Frequency–magnitude distribution of extreme storm surges. Storm surge heights (mm) were modelled using GPD fitted to peaks-over-threshold data, and using GEV fitted to annual maxima.

AEP	ARI	Whitianga		Tararu		Kawhia	
		GPD	GEV	GPD	GEV	GPD	GEV
0.63	1	291	288	444	444	602	595
0.39	2	338	344	510	511	667	663
0.18	5	407	413	605	605	777	776
0.10	10	465	464	682	679	879	881
0.05	20	528	513	762	757	998	1008
0.02	50	619	574	875	864	1188	1218
0.01	100	694	619	965	950	1360	1414

6.2 Descriptive analysis of the largest storm surge events

The largest storm surge events on record for each sea level gauge are described in this Section. The largest five independent storm surges were chosen for Whitianga and Tararu, and the largest three for the shorter Kawhia record.

The inverse barometer (IB) correlation to storm surge was analysed at each sea level gauge. In the deep ocean, far from land, changing atmospheric pressure results in the IB effect:

- a 1 hPa fall in pressure results in approximately a 10 mm rise in sea level; and
- a 1 hPa rise in pressure results in approximately a 10 mm fall in sea level.

The IB effect at each site was determined by processing mean sea level pressure (MSLP) data using Equation 6-1:

Equation 6-1: Inverse barometer equation.

$$(m - ssMSLP) * 10 \text{ mm}$$

where m is the long term mean MSLP; and $ssMSLP$ is the instantaneous MSLP. $ssMSLP$ was calculated by wavelet filtering MSLP to obtain only the periods of motion between 24 hours and 1 month, which is consistent with the processing of sea-level data into storm surge.

For each event described, synoptic weather maps are provided (where possible) to show the individual storms and give context to the storm surge events. Finally, monthly boxplots of the largest storm surge events each year are constructed to highlight seasonality in storm-surge hazard.

Table 6-2 shows the source of meteorological data used for the descriptive storm surge analysis. Other than at Tararu, more than one wind source was required for the descriptive analysis. This does not affect the general description of storm surge response to meteorological conditions.

Table 6-2: Source of meteorological data used for storm surge descriptive analysis.

Description	Source	Distance away from sea-level gauge (km)	Latitude	Longitude
Tararu Sea level	Tararu tide gauge	0	-37.128	175.521
Tararu MSLP (1991-1997)	Paeroa AWS	30.8	-37.373	175.684
Tararu MSLP (1998-present)	Tararu MSLP	0	-37.128	175.521
Tararu Wind (1991-present)	Tararu wind station	0		
Whitianga Sea level	Whitianga tide gauge	0	-36.833	175.709
Whitianga MSLP (1999-2006)	Whitianga aero AWS	2.8	-36.834	175.677
Whitianga MSLP (2007-2014)	Whitianga MSLP	0	-36.833	175.709
Whitianga wind (1995-2004)	Whitianga Aero AWS	2.8	-36.834	175.677
Whitianga wind (2005-2012)	Slipper Island AWS	32	-37.052	175.943
Whitianga wind (2013-2014)	FOT EWS NIWA	48.3	-37.21622	175.4503
Kawhia Sea level	Kawhia tide gauge	0	-38.0659	174.8232
Kawhia MSLP (2008-June 2010)	Port Taharoa AWS4	15.5	-38.171	174.707
Kawhia MSLP (June 2010-present)	Kawhia MSLP	0	-38.0659	174.8232
Kawhia wind (2008-2012)	Port Taharoa AWS5	15.5	-38.171	174.707
Kawhia wind (2013-2014)	Whatawhata2 (Cliflo)	37.6	-37.78832	175.06906

6.2.1 Whitianga

The largest five storm surges are listed in Table 6-3. Three out of the five large events occurred during winter. MSLP data for Whitianga was supplied for the duration of the sea level gauge record, from Metservice and NIWA. Figure 6-3 shows the storm surge and IB for Whitianga during 2008 (for example), when the highest storm surge occurred. Both the storm surge and IB generally rise and fall in unison, however there is often a lag between the two, with storm surge peaking before IB during the July 2008 storm and during April 2008. Figure 6-3 indicates that storm surge is strongly correlated with IB at Whitianga.

A cross correlation analysis reveals a peak correlation of 0.74 between storm-surge and the IB lagged by 1 hour over the record (Figure 6-4). A correlation of 0.74 means that 74% of the variability in storm surge is explained by inverted barometer, on average. The barometric factor obtained with a 1 hour lag is 0.87; in other words, divide IB by 0.87 to predict storm-surge magnitude.

Table 6-3: The top five storm surges on record at Whitianga.

Date	Storm surge (mm)	Lowest barometric pressure (hPa)	Maximum expected IB sea level (mm)	Remaining wind setup component (mm)
26-Jul-08	502	968	407	94
25-Sep-13	494	989	224	270
29-Jan-11	468	992	204	265
21-Aug-03	416	985	261	155
21-Jun-02	412	991	209	203

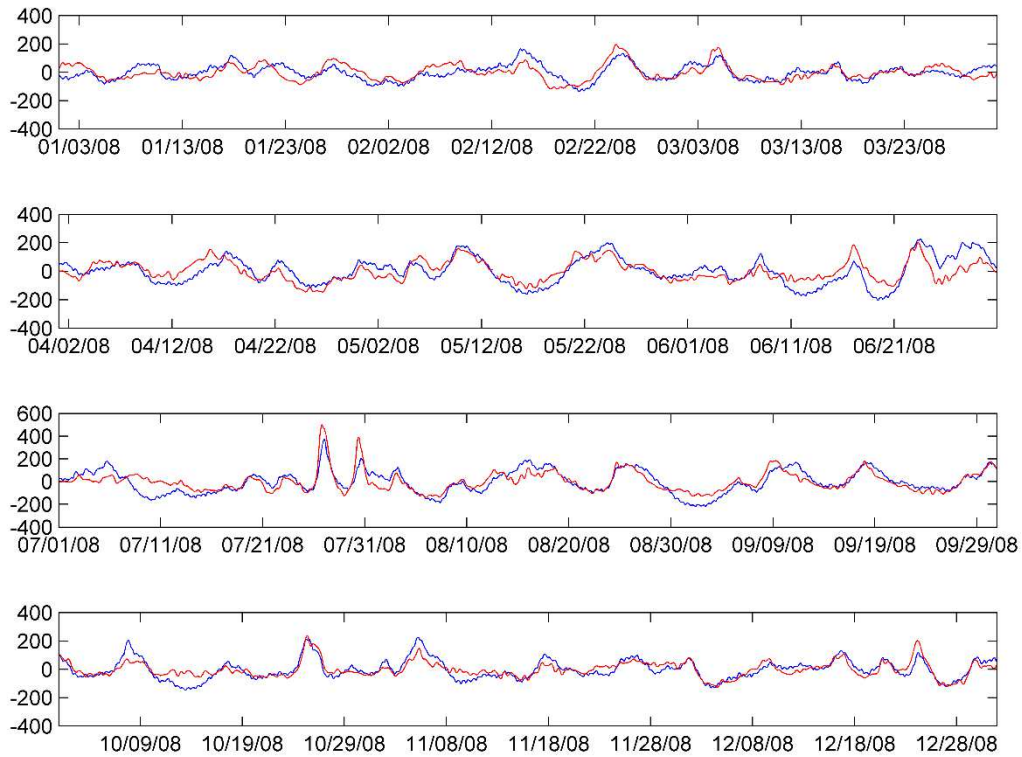


Figure 6-3: Storm surge (red line) and inverted barometer (blue line) at Whitianga for 2008, in mm above gauge zero. Records divided into 3 month periods with Jan-Mar (top), Apr-Jun (2nd from top), Jul-Sep (2nd from bottom) and Oct-Dec (bottom). Largest storm-surge for this year observed as spike on 26-July.

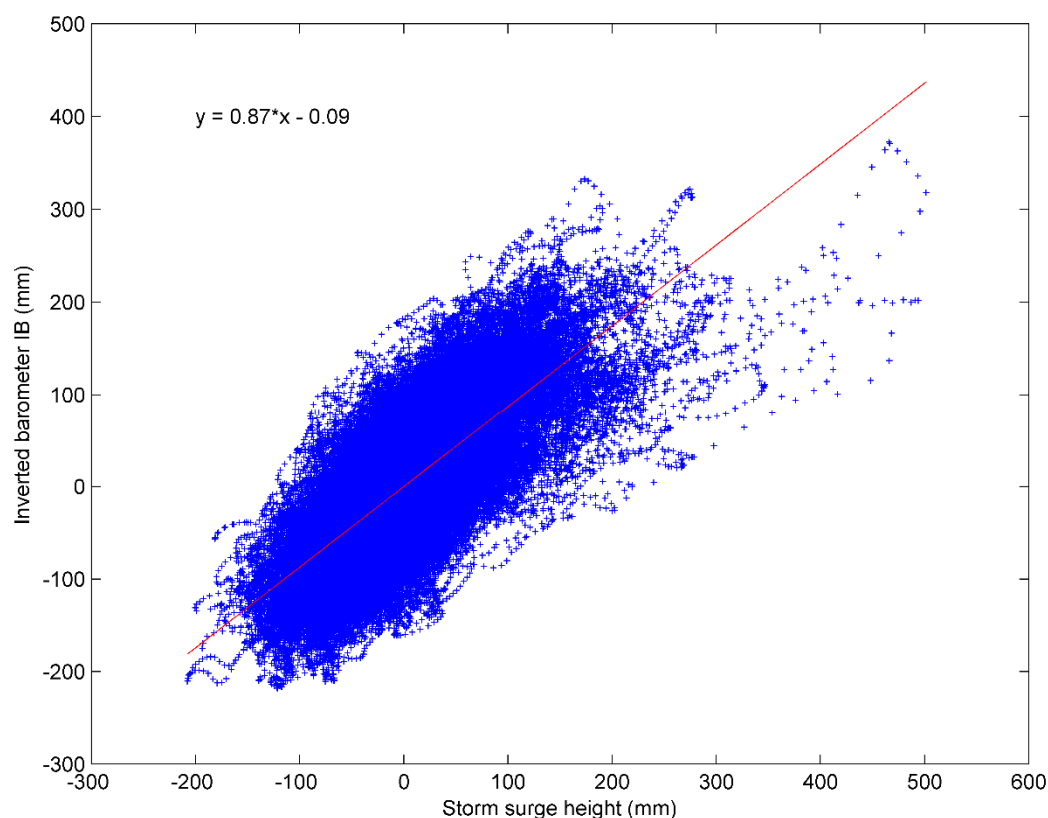


Figure 6-4: Variability of storm surge height relative to the inverted barometer (IB) height for Whitianga. A 1 hour time lag was applied to the IB height, shifting it back an hour. The barometric factor for the best-fit linear regression line is 0.87 and the correlation coefficient is 0.74.

26 July 2008 storm

A deep low moved over the North Island from the north west to the south east over 2 days, producing a storm surge of 502 mm at Whitianga. Barometric pressure reached as low as 965 hPa in the Coromandel (968 hPa at Whitianga). In the deep ocean this would produce around 50 cm of inverse-barometer sea level; applying an inverse-barometric factor of 0.87 would predict 41 cm of inverse-barometer sea-level, plus 9 cm of additional wind setup. This storm brought high winds, seas and rainfall to the North Island. Here, the MSLP and IB rose and fell in unison, but the storm surge peaked a few hours before the IB (Figure 6-3), this may be due to strong NE to E winds that occurred during the storm. These wind stresses would push water down-wind, piling it up against the Whitianga coastline, causing a rise in storm surge before the IB. Peak wind speeds of 28.3 m s^{-1} were recorded at Slipper Island nearby two hours before the peak storm surges (1900 hours at 26 July 2008). Figure 6-5 shows the weather situation at 0000 hours, 27 July 2008.

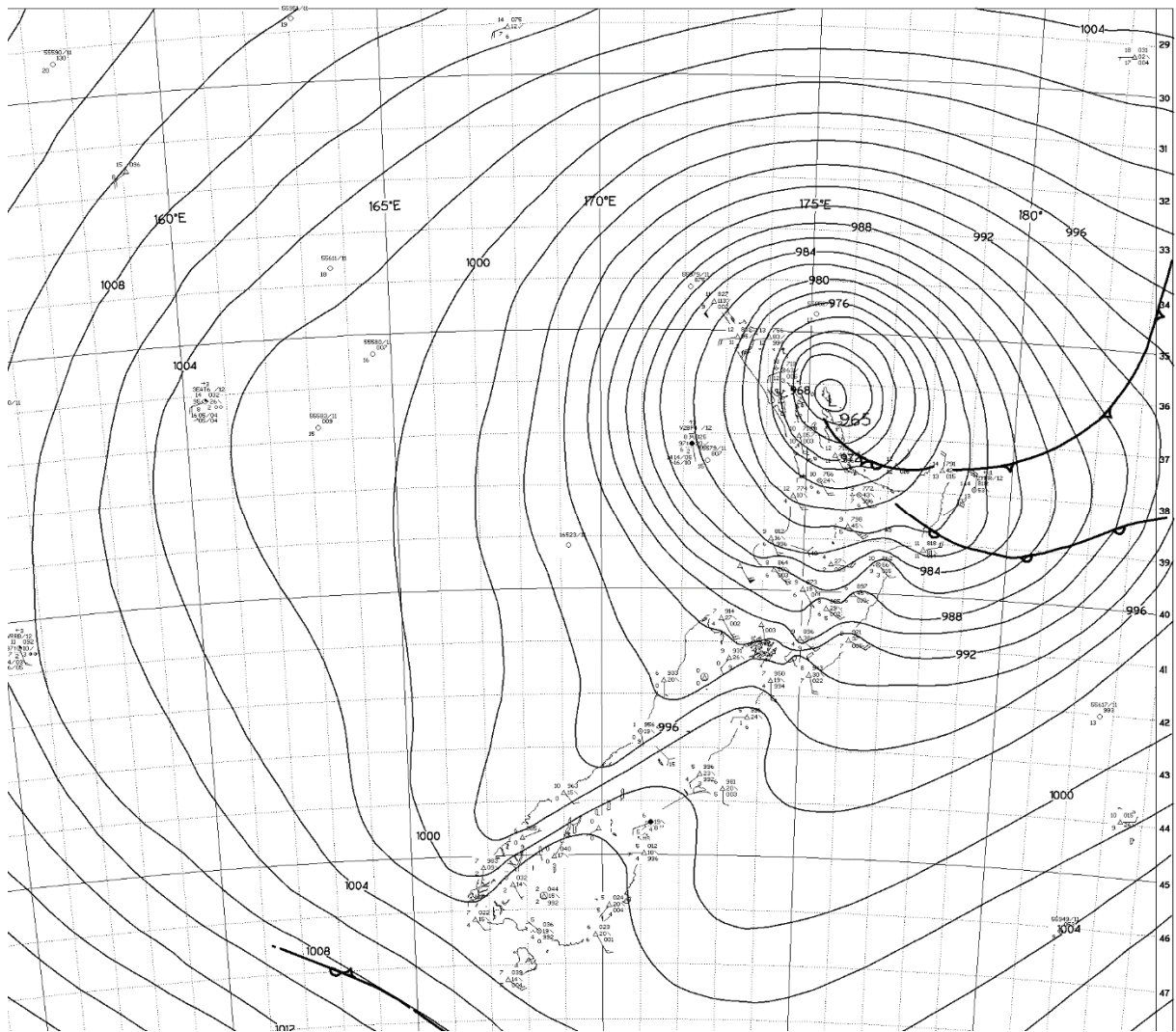


Figure 6-5: Mean sea level pressure map at 0000 hrs, 27 July 2008 around the time of the largest measured storm surge (502 mm) at Whitianga.

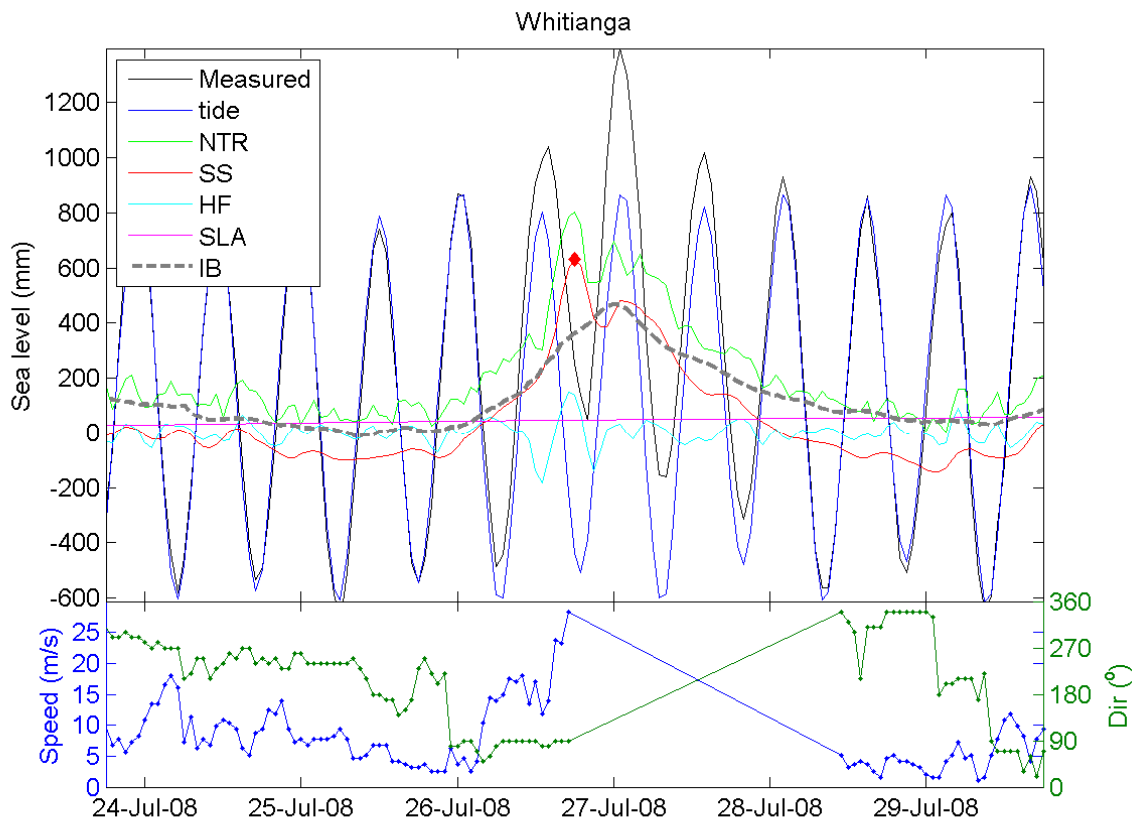


Figure 6-6: Measured sea level and its components during 26 July 2008 storm surge at Whitianga. NTR = non-tidal residual; SS = storm surge; HF = high-frequency sea-level; SLA = sea-level anomaly; IB = inverse barometer.

25 September 2013 storm

During the 24th to 25th September a complex low pressure system moved from the northern North Island to the south east, with a minimum barometric pressure of 989 hPa (23 cm expected IB) recorded at Whitianga during the storms peak. Storm-surge peaked at 494 mm. There is no apparent lag between the storm surge and IB, but there are some differences in the behaviour of the two during this storm. After the peak storm surge at midnight 25th September, it dropped sharply before rising again around 1500 hours 25th September. IB was mostly flat, while barometric pressure remained approximately constant until it fell when the storm surge rose the second time. Why did the barometric pressure and IB remain mostly constant while storm surge decreased? This is because the dominant wind approaching toward the Whitianga coastline from 50-130 degrees, decreased during that time (based on winds observed in Firth of Thames). The second peak in storm surge (and trough in barometric pressure) was caused by the low pressure system having two distinct troughs. Figure 6-8 shows the weather situation at midnight, 25 September 2013.

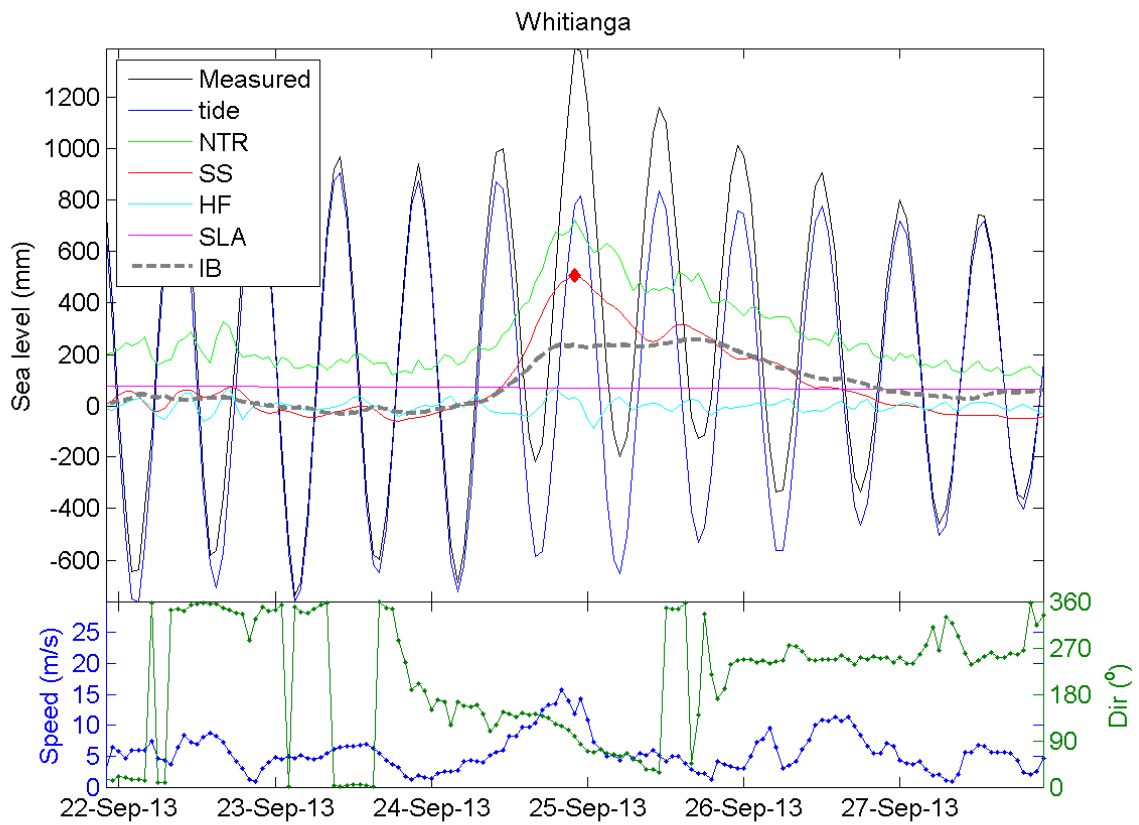


Figure 6-7: Measured sea level and its components during 25 September 2013 storm surge at Whitianga. NTR = non-tidal residual; SS = storm surge; HF = high-frequency sea-level; SLA = sea-level anomaly; IB = inverse barometer. Inverse barometer is based on MSLP measured at Whitianga, but wind data was from Firth of Thames, and is unlikely to represent the local situation well.

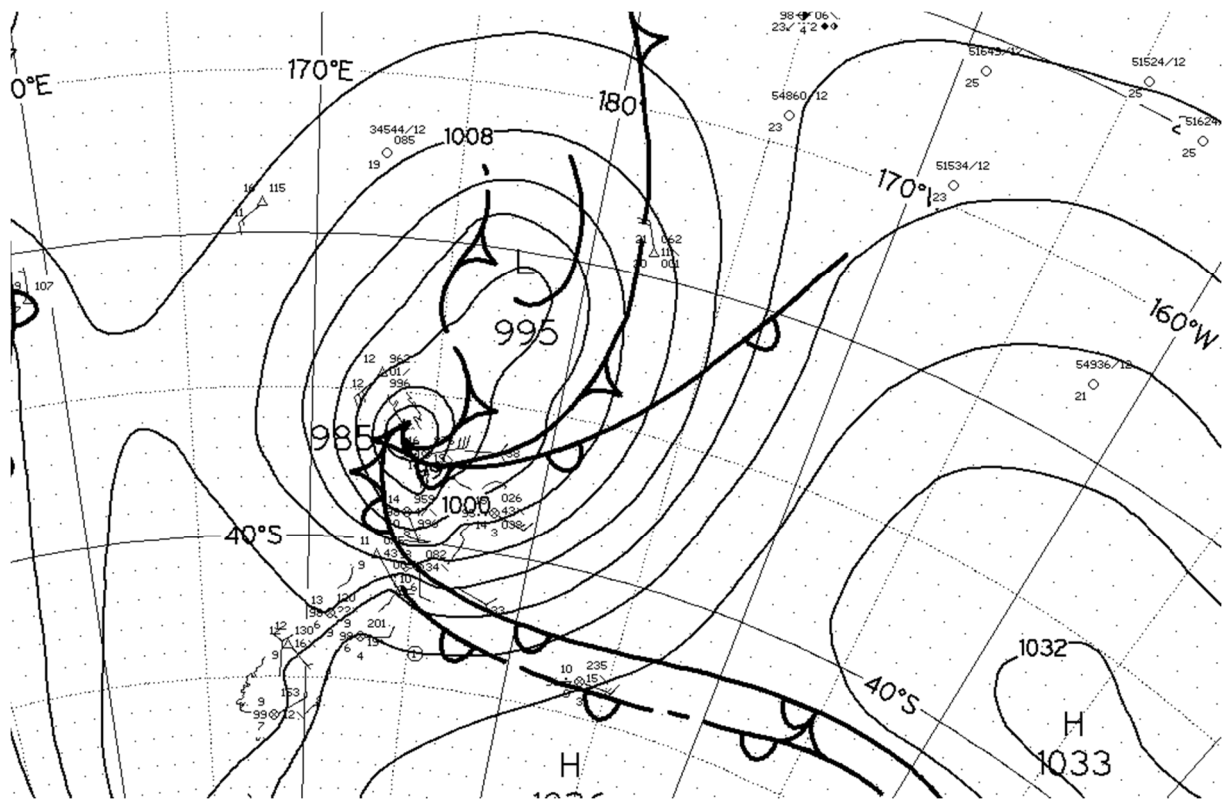


Figure 6-8: Mean sea level pressure at 0000 hours, 25 September 2013 around the time of the second largest measured storm surge (494 mm) at Whitianga.

29 Jan 2011 storm

During 28th to 29th January tropical cyclone Wilma moved across the north eastern North Island, bringing very heavy rainfall and severe flooding. Storm-surge peaked at 468 mm. Rainfall rates as heavy as 31 mm an hour were recorded in the Coromandel peninsula. IB peaked at 237 hPa (20.4 cm expected IB) approximately 3 hours before storm surge. During peak storm intensity, moderately strong winds peaking at 14.9 m/s were recorded at Slipper Island, swinging from a SE to SW direction. The position of the cyclone relative to Whitianga and the dominant wind directions may explain why there was a 3 hour lag between IB and storm surge. Figure 6-10 shows the weather situation at 0600 hours, 29 January 2011.

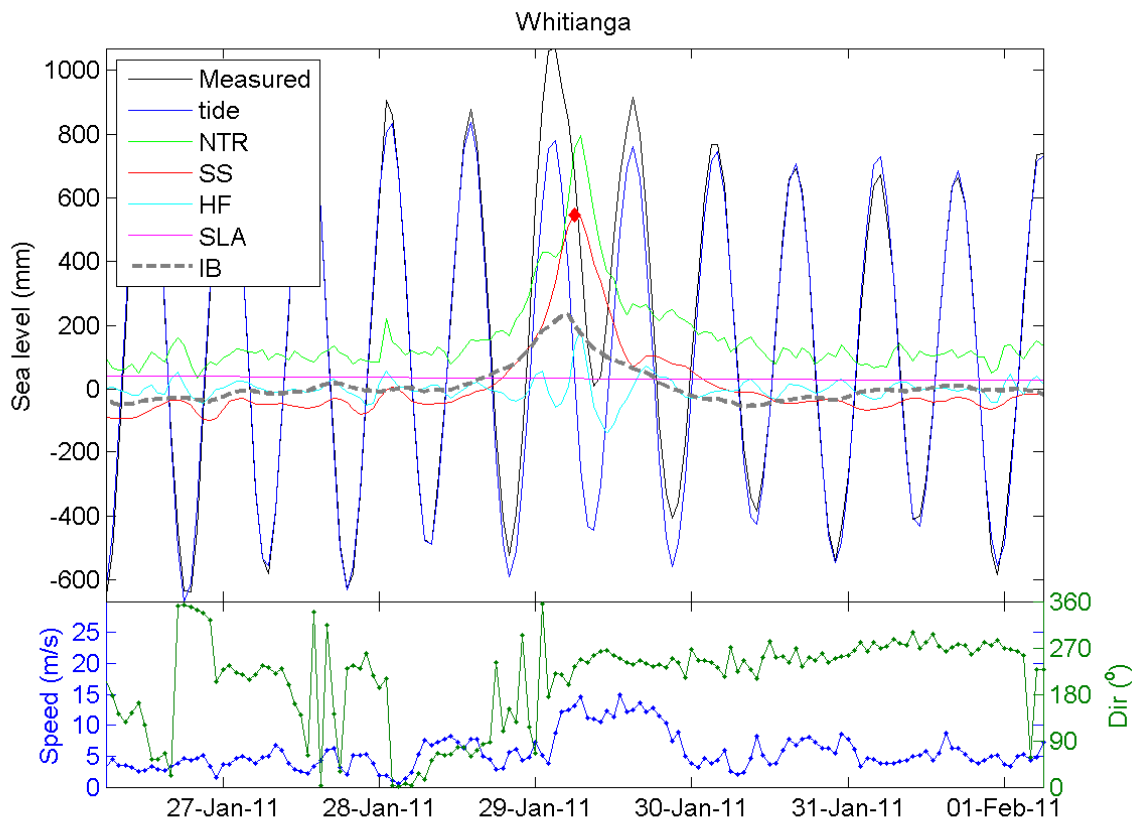


Figure 6-9: Measured sea level and its components during 29 Jan 2011 storm surge at Whitianga. NTR = non-tidal residual; SS = storm surge; HF = high-frequency sea-level; SLA = sea-level anomaly; IB = inverse barometer. Inverse barometer is based on MSLP measured at Whitianga, and wind data was sourced from Slipper Island.

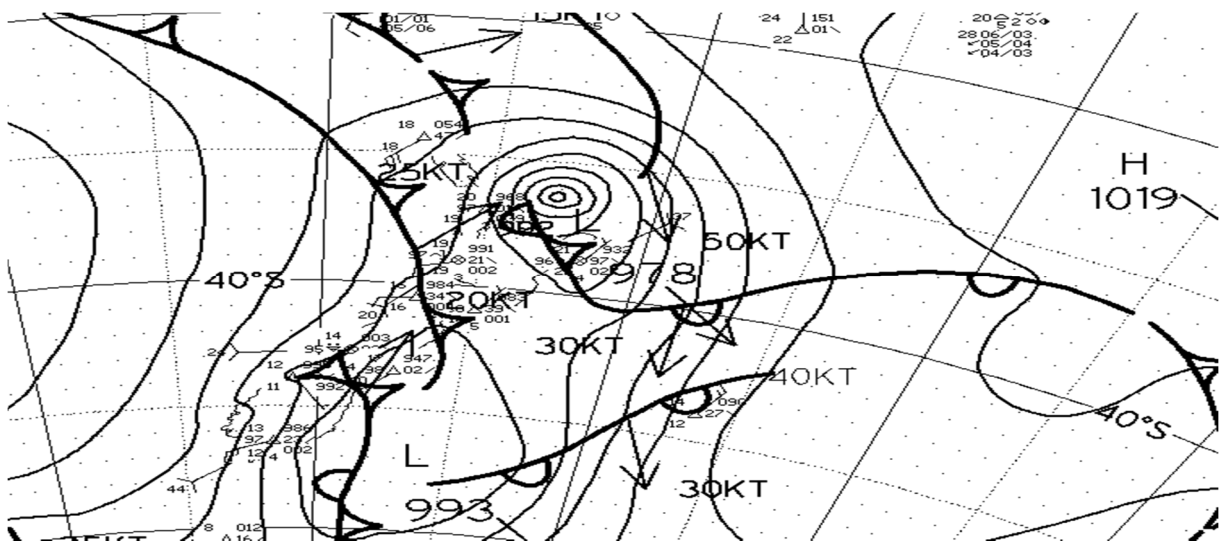


Figure 6-10: Mean sea level pressure map at 0600 hrs, 29 January 2011 around the time of the third largest measured storm surge (468 mm) at Whitianga.

21 August 2003 storm

During the 20th August 2003, a slow moving front-embedded low-pressure system moved from the north of New Zealand onto the North Island, intensifying as it did so. Storm-surge peaked at 416 mm. MSLP dropped to 985 hPa resulting in an expected inverse-barometer effect of 26.1 cm (87% of the measured storm surge). By 2100 hours, the centre of the low-pressure system had moved over to the Tasman Sea west of Auckland, before making landfall again over Northland, and then gradually weakening. Wind directions at Whitianga were predominantly 100-150 degrees (SE) initially, before changing direction to be mostly northerly around the time of peak storm surge, with winds peaking at 12.9 m/s at peak storm surge (21st August 2003 at midnight). There was a two hour lag between storm surges and IB (storm surge peaking first). Both gradually rose (along with falling barometric pressure) until storm surge peaks, before the reverse occurred after 0300. Figure 6-12 shows the weather situation at 0300 hours, 21 August 2003.

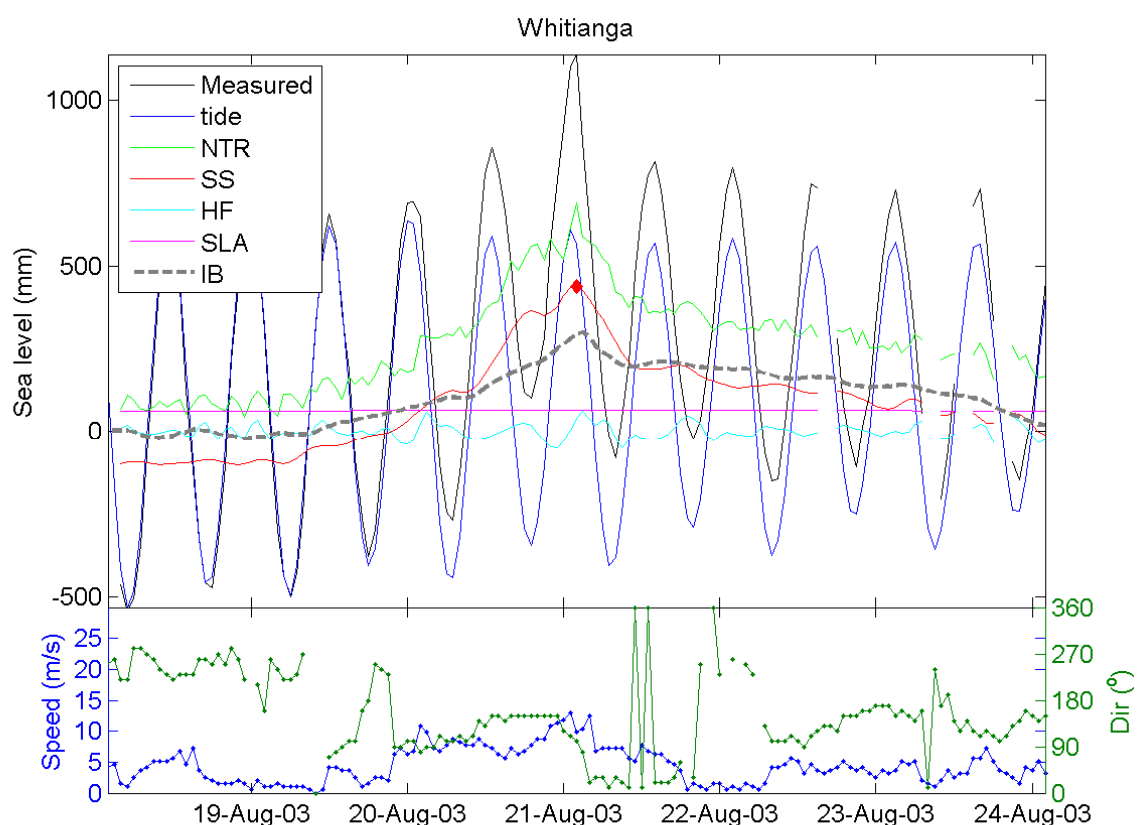


Figure 6-11: Measured sea level and its components during 21 Aug 2003 storm surge at Whitianga. NTR = non-tidal residual; SS = storm surge; HF = high-frequency sea-level; SLA = sea-level anomaly; IB = inverse barometer. Inverse barometer is based on MSLP measured at Whitianga, and wind data was sourced from Whitianga.

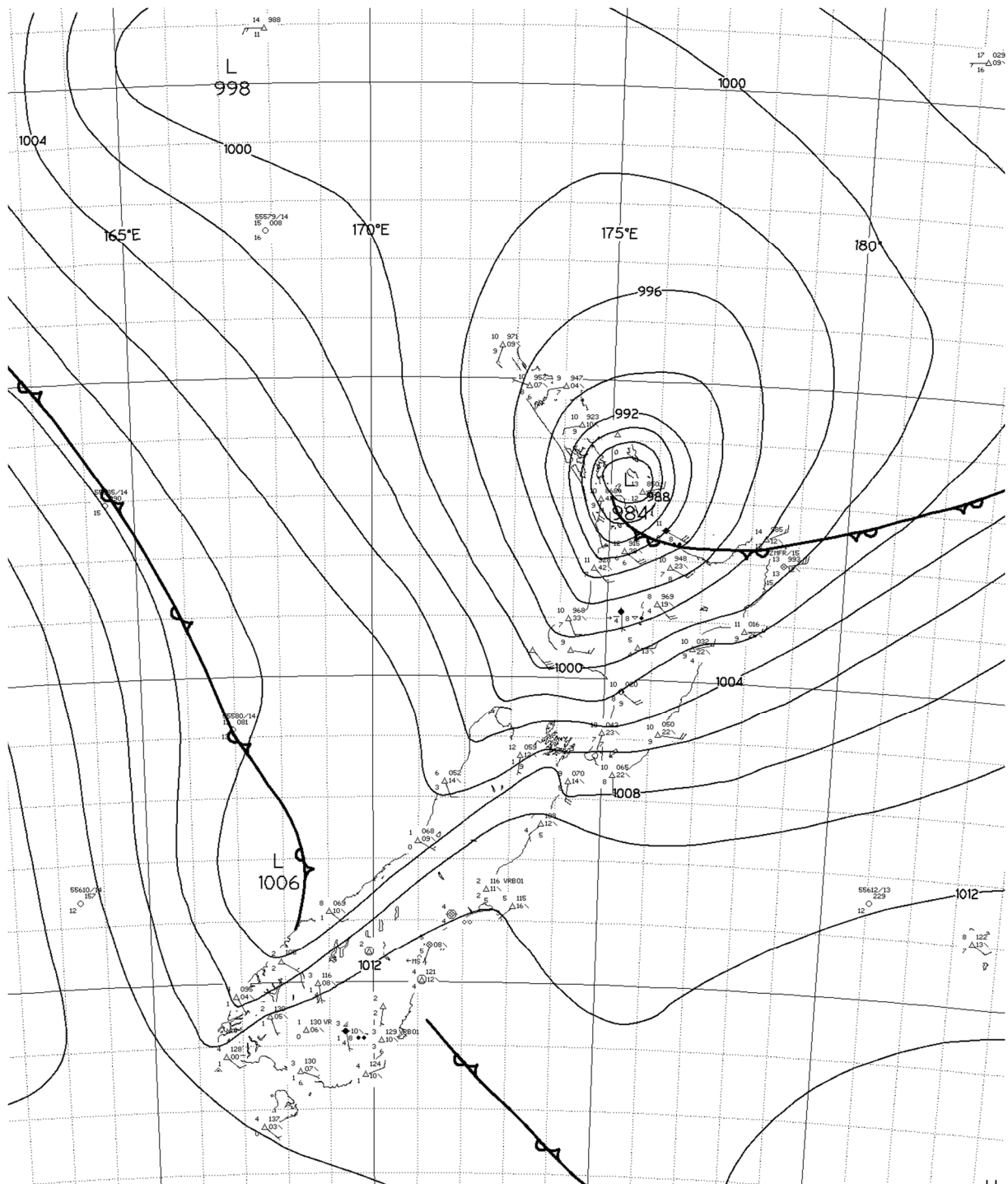


Figure 6-12: Mean sea level pressure at 0300 hours, 21 August 2003 around the time of the fourth largest measured storm surge (416 mm) at Whitianga.

21 June 2002 storm

A 'weather bomb' struck the North Island from 20-21 June 2002. Storm-surge at Whitianga peaked at 412 mm. This storm approached from the far north and moved southwards across the North Island. In its wake, it brought torrential rain and damaging gales to many northern districts, in particular the Coromandel Peninsula, where over 215.5 mm of rain was recorded in 24 hours. At the Whitianga Aero gauge, maximum hourly wind speeds reached 17.5 m.s^{-1} , but gusts would have reached much

higher, being recorded over 30 m.s^{-1} on the Coromandel Peninsula. States of civil emergency were declared in nearby Thames and Putaruru after severe flooding of roads and properties, with homes evacuated and water supplies cut.

Analysis of IB and storm surge data shows a significant lag between peak storm surge and IB during this storm. Storm surge peaked at 0200 hours 21st June, 7 hours before peak IB at 0900 hours on 21st June. Such a large time lag may be due to strong NE to E winds piling wind against the Whitianga coastline, causing a rise in storm surge before IB (Figure 6-13). After the peak storm surge, wind speed dropped significantly, but barometric pressure continued to drop, which would increase the storm surge component of sea level. Over the entire storm, barometric pressure dropped from 1020 hPa down to 991 hPa (21 cm of expected IB sea level) at Whitianga.

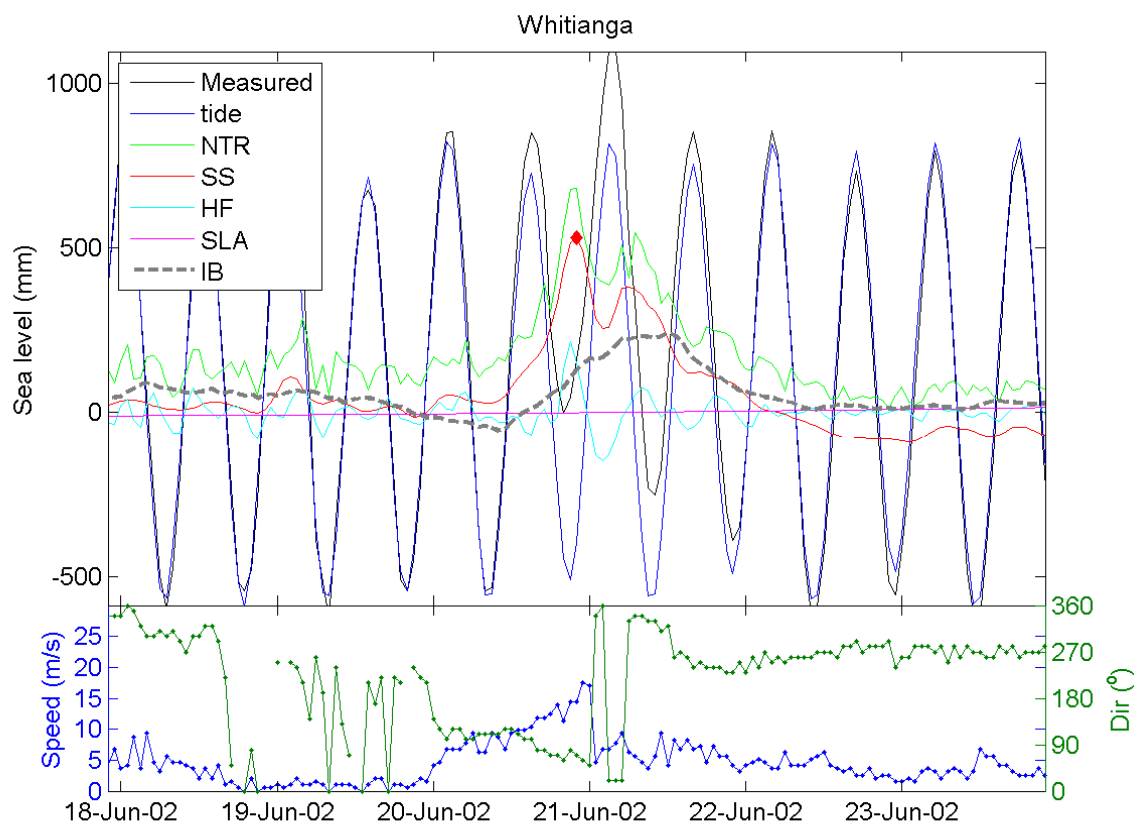


Figure 6-13: Measured sea level and its components during 20 Jun 2002 storm surge at Whitianga. NTR = non-tidal residual; SS = storm surge; HF = high-frequency sea-level; SLA = sea-level anomaly; IB = inverse barometer. Inverse barometer is based on MSLP measured at Whitianga, and wind data was sourced from Whitianga.

Seasonality of storm surges

A monthly boxplot was constructed for the 5 largest storm surge events each year at Whitianga to highlight any seasonality in storm surge hazard (Figure 6-14). It is apparent that the median storm surge was highest during summer and early autumn, and particularly in January, corresponding to the tropical cyclone season, which included ex-tropical cyclone Wilma. Otherwise, the largest storm

surges occurred during winter, especially in June through August. A frequency count of the top 5 storm surges each month reveals mostly a uniform distribution of large storm surges across all months, but with a spike in frequencies during June and July. July records 19 of the largest storm surges, June records 11, while every other month records 8 or less.

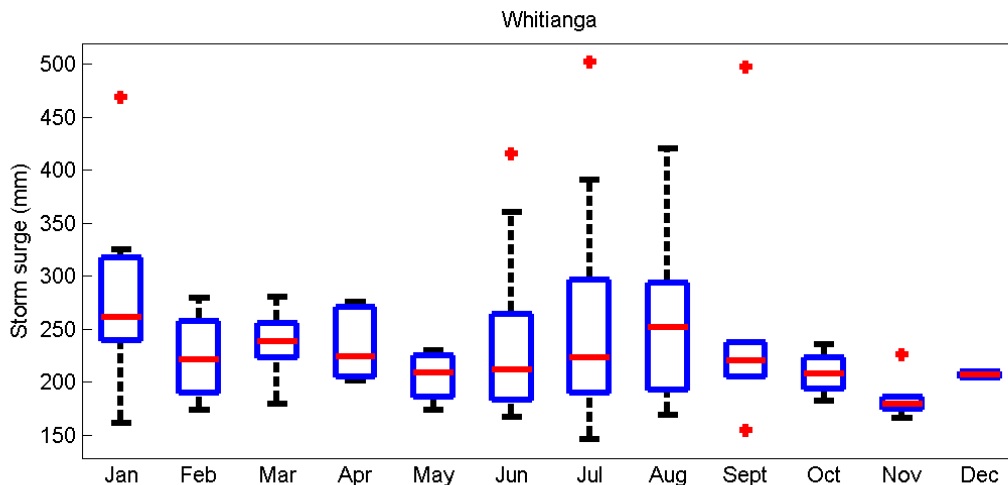


Figure 6-14: Monthly boxplot of the 5 largest storm surge events per year at Whitianga. Median (red line), top and bottom of boxes represent 3rd and 1st quartiles respectively. Maximum and minimum (excluding outliers) (black lines), outliers (red dots) correspond to values greater than $Q3 + 1.5(Q3-Q1)$ or less than $Q1 - 1.5(Q3-Q1)$.

Cyclone Pam

Ex-tropical cyclone Pam passed offshore from Whitianga on 16 March 2015. Cyclone Pam was an energetic event that brought strong winds, heavy rainfall and large waves to the Whitianga region. Since the event lies outside the gauge record analysed in this report, WRC requested a brief comment on the significance of cyclone Pam against the otherwise-analysed sea-level record. Figure 6-15 shows the measured sea level (at 1-minute intervals) and the various components of sea level as cyclone Pam passed by. There is some high-frequency seiche of approximately 5-minute period within the harbour, with a maximum amplitude of about 0.4 m. This peaked close to low tide. The storm surge (SS) peaked an hour or two before low tide at 0.33 m, which has an ARI of less than 2 years (Table 6-1). The storm surge at the time of the nearest high-tide peak was several cm lower. The total storm tide elevation reached during cyclone Pam was unremarkable, with several larger peaks occurring during 2014 alone.

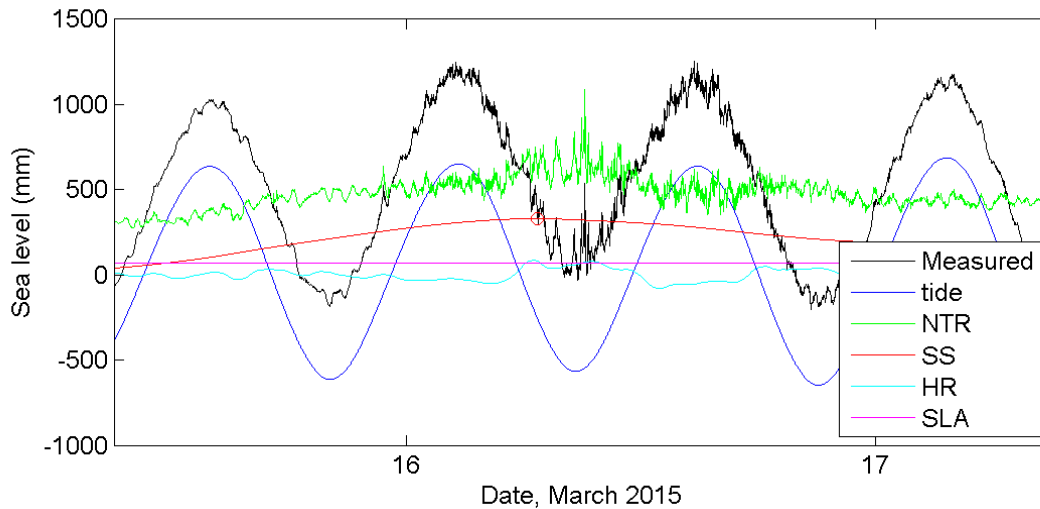


Figure 6-15: Sea level at Whitianga during Cyclone Pam. The measured data and NTR are shown relative to MVD-53; all other sea-level components are shown relative to MSL = 0. NTR = non-tidal residual; SS = storm surge, HF = high-frequency energy with periods of motion 3-12 hours; SLA = sea-level anomaly.

Summary of storm surge analysis for Whitianga

The largest storm surges at Whitianga occur during compact intense low-pressure systems, often ex-tropical cyclones that move down the northeast coast of the north island. The inverse-barometer component, or MSLP, is responsible for most of the storm surge. However, due to the cyclonic nature of these storms, the strongest onshore winds precede the peak in IB, raising the storm surge above the IB and causing the peak storm surge to occur 2–3 hours before the IB peak. The largest storm surges in the record are 0.4–0.5 m. Extreme storm surge analyses indicate that 1% annual exceedance probability storm surges have a maximum likelihood of about 0.65 m (Section 7).

6.2.2 Tararu

The largest five storm events at Tararu are summarised in Table 6-4. As is the case for Whitianga, 3 out of 5 of the largest storm surges occur during winter. However, with the exception of the 21 August 2003 event, the storm surge events are different. MSLP data for Tararu was provided by NIWA after February 1997. Before February 1997, MSLP was obtained from a weather station at Paeroa which is 31 km away from the Tararu gauge. An offset of -1.2 hPa was added to the Paeroa data to match the overlapping NIWA record. Figure 6-16 shows the storm surge and IB for Tararu during 2013, which is when the highest storm surge occurred. Both the storm surge and IB rise and fall in unison.

A cross correlation analysis reveals a peak correlation of 0.75 between the IB sea level and storm surges with an average lag of 3 hours for the entire sea level record (Figure 6-27). The barometric factor obtained with a 3 hour lag is 0.7.

A correlation of 0.75 means that 75% of the variability in storm surge is explained by inverted barometer, on average. Thus 25% of variability is explained by other factors such as wind setup. The barometric factor obtained with a 3 hour lag was 0.7; in other words, the inverse-barometer sea-level is generally 70% of the measured storm-surge height. It is important to note that the cross-correlation analysis includes all storm-surge data, but the below analysis of the largest 5 storm surges

shows that the largest storm surges appear to be driven by wind blowing along the Firth of Thames and that inverse-barometer plays a relatively minor role.

Table 6-4: The top five storm surges on record at Tararu.

Date	Storm surge (mm)	Lowest barometric pressure (hPa)	Maximum expected IB Remaining wind setup sea level (mm)	Remaining wind setup component (mm)
12-Jun-2006	970	990	173	797
06-Sep-1995	721	987	197	524
31-Aug-2009	640	997	126	514
21-Oct-1998	639	989	179	460
21-Aug-2003	582	984	214	368

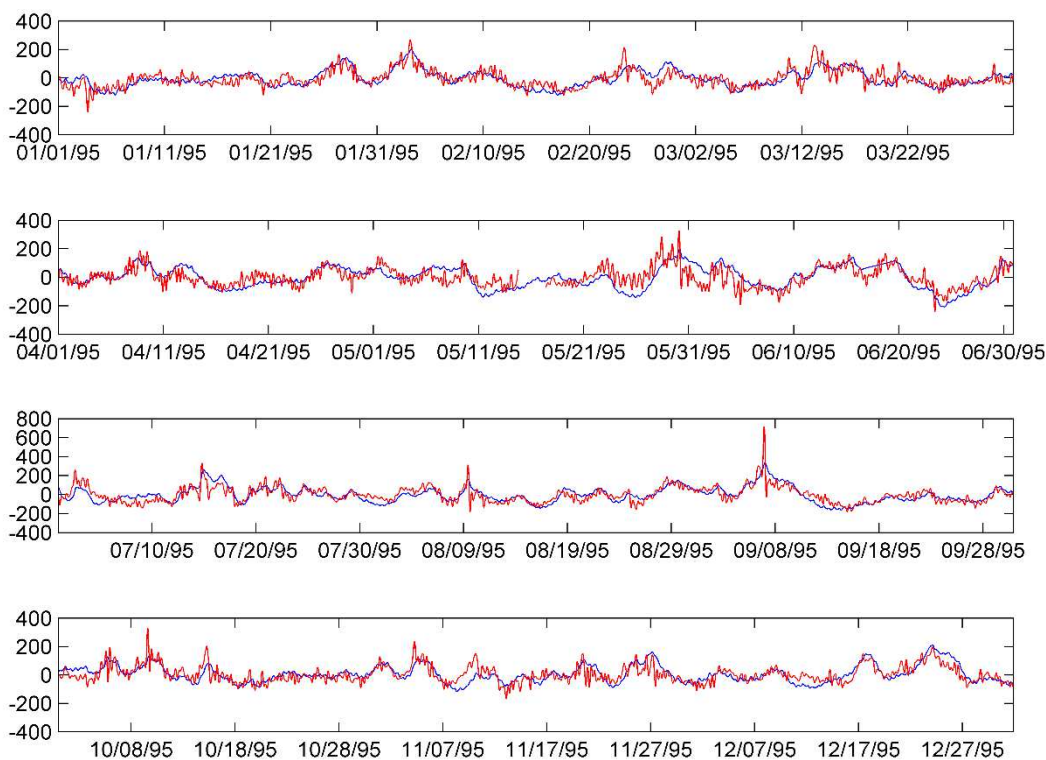


Figure 6-16: Storm surge (red line) and inverted barometer (blue line) at Tararu for 1995, in mm above gauge zero. Records are divided into 3 month periods with Jan-Mar (top), Apr-Jun (2nd from top), Jul-Sep (2nd from bottom) and Oct-Dec (bottom). Largest storm-surge for this year observed as spike in September.

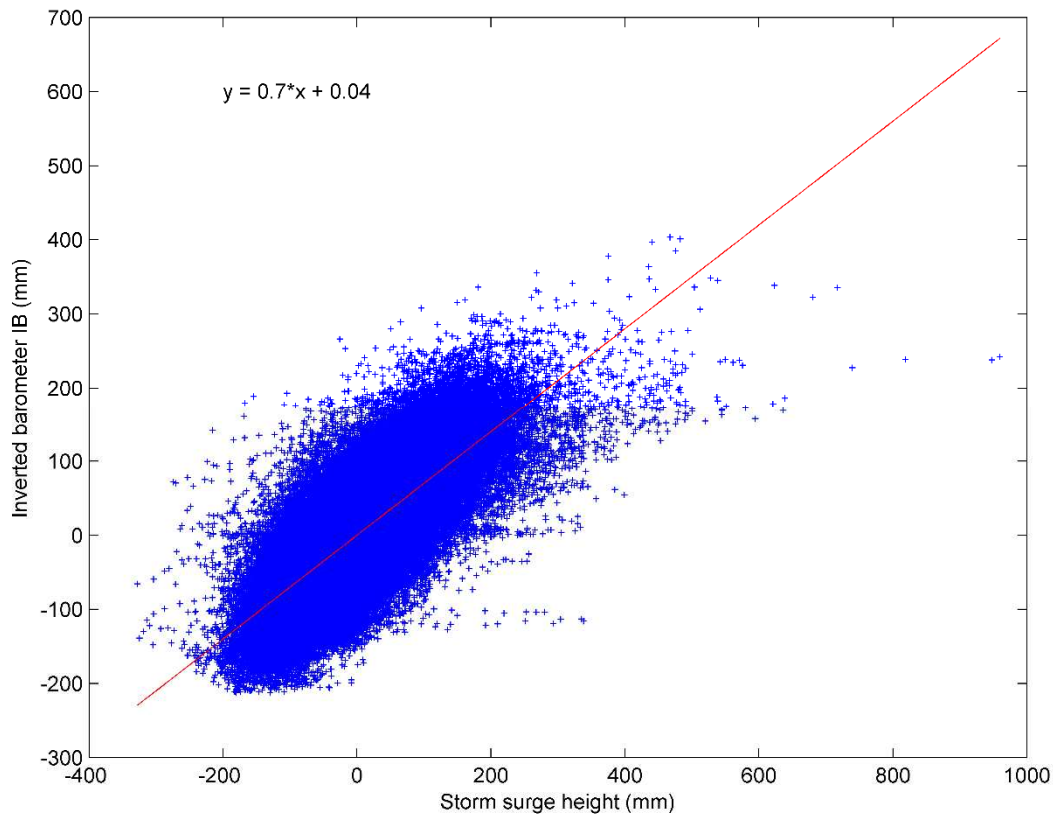


Figure 6-17: Variability of storm surge height relative to the inverted barometer (IB) height for Tararu. A 3 hour time lag was applied to the IB height, shifting it back three hours. The barometric factor for the best-fit linear regression line is 0.7 and the correlation coefficient is 0.75.

12 June 2006 storm

From 11-13th June 2006, a severe snowstorm brought snow down to sea level in Canterbury, and caused approximately 40 million dollars of insurance costs on the South Island. At that time, it was the third most expensive weather event, and caused temperatures to be the lowest in the South Island in 35 to 50 years. This snowstorm was the result of a rapidly deepening depression moving from the Tasman Sea south-eastward across New Zealand, with a strong moist north-westerly air stream ahead and a very cold southerly airflow behind. The very cold air undercutting the front from the southwest meant that the precipitation fell as snow rather than rain.

The cold front associated with this depression crossed the North Island by the 12th June, and brought heavy rain, with severe and damaging north-westerly gales to many areas. Wind data from Tararu shows high wind speeds up to 23 m.s⁻¹ coming from an N-NW direction around the time of the storm surge peak (1000 hours 12th June), Figure 6-18. During this storm, the storm surge peaked three hours ahead of the IB. The strong winds, compounded by a sudden drop in barometric pressure (1025 down to 990 hPa in 24 hours) contributed to a very large storm surge at Tararu. With only 250 mm of expected inverse-barometer sea-level, wind blowing down the Firth appears to have been responsible for most of the 970 mm of storm surge. The north-south orientation of the Firth of Thames, combined with winds from an N-NW direction would have enhanced the storm surge, and probably caused the peak in storm surge before IB at Tararu. Figure 6-19 shows the weather situation at 0900 hours, 12 June 2006.

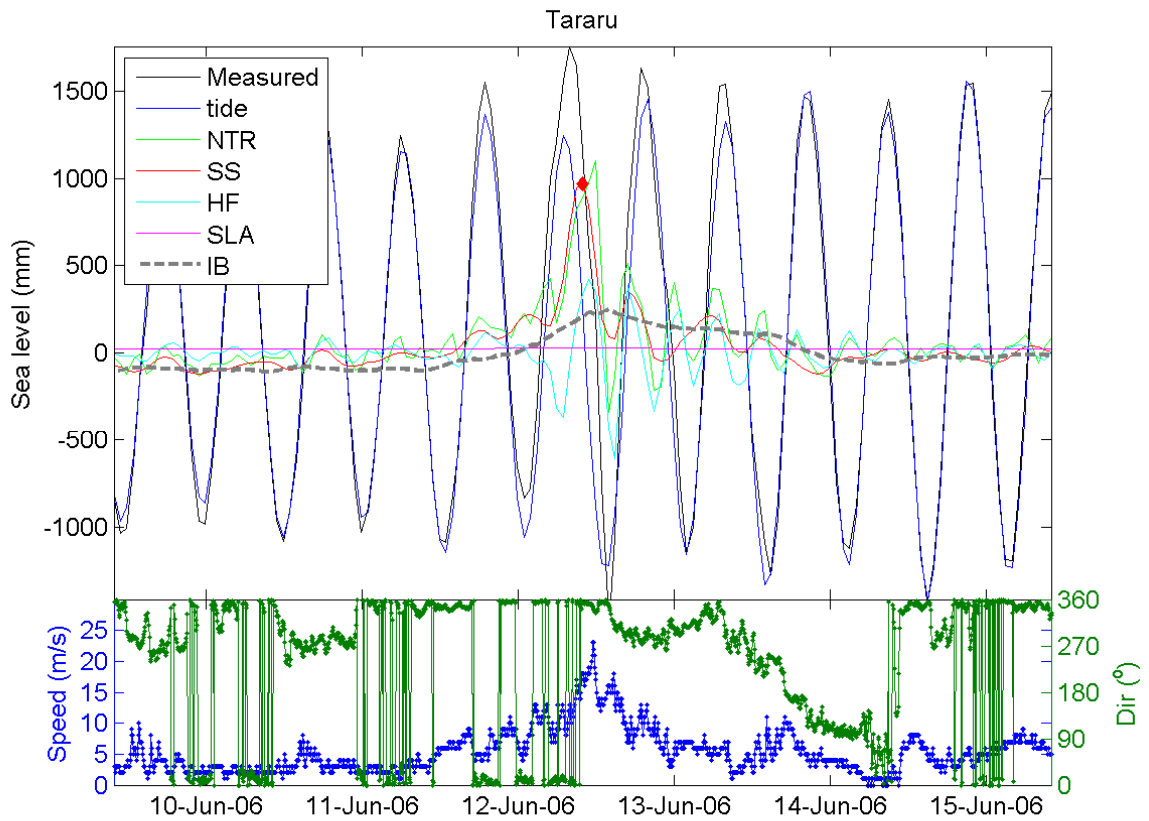


Figure 6-18: Measured sea level and its components during 12 Jun 2006 storm surge at Tararu. NTR = non-tidal residual; SS = storm surge; HF = high-frequency sea-level; SLA = sea-level anomaly; IB = inverse barometer. Inverse barometer and wind data was sourced from Tararu.

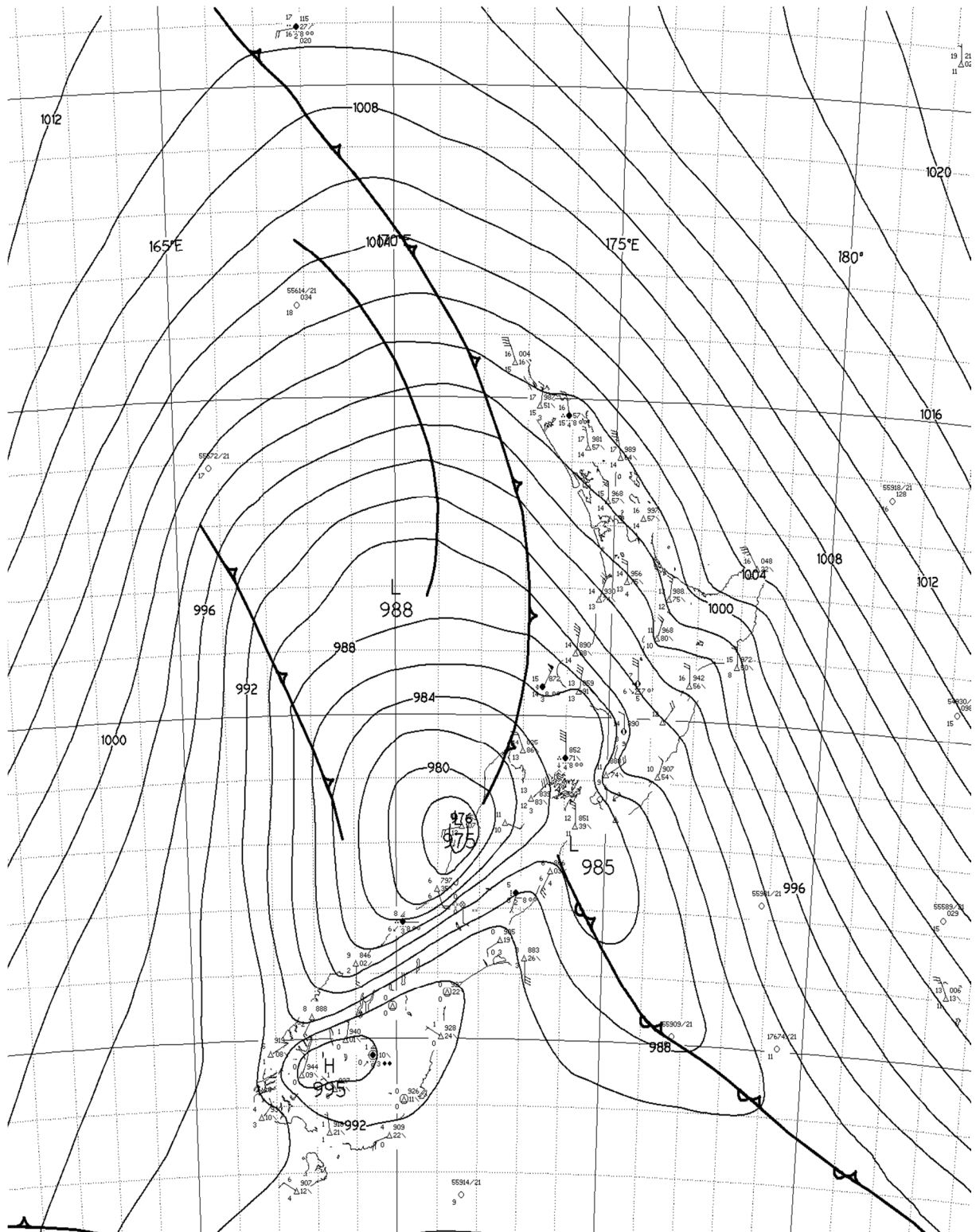


Figure 6-19: Mean sea level pressure map at 0900 hrs, 12 June 2006 around the time of the largest measured storm surge (970 mm) at Tararu.

6 September 1995 storm

Apart from barometric pressure and wind readings, little is known about how this storm event affected the North Island. There were two days of snowfall on the South Island from 6th to 7th September, which was classified as an event with an average recurrence interval of 20 years. Peak IB occurred around midnight on 7 September 1995, approximately 90 minutes after the peak storm surge at Tararu. The peak hourly wind speeds were up to $14.4\text{m}\cdot\text{s}^{-1}$ which is moderately strong, and mostly from a NW-NE direction. These winds would cause water to pile up against the Firth of Thames coastline, and enhance storm surge there. Barometric pressure dropped from around 1010 hPa during the 5th September down to 987 hPa during the peak storm-surge (28 cm of expected IB sea level).

From the information supplied, it appears that this storm was a deep depression which brought cold southerly weather (and fronts) over the South Island, followed by the North Island. If this was the case, it would be a similar weather system to the June 2006 storm, albeit less severe.

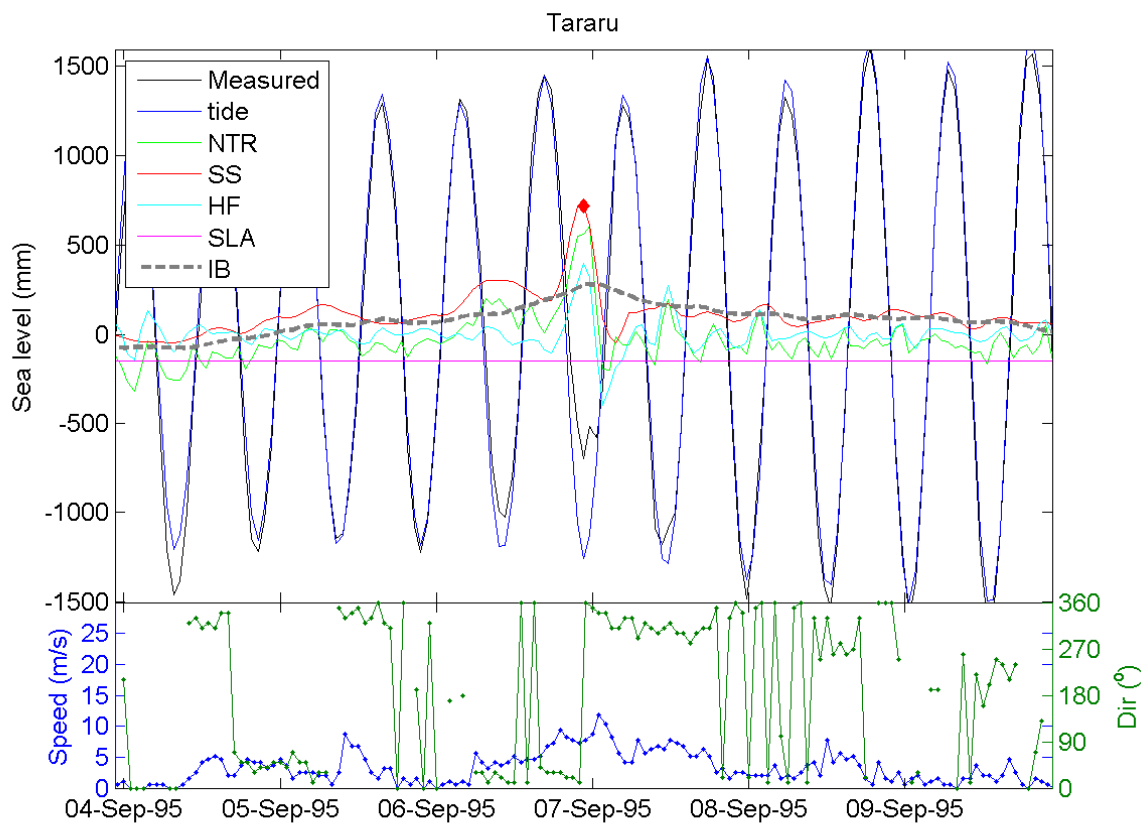


Figure 6-20: Measured sea level and its components during 6 Sep 1995 storm surge at Tararu. NTR = non-tidal residual; SS = storm surge; HF = high-frequency sea-level; SLA = sea-level anomaly; IB = inverse barometer. Inverse barometer was sourced from Tararu, while wind was sourced from Paeroa.

31 August 2009 storm

From 30th August to 1st September a deep low southwest of New Zealand sent a series of cold fronts over New Zealand from the Tasman Sea. As the low pressure system moved east, the fronts brought high winds and heavy rain due to a high air pressure gradient across the fronts. Figure 6-22 shows the weather situation at midnight 31 August 2009, 55 minutes before the peak storm surge was recorded. Note the closely spaced isobars and series of cold fronts that have just passed through. Wind data from Tararu reveals a peak hourly wind speed of 21 m.s⁻¹ around the time of maximum storm surge. The wind blew consistently from the north during the storm surge build up and at its peak, before turning northwest. IB peaked at 12.6 cm two hours after maximum storm surge.

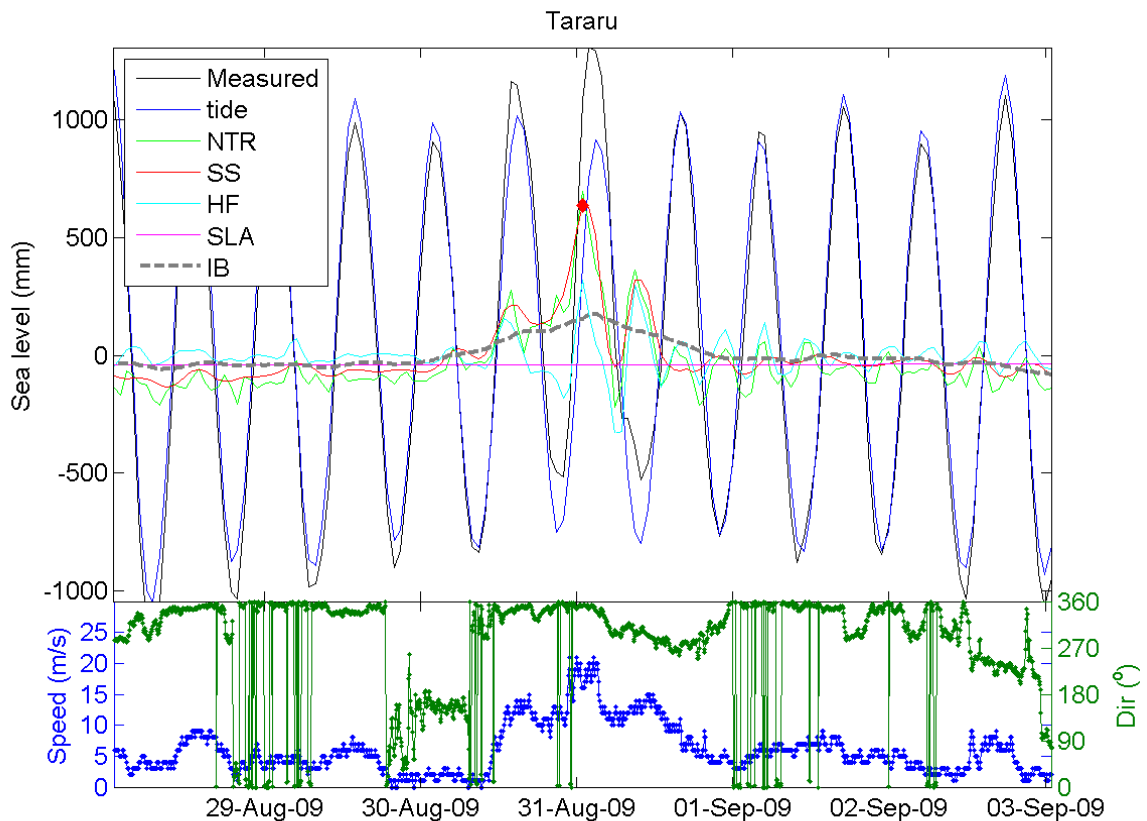


Figure 6-21: Measured sea level and its components during 31 Aug 2009 storm surge at Tararu. NTR = non-tidal residual; SS = storm surge; HF = high-frequency sea-level; SLA = sea-level anomaly; IB = inverse barometer. Inverse barometer and wind data was sourced from Tararu.

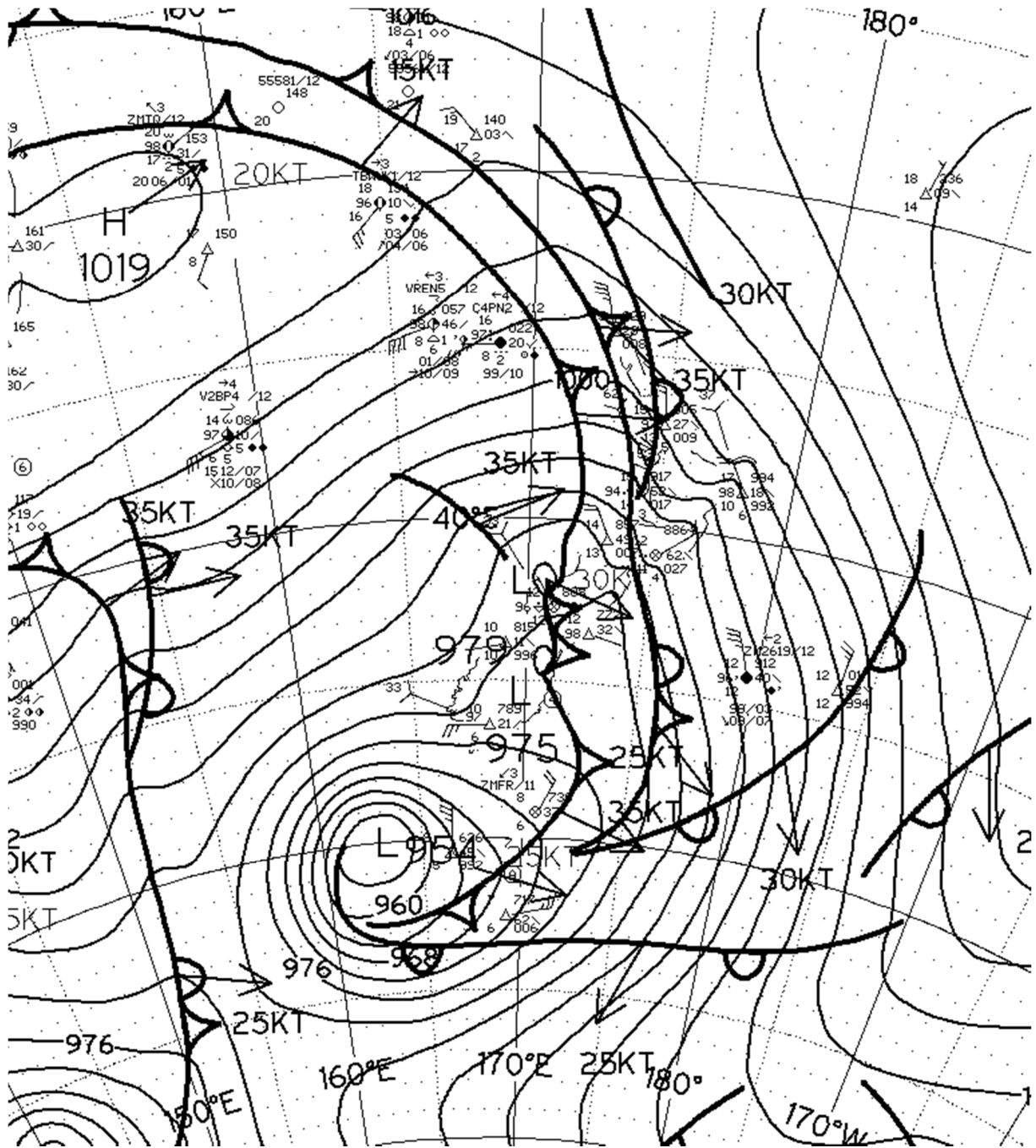


Figure 6-22: Mean sea level pressure map at midnight, 31 August 2009 around the time of the third largest measured storm surge (640 mm) at Tararu.

21 October 1998 storm

On the 18th October 1998, a broad active trough moved into the Tasman Sea, and a very strong NW pressure gradient built up over the South Island, bringing gales to eastern South Island districts. By the 20th October, a slow moving cold front associated with this trough moved onto the southern North Island. This front became occluded and very active while it brought rain over a broad area from Taranaki to Wellington. Analysis of storm surge and MSLP at Tararu reveals zero lag between the IB and storm surge, which peaked around 0100 hours on the 21 October 1998. From the 19th October to the storm surge peak, barometric pressure gradually decreased from 1015 down to 989 hPa (26 cm of expected IB sea level) while wind speed increased, with a maximum hourly wind speed of 12.4 m.s⁻¹. Recorded wind gusts at the Coromandel would have been much higher however, as northerly gales blew boats off their moorings there.

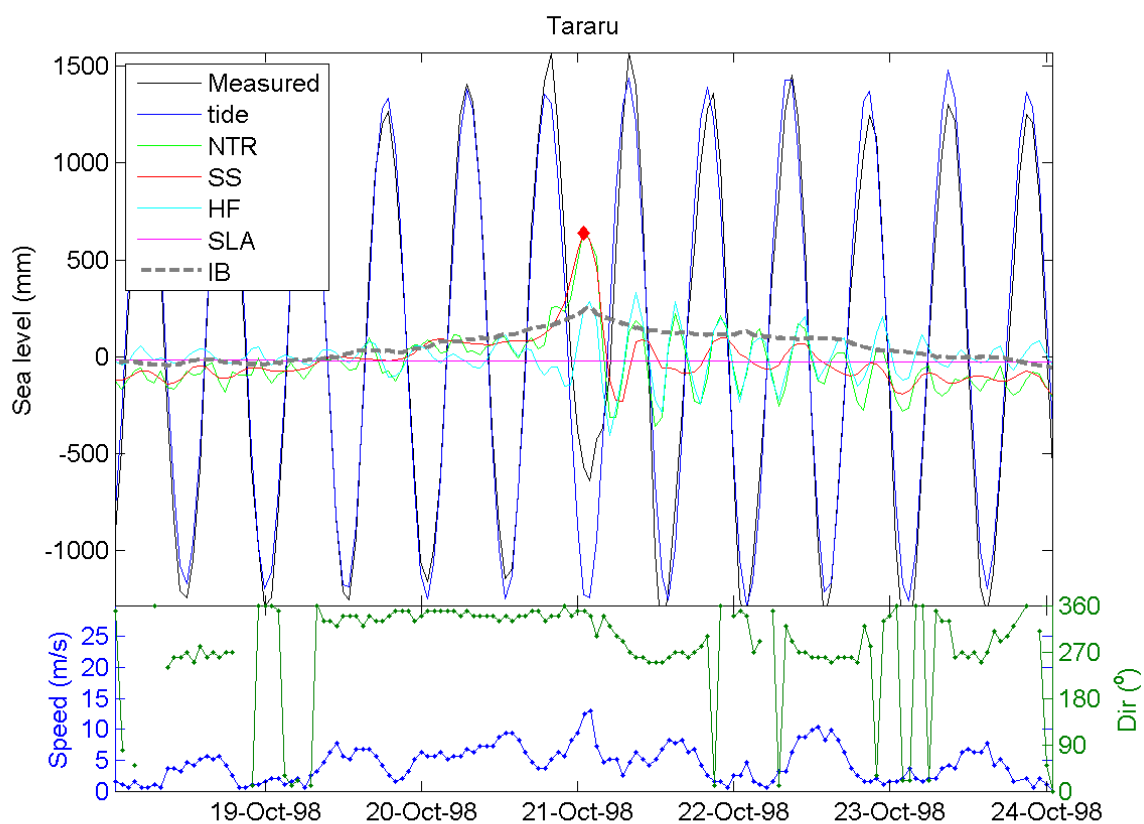


Figure 6-23: Measured sea level and its components during 21 Oct 1998 storm surge at Tararu. NTR = non-tidal residual; SS = storm surge; HF = high-frequency sea-level; SLA = sea-level anomaly; IB = inverse barometer. Inverse barometer was sourced from Tararu, while wind was sourced from Paeroa.

21 August 2003 storm

This storm event was also recorded at Whitianga. Refer to Section 6.2.1 for a description of the weather event and Figure 6-12 for a map of the weather situation. Tararu recorded a larger storm surge of 582 mm compared with only 446 mm at Whitianga. While the air pressure difference between the two sites was small, the northerly winds recorded during the storm surge peak would have enhanced the storm surge at Tararu (Figure 6-24). So the difference in geography of both sites is the probable cause for the different storm surge sizes. When comparing the IB at Whitianga and Tararu for this event, the expected IB here only accounts for 37% of the total storm surge, compared with 56% at Whitianga, so the storm surge at Tararu had a larger wind-driven component. The storm surge peaked a couple of hours after wind speed peaked at 19 m s^{-1} .

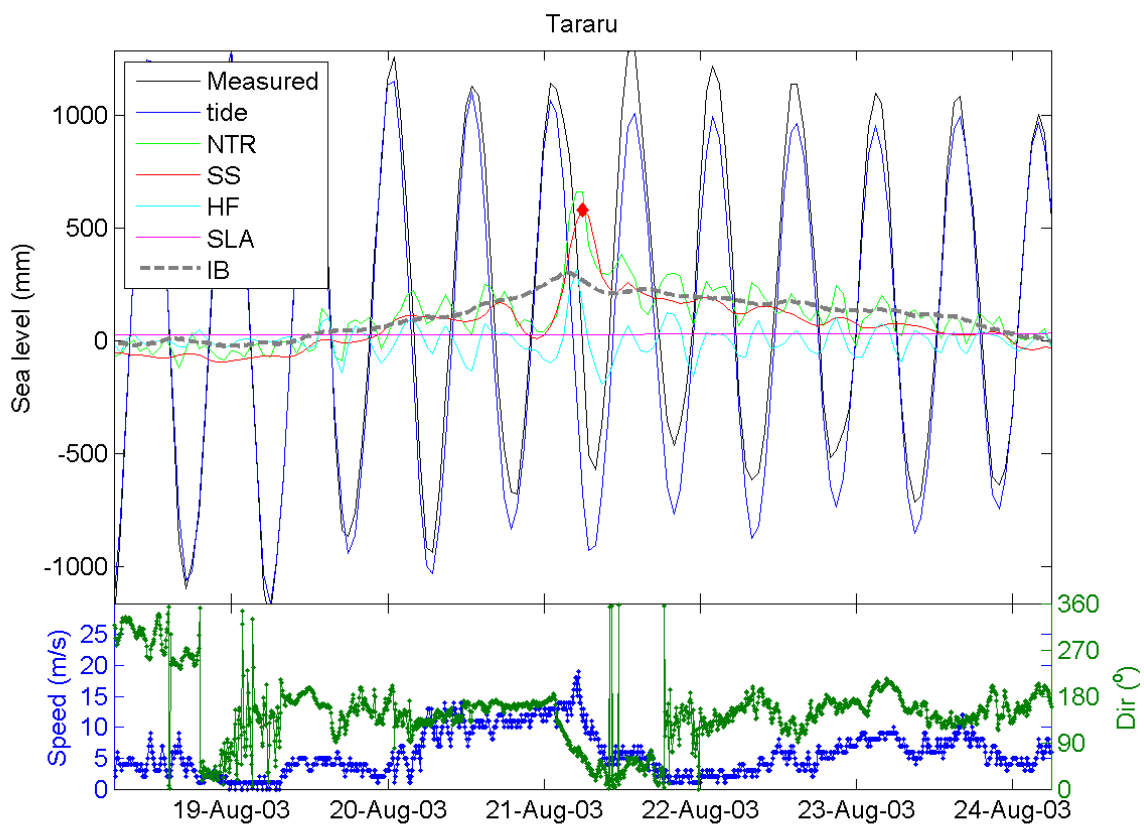


Figure 6-24: Measured sea level and its components during 21 Aug 2003 storm surge at Tararu. NTR = non-tidal residual; SS = storm surge; HF = high-frequency sea-level; SLA = sea-level anomaly; IB = inverse barometer. Inverse barometer and wind data was sourced from Tararu.

Seasonality of storm surges

At Tararu, a monthly boxplot was constructed for the 5 largest storm surge events each year to highlight any seasonality in storm surge hazard (Figure 6-25). With a sea-level record close to 25 years, storm surge seasonality should be more robustly defined than at Kawhia or Whitianga. Storm surges larger than 500 mm occur from late autumn to late spring, with August to October being particularly stormy and the summer months being more quiescent. A frequency count of the top 5 storm surges each month reveals that months May to November have the most storm surges (11-15), with October having the most (15), followed by May and July (14). From November to April, the

frequency of largest storm surges drops off, with large storm surges varying from 6-8 each month. Figure 6-25 contrasts with the similar plot from Whitianga (Figure 6-14). Whereas Whitianga has numerous surges driven by late-summer ex-tropical cyclones, large storm surges at Tararu are driven more by late-winter storm systems, which drive wind southward into the enclosed Firth of Thames. In contrast to Whitianga, there are an absence of late-summer ex-tropical cyclones at Tararu.

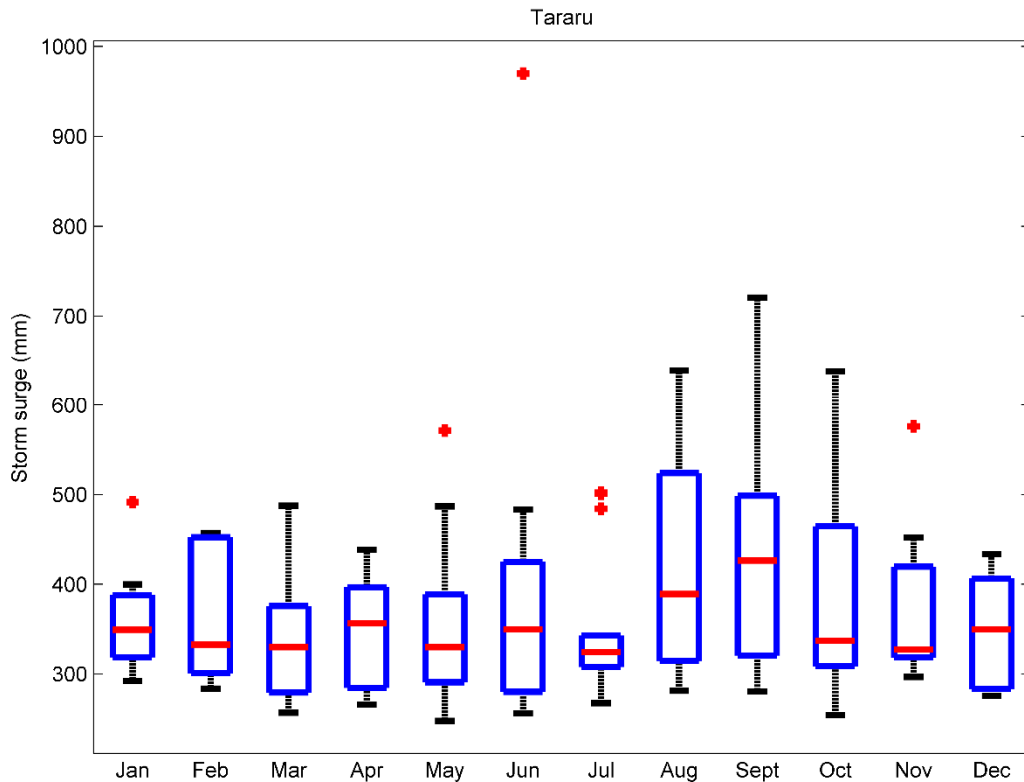


Figure 6-25: Monthly boxplot of the 5 largest storm surge events per year at Tararu. Median (red line), top and bottom of boxes represent 3rd and 1st quartiles respectively. Maximum and minimum (excluding outliers) (black lines), outliers (red dots) correspond to values greater than $Q3 + 1.5(Q3-Q1)$ or less than $Q1 - 1.5(Q3-Q1)$.

Summary of storm surge analysis for Tararu

The largest storm surges at Tararu are driven by wind stress, with a relatively small IB component, although IB is more important than at Kawhia (Section 6.2.3). The large storm surges are observed when low-pressure troughs pass over the north island causing strong wind speeds from the northwest, sustained over several hours. These winds blow southward into the enclosed Firth of Thames, causing the surge to pile up along the southern Firth shoreline. These weather systems are larger in scale and slower moving than the cyclones that are responsible for large surges at Whitianga. Extreme storm surge analyses indicate that 1% AEP storm surges have a maximum likelihood of about 1 m – as discussed in Section 6.1.

6.2.3 Kawhia

The largest three storm events at Kawhia are summarised in Table 6-5. Storm surges at Kawhia appear to be significantly larger than at Whitianga, despite only a 6-year long record. It would appear likely that storm surges larger than 900 mm have occurred here, although it is possible that the record captures a particularly energetic 5 years. MSLP data for Kawhia was provided by NIWA after

June 2010. Before June 2010, MSLP is provided from Port Taharoa which is 15 km away from the Kawhia gauge. An offset of -3.4 hPa was added to the Port Taharoa data, to match the overlapping portion of the NIWA record. Figure 6-26 shows the storm surge and IB for Kawhia during 2013, which is when the highest storm surge occurred. Both the storm surge and IB rise and fall in unison, however there is often a lag between the two, with IB peaking before storm surges, such as during the May 2013 storm and during October 2013. Table 6-5 and Figure 6-26 show that the largest storm surges contain a substantial non-IB component.

A cross correlation analysis reveals a peak correlation of 0.73 between the IB effect and storm surges with an average lag of -2 hours for the entire sea level record (Figure 6-27). A correlation of 0.73 means that 73% of the storm surge height is explained by inverted barometer on average. The barometric factor obtained with a -2 hour lag is 0.48, which is a lot smaller than the 0.83 found at Whitianga. This means that inverse-barometer sea level generally only reaches half the measured storm-surge, so other processes such as wind setup must be important in Kawhia.

Table 6-5: The top three storm surges on record at Kawhia.

Date	Storm surge (mm)	Lowest barometric pressure (hPa)	Maximum expected IB sea level (mm)	Remaining wind setup component (mm)
06-May-2013	899	985	143	756
26-May-2010	815	982	160	655
11-Sep-2008	707	994	99	608

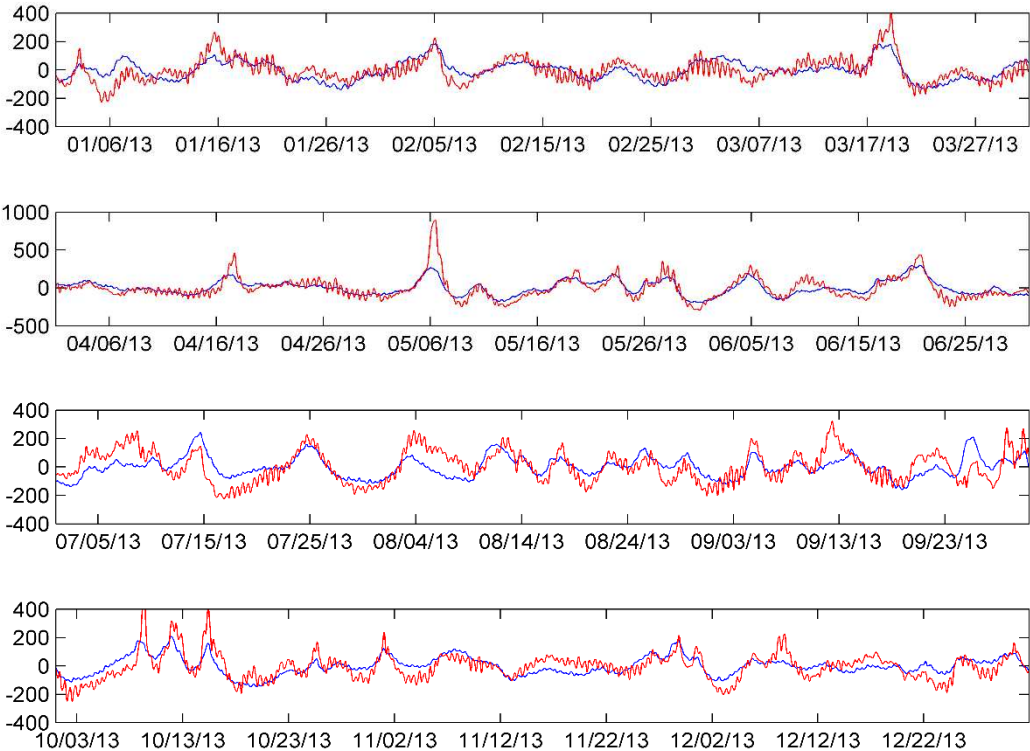


Figure 6-26: Storm surge (red line) and inverted barometer (blue line) at Kawhia for 2013, in mm above gauge zero. Records divided into 3 month periods with Jan-Mar (top), Apr-Jun (2nd from top), Jul-Sep (2nd from bottom) and Oct-Dec (bottom). Largest storm-surge for this year observed as spike in May

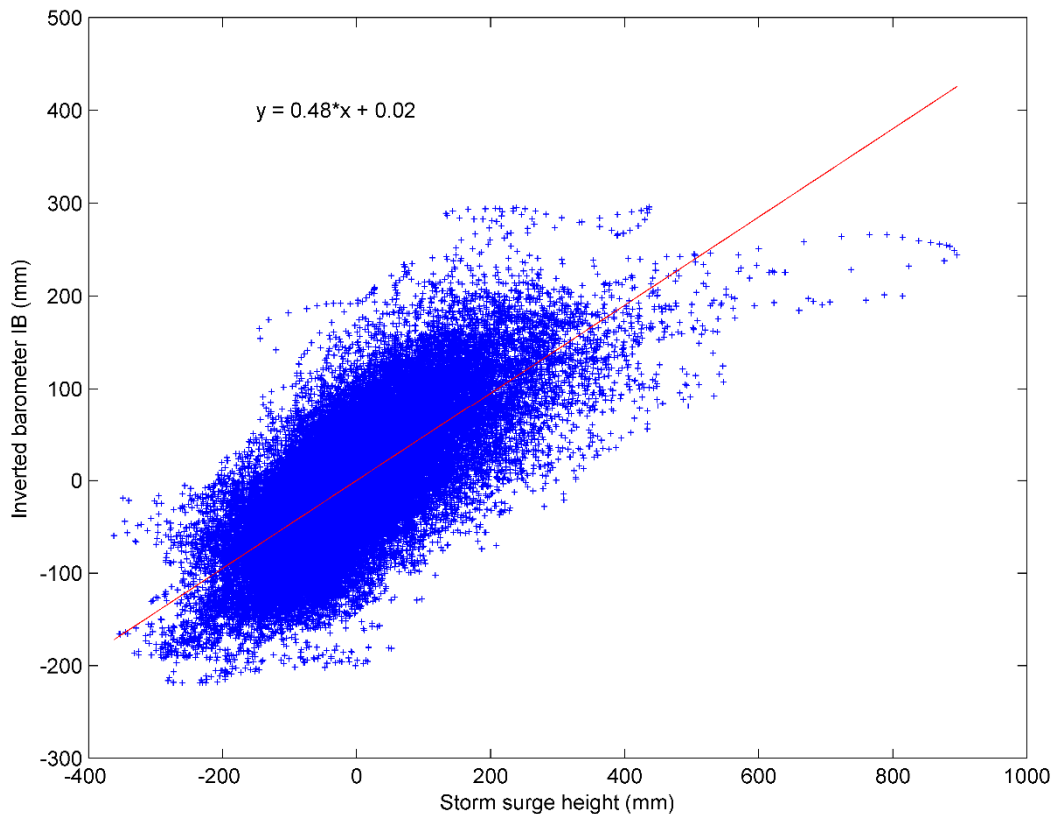


Figure 6-27: Variability of storm surge height relative to the inverted barometer (IB) height for Kawhia. A - 2 hour time lag was applied to the IB height, shifting it forward two hours. The barometric factor for the best-fit linear regression line is 0.48 and the correlation coefficient is 0.73.

6 May 2013 storm

This storm lasted approximately three days from the 4th to the 6th May. During the 4th, a low to the west of Northland was strengthened by an advancing trough moving in from the south Tasman Sea. A warm north-easterly flow covered New Zealand. Overnight on the 4th, the trough moved onto the South Island and combined with the low to create a much deeper low pressure system centred to the west of central New Zealand during the 5th. This system brought heavy falls of rain and thunderstorms to northern and western areas, with gale force NW winds in exposed areas. By the 6th May, this low moved onto the North Island.

Analysis of IB and storm surge data revealed a 10-11 hour lag between storm surge and IB at Kawhia (Figure 6-28). IB peaked at 278 hPa (14.3 cm of expected IB sea level) midnight on 5–6th May while storm surge continued to rise until 1046 hours 6th May, with a peak of 899 mm. The position of the low, westward of the North Island, combined with high wind speeds from the NW over a duration of several hours, would have been responsible for the high storm surge at Kawhia. Figure 6-29 shows the weather situation at 1200 hours, 6 May 2013.

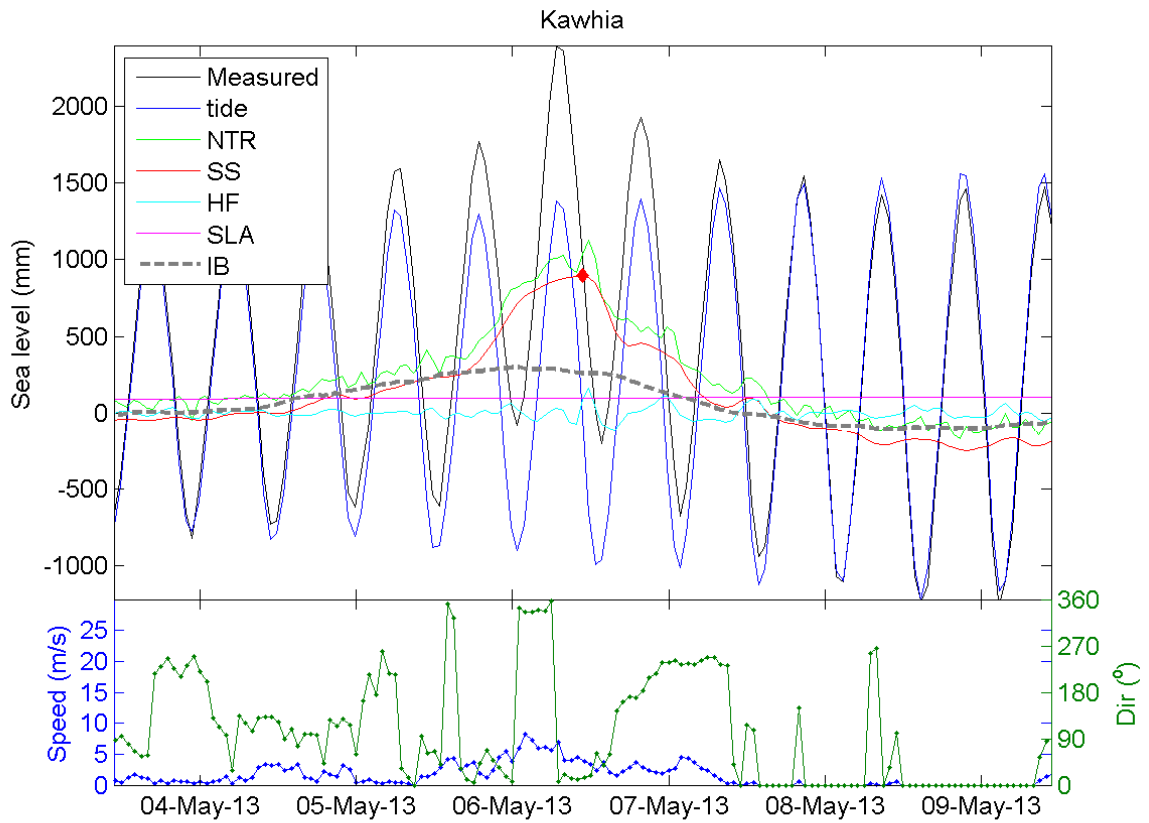


Figure 6-28: Measured sea level and its components during 6 May 2008 storm surge at Kawhia. NTR = non-tidal residual; SS = storm surge; HF = high-frequency sea-level; SLA = sea-level anomaly; IB = inverse barometer. Inverse barometer is based on MSLP measured at Kawhia, but wind data was sourced from Whatawhata, and is unlikely to represent the local situation well.

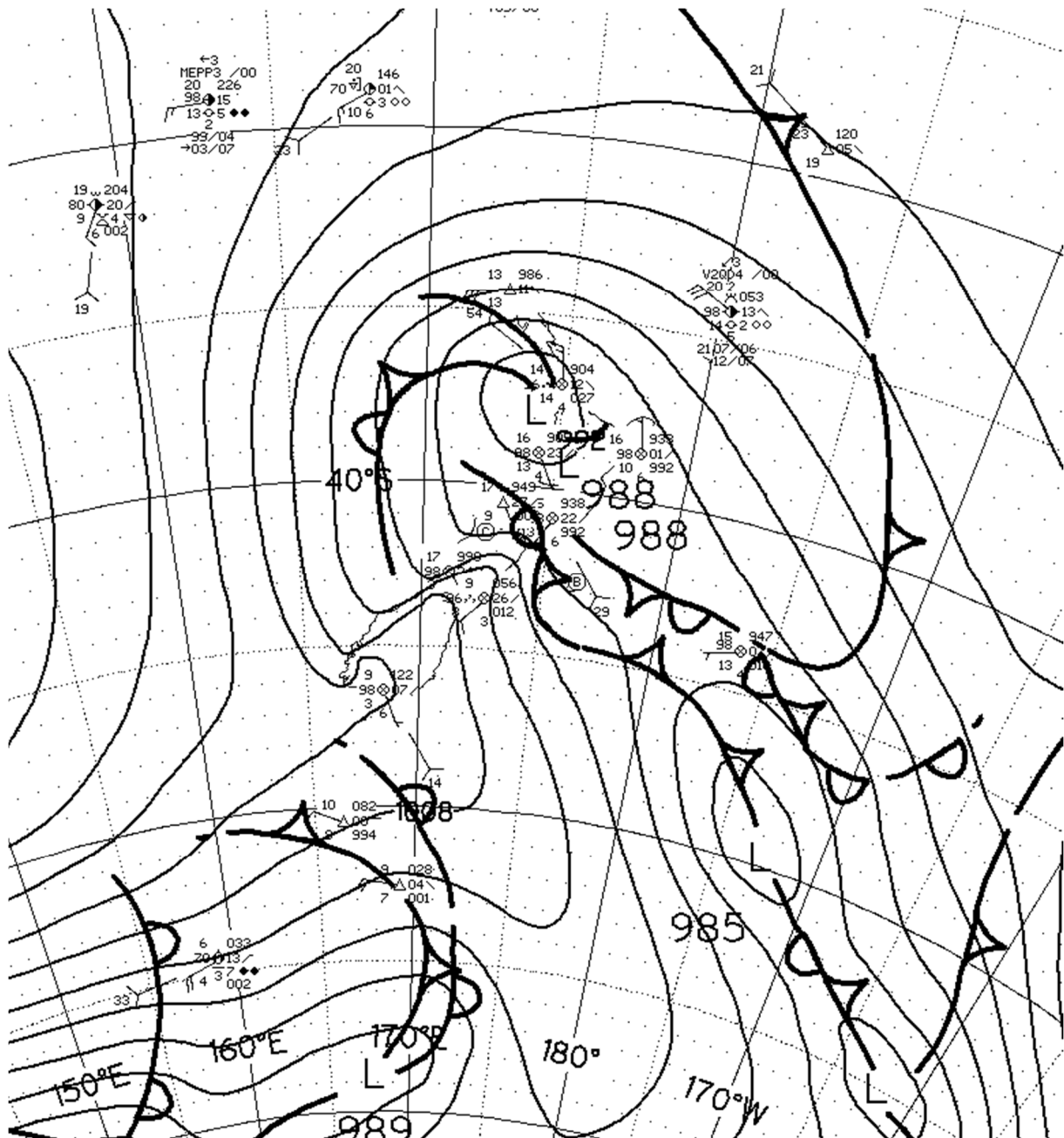


Figure 6-29: Mean sea level pressure at 1200 hours, 6 May 2013 around the time of the largest measured storm surge (889 mm) at Kawhia.

26 May 2010 storm

This storm lasted several days, affecting New Zealand from May 24 to May 30 2010. A front carrying heavy rain moved down the North Island on the 24th May. This front was pinned in place by a low pressure system over the Tasman Sea. Weather maps show a series of fronts, both cold and occluded, crossing the North Island from the Tasman Sea on the 24th May. The low pressure system in the Tasman followed the path of the fronts and made landfall on the 25th May. After the 25th May, the low pressure system moved SE across New Zealand. Figure 6-31 shows the weather situation at midnight 26 May 2010.

Analysis of storm surge and IB data at Kawhia revealed the lowest barometric pressure of 982 hPa (33 cm of expected IB sea-level) at 2100 hours 25 May 2010. Wind speeds and storm surge continued to rise until midnight, with a peak hourly wind speed of 19.7 m.s⁻¹ at Taharoa, and a peak storm surge of 815 mm (Figure 6-30).

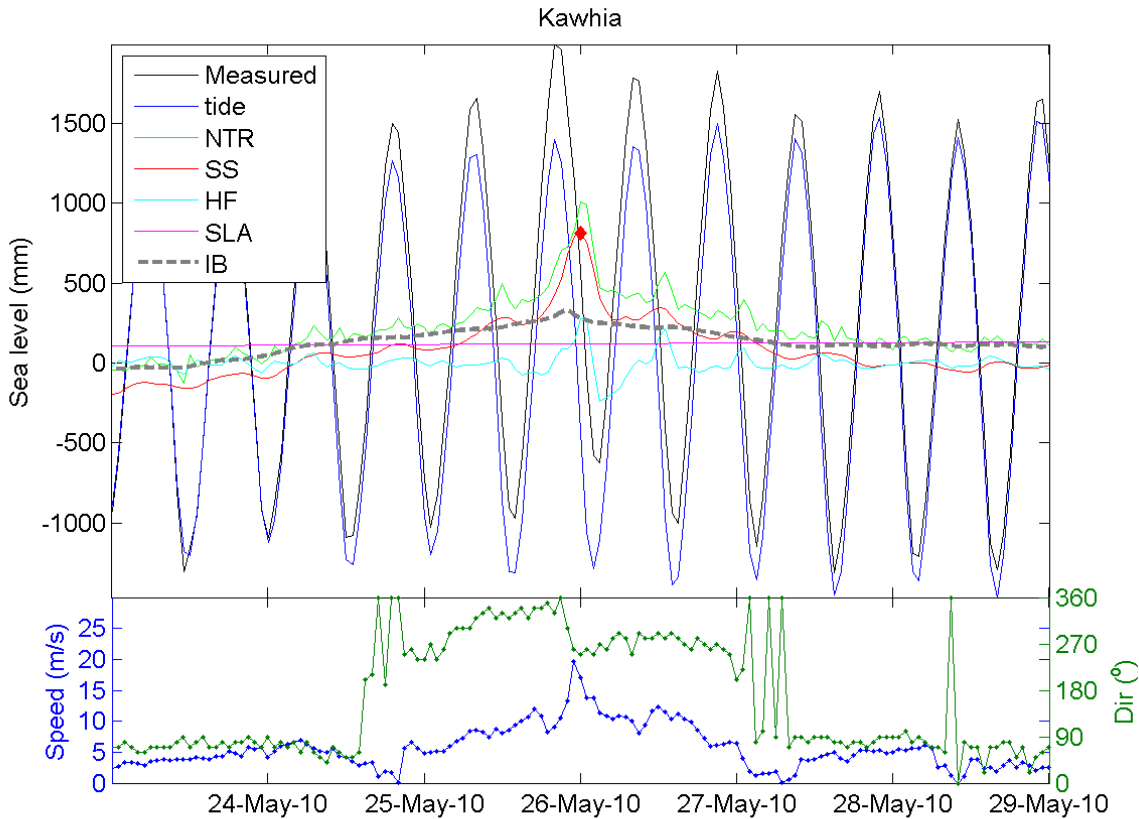


Figure 6-30: Measured sea level and its components during 26 May 2010 storm surge at Kawhia. NTR = non-tidal residual; SS = storm surge; HF = high-frequency sea-level; SLA = sea-level anomaly; IB = inverse barometer. Inverse barometer and wind were measure at Taharoa.

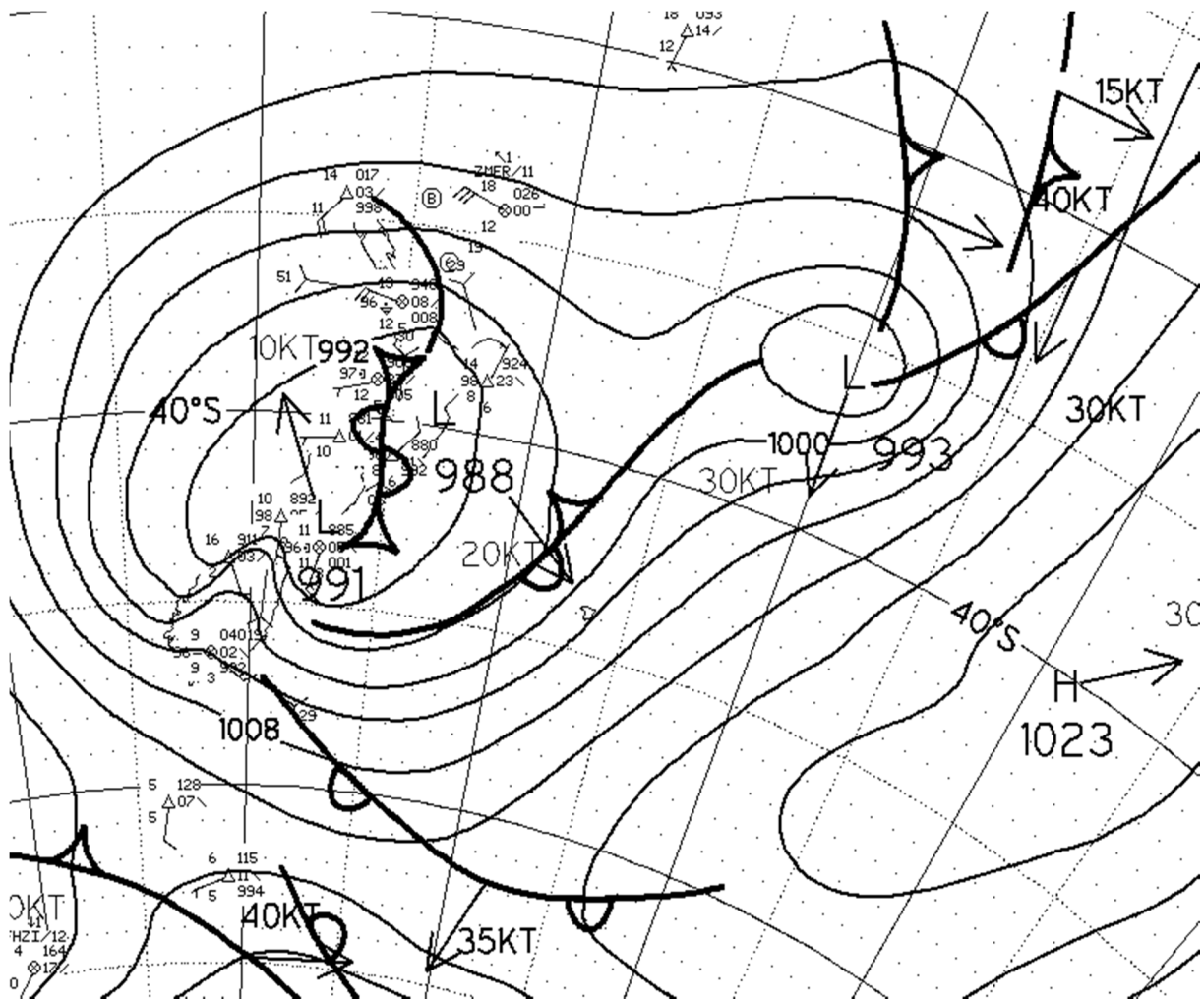


Figure 6-31: Mean sea level pressure at midnight, 26 May 2010 around the time of the second largest measured storm surge (815 mm) at Kawhia.

11 September 2008 storm

On the 10th September 2008, a low pressure system in the Tasman Sea began to move towards New Zealand with an occluded front on the N-NE part of the low. By the 11th September, this low merged with another low to become complex, having three troughs. Around the time of peak storm surge, a trough of low pressure reached from Auckland, over the Tasman Sea to Greymouth on the South Island (Figure 6-33).

Analysis of IB and storm surge data at Kawhia shows a peak IB of 228 hPa (9.9 cm of expected sea-level rise) at 0700 hours 11 September 2008, which is 3 hours before the peak storm surge at 1000 of 707 mm. During the time of peak storm surge, the wind approached from N-NW and peaked at 12.9 m/s at Taharoa.

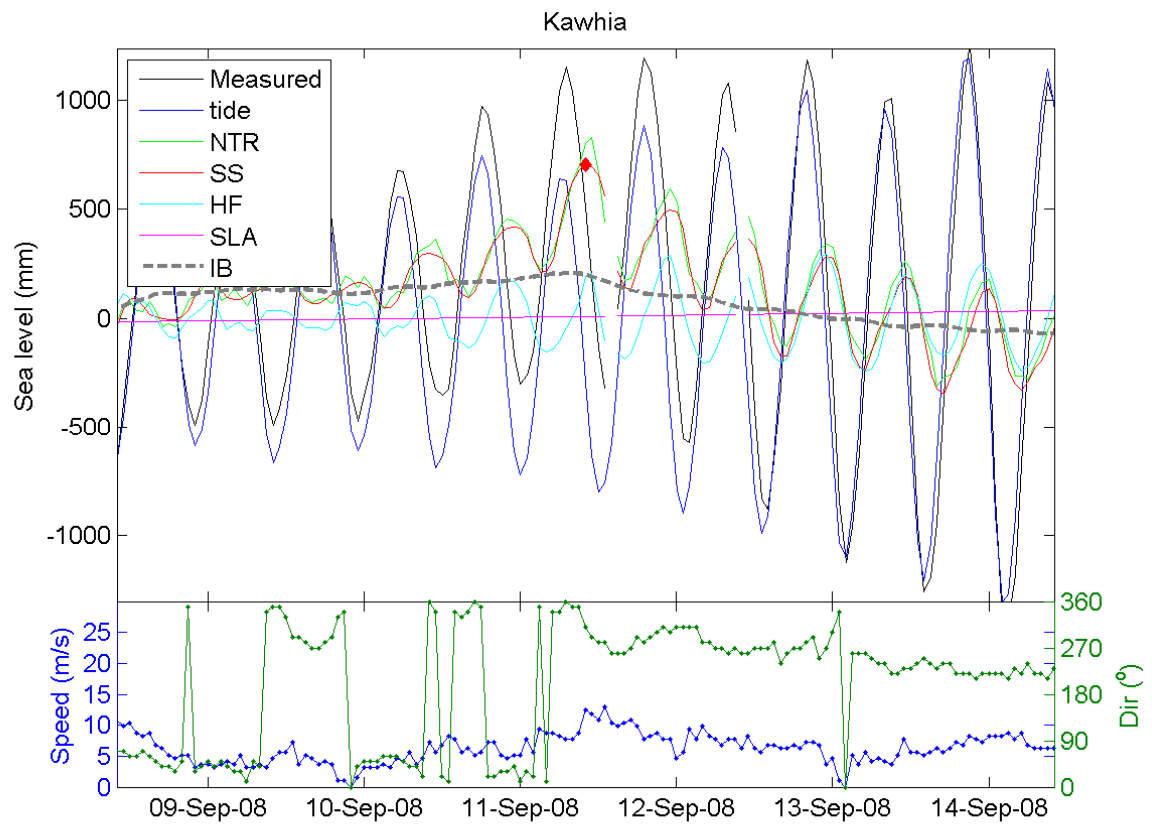


Figure 6-32: Measured sea level and its components during 11 September 2008 storm surge at Kawhia. NTR = non-tidal residual; SS = storm surge; HF = high-frequency sea-level; SLA = sea-level anomaly; IB = inverse barometer. Inverse barometer and wind were measure at Taharaoa.

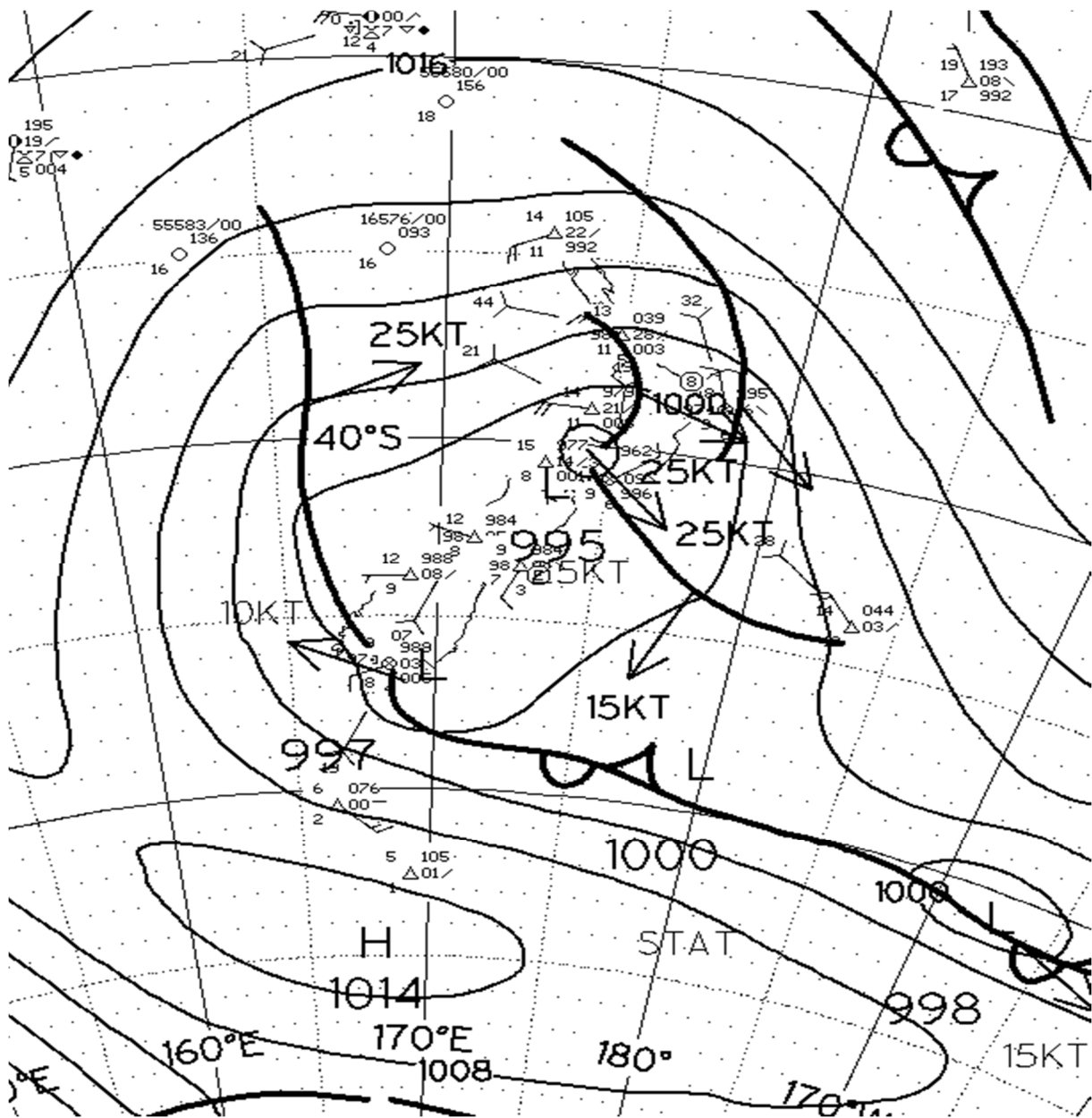


Figure 6-33: Mean sea level pressure at 1200 hours, 11 September 2008 around the time of the third largest measured storm surge (707 mm) at Kawhia.

Seasonality of storm surges

The sea-level record at Kawhia is too short to meaningfully examine the seasonality of storm surge.

Summary of storm surge analysis for Kawhia

The largest storm surges at Kawhia are driven by wind stress, with only a relatively small IB component. The large storm surges occur during complex low-pressure systems or troughs that result in strong wind speeds from the northwest, sustained over many hours. These weather systems are larger in scale and slower moving than the cyclones that are responsible for large surges at Whitianga. With three surges greater than 0.7 m in just 6 years of record, it appears that Kawhia Harbour (and likely other west-coast estuaries) are subject to large wind-driven storm surges that could conceivably reach well over 1 m in magnitude.

6.2.4 Summary of storm-surge records

The weather-map analysis shows a very different storm-surge climate between the east (Whitianga) and west (Kawhia) coasts of New Zealand. Storm surges at Whitianga were dominated by the drop in MSLP (inverse-barometer) associated with tight, fast-moving, low-pressure weather systems and onshore wind speeds are not sustained for long enough to produce surges much larger than 0.5 m. Conversely, storm surges at Kawhia were dominated by the wind setup associated with persistently strong north-westerly winds from weather fronts blowing over several hours to days; they drive surges almost double those experienced at Whitianga with likely maximum storm surges of over 1 m. Likewise, wind fronts that align with the Firth of Thames are the dominant cause of the largest storm surges occurring at Tararu, and again these surges are larger than those experienced at Whitianga, and likely to reach over 1 m at times.

7 Storm tide extreme-value analysis

7.1 Monte Carlo joint-probability analysis

Storm-tide is defined as the sea-level peak reached during a storm event, from a combination of **SLA + tide + storm surge**. It is the storm-tide that is primarily measured by sea-level gauges such as the Whitianga, Kawhia and Tararu gauges analysed here. The Monte Carlo joint-probability method (Goring et al. 2011) was used to predict the storm-tide height for a range of Annual Exceedance Probabilities (AEP's). The method is described below:

1. Decompose the non-tidal residual using a wavelet filter (see Section 2.3 for details).
2. Use the Monte Carlo joint-probability method to predict storm tide heights with AEP of 99% to 0.5% (0.2–200 year ARI).
3. Adjust extreme storm-tide distribution to local datum.

The Monte-Carlo joint-probability method takes extreme value distributions of the various components of storm tide (SS, SLA, HF), as well as 100 years of predicted tides to determine the AEP of various extreme storm tide levels. The MCJP method not only draws from the existing data, but also uses the extreme value distributions of the storm tide components to simulate thousands of years of storm tide; this narrows the confidence intervals and provides a more robust estimate for extreme storm tide estimates. For each site, the annual maximum storm tide was compared alongside the storm tide heights (Figure 7-1, Figure 7-2 and Figure 7-3).

Kawhia and Tararu record larger extreme storm tides than Whitianga. The storm-tide levels corresponding to a 1% AEP event were 2.44 and 2.63 m at Tararu and Kawhia respectively (Table 7-2 and Table 7-3) while at Whitianga it was 1.46 m (Table 7-1 and Figure 7-1). This is because the tide makes up the largest component of total storm tide recorded and the tidal range is larger at Kawhia and Tararu than at Whitianga (Table 5-1). Storm surges, the second largest sea-level component, are also larger at Kawhia and Tararu than Whitianga (Section 5.2).

Table 7-1: Extreme storm-tide distribution at Whitianga. Elevations for the median and 95% confidence bounds are based on a Monte Carlo joint-probability analysis of sea level data at Whitianga wharf. The storm-tide elevations presented here are given relative to a zero MSL. To calculate the elevations relative to MVD-53, add the present-day MSL datum offsets in Table 4-2.

AEP (%)	ARI (years)	Median (mm)	Lower 95% C.I (mm)	Upper 95% C.I (mm)
39	2	1142	1140	1145
18	5	1205	1200	1210
10	10	1256	1249	1263
5	20	1312	1302	1322
2	50	1392	1374	1407
1	100	1461	1435	1496
0.5	200	1545	1499	1597

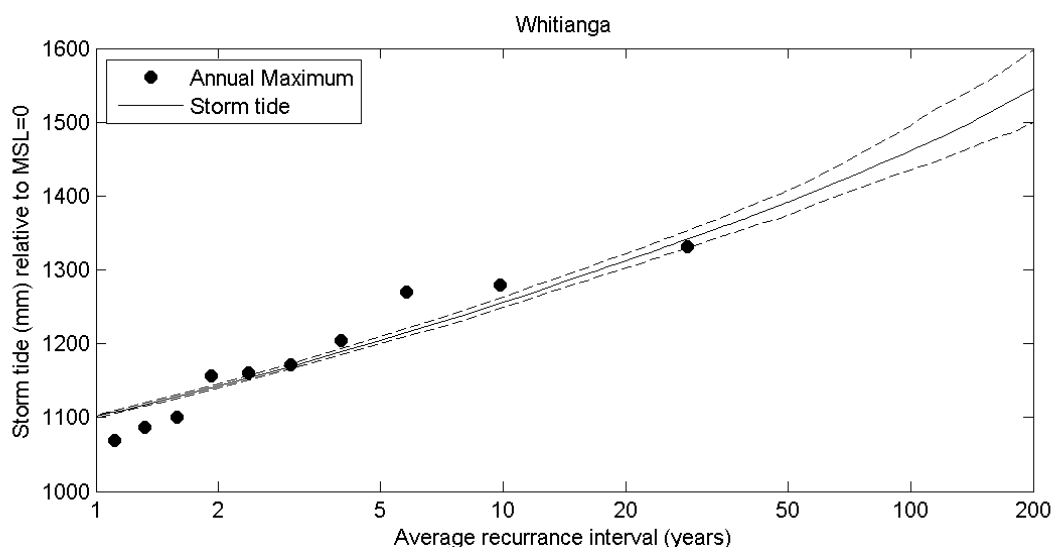


Figure 7-1: Extreme storm tide prediction levels, and annual maximum sea levels for Whitianga. Predicted storm tide levels make use of the Monte Carlo joint-probability method. Dashed lines indicate 95% confidence intervals. Refer to Table 7-1 for the data in table form.

Table 7-2: Extreme storm-tide distribution at Kawhia. Elevations for the median and 95% confidence bounds are based on a Monte Carlo joint-probability analysis of sea level data at Kawhia Harbour. The storm-tide elevations presented here are given relative to a zero MSL. To calculate the elevations relative to MVD-53, add the present-day MSL datum offsets in Table 4-2.

AEP (%)	ARI (years)	Median (mm)	Lower 95% C.I (mm)	Upper 95% C.I (mm)
39	2	2141	2137	2146
18	5	2244	2236	2252
10	10	2328	2317	2340
5	20	2418	2403	2435
2	50	2535	2513	2562
1	100	2627	2589	2673
0.5	200	2734	2672	2827

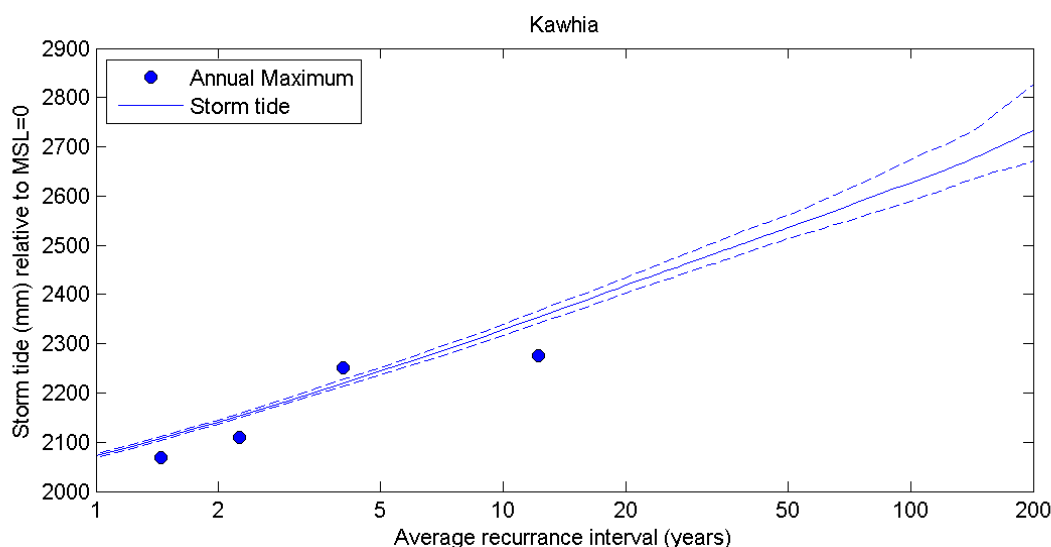


Figure 7-2: Extreme storm tide prediction levels, and annual maximum sea levels for Kawhia. Predicted storm tide levels make use of the Monte Carlo joint-probability method. Dashed lines indicate 95% confidence intervals. Refer to Table 7-2 for the data in table form.

Table 7-3: Extreme storm-tide distribution at Tararu. Elevations for the median and 95% confidence bounds are based on a Monte Carlo joint-probability analysis of sea level data at Tararu. The storm-tide elevations presented here are given relative to a zero MSL. To calculate the elevations relative to MVD-53, add the present-day MSL datum offsets in Table 4-2.

AEP (%)	ARI (years)	Median (mm)	Lower 95% C.I (mm)	Upper 95% C.I (mm)
39	2	2016	2013	2018
18	5	2095	2089	2100
10	10	2168	2160	2179
5	20	2251	2237	2266
2	50	2358	2339	2381
1	100	2440	2409	2478
0.5	200	2526	2482	2579

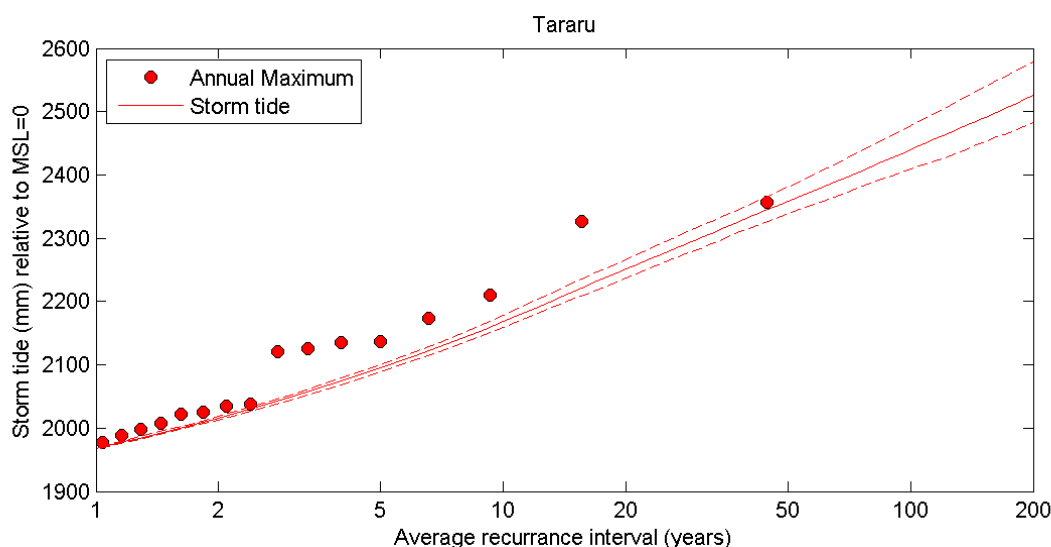


Figure 7-3: Extreme storm tide prediction levels, and annual maximum sea levels for Tararu. Predicted storm tide levels make use of the Monte Carlo joint-probability method. Dashed lines indicate 95% confidence intervals. Refer to Table 7-3 for the data in table form.

7.2 Breakdown of the largest storm-tide events

For each sea level gauge, the highest 20 storm tide events and their contributing component elevations (SLA, tide, storm surge, remaining high-frequency oscillations) were determined (Table 7-4, Table 7-5 and Table 7-6). To ensure independent events, storm-tide peaks separated by at least 3 days were chosen. A 3-day threshold is sufficient to separate storm tide peaks to ensure they are generated by separate storm events; weather systems typically pass over New Zealand every 4–7 days. The contributing component elevations were determined by decomposing the quality assured sea level at each gauge as described in Section 2.3.

The data is plotted in Figure 7-4 to Figure 7-6. The following points can be observed:

- The tide forms the dominant component of storm-tide in all cases.
- Large storm-tides can consist almost exclusively of tide, compounded by SLA (e.g., Figure 7-4, Figure 7-5).
- The great majority of storm tides have some positive storm surge component also, but often it is relatively small, especially at Tararu and Kawhia.
- Only one of the storm-surge annual maxima were observed in the top 20 storm-tides at Tararu (23–24 Jan 2011) and Kawhia (6 May 2013); storm tides at these sites were generally dominated by the tide, despite large surges being observed. The large storm tides that did include an annual maximum storm surge were still not the largest storm tides at these sites, because peak storm-surge did not coincide with the peak of a high high-tide.
- Given the large size of some storm surge events at Tararu and Kawhia, there is potential for storm tides to occur that are very much larger than those observed in the existing gauge records, should they peak at the same time as a high spring tide. Maximum combinations of tide, storm surge and SLA are shown in Table 7-7.

- Four storm-surge annual maxima were observed in the top-20 storm tides at Whitianga. Whitianga is more storm dominated despite its smaller storm-surge climate, because it has a smaller tidal range.

Table 7-4: The top 20 storm tide events and list of contributing components elevations for Kawhia. Storm tides are relative to MSL=0. A MSL offset of +0.13 mm (2008–2014) should be added to the storm tide values to adjust them relative to MVD-53 (Table 4-2).

Date	Storm tide (mm)	SLA (mm)	Storm surge (mm)	Unexplained tidal energy (mm)	Predicted tide (mm)
23-Jul-2009	2276	78	316	-4	1823
06-May-2013	2251	98	868	33	1243
27-May-2013	2199	111	184	-72	1897
24-Jul-2013	2134	-19	159	-22	1950
12-Aug-2014	2109	-40	156	-39	1977
14-Jan-2013	2092	-41	111	36	1963
15-Nov-2012	2068	67	26	-15	1944
18-Oct-2012	2045	29	109	-3	1858
13-Oct-2012	2044	4	479	106	1447
18-Apr-2011	2037	-12	237	-26	1774
13-Jul-2014	2035	37	84	-11	1880
26-Apr-2013	2032	77	17	-43	1909
05-Jan-2014	2030	-1	228	31	1767
21-Aug-2013	1999	90	25	-35	1851
17-Apr-2014	1993	26	370	-35	1564
03-Mar-2014	1986	-41	109	34	1861
08-Apr-2012	1977	-42	127	32	1836
17-Sep-2012	1975	-69	204	-16	1778
30-Aug-2011	1957	-48	94	4	1877
14-Aug-2010	1954	65	129	-31	1705

Table 7-5: The top 20 storm tide events and list of contributing components elevations for Tararu. Storm tides are relative to MSL=0. A MSL offset of +0.19 mm (1999–2014) should be added to the storm tide values to adjust them relative to MVD-53 (Table 4-2). A MSL offset of +0.08 m (1999–2014) should be added to the storm tide values to adjust them relative to TVD-52.

Date	Storm tide (mm)	SLA (mm)	Storm surge (mm)	Unexplained tidal energy (mm)	Predicted tide (mm)
14-Jul-1995	2357	11	303	158	1834
23-Jan-2011	2327	47	414	143	1833
02-Aug-2008	2211	80	171	151	1720
18-Sep-2005	2173	34	157	156	1750
17-Apr-1999	2136	74	195	108	1716
26-Nov-2003	2135	-72	186	138	1894
15-Jan-2013	2126	4	172	163	1838
18-Oct-2012	2121	-12	201	171	1780
05-Jun-2012	2101	76	257	30	1785

Date	Storm tide (mm)	SLA (mm)	Storm surge (mm)	Unexplained tidal energy (mm)	Predicted tide (mm)
22-Feb-2011	2065	-15	148	63	1892
28-Oct-2003	2064	-57	164	46	1896
16-Jun-1999	2043	16	72	-1	1871
05-Jan-2014	2038	-24	166	16	1868
12-Aug-2014	2037	-48	75	52	1942
02-Mar-2002	2035	0	159	82	1848
08-May-2012	2026	85	91	-19	1835
23-Jul-2009	2025	55	173	-35	1798
03-Mar-2006	2021	27	101	12	1880
17-Nov-2012	2021	-60	198	-93	1937
02-Feb-2014	2020	12	65	48	1891

Table 7-6: The top 20 storm tide events and list of contributing components elevations for Whitianga. Storm tides are relative to MSL=0. A MSL offset of +0.11 mm (1999–2014) should be added to the storm tide values to adjust them relative to MVD-53 (Table 4-2).

Date	Storm tide (mm)	SLA (mm)	Storm surge (mm)	Unexplained tidal energy (mm)	Predicted tide (mm)
23-Jan-11	1332	61	273	5	959
27-Jul-08	1280	54	462	33	747
24-Sep-13	1270	72	480	40	663
22-Mar-11	1210	63	240	-14	882
3-Jul-00	1205	94	185	-1	901
6-Jun-12	1171	66	132	14	945
30-Jul-08	1168	63	265	-37	833
9-May-12	1167	88	109	-6	949
20-Jul-14	1161	155	233	-24	789
3-Jul-12	1157	69	222	30	818
29-Jun-09	1157	77	193	-3	922
9-May-08	1145	79	149	-6	910
1-Feb-14	1132	73	123	-22	940
22-Feb-11	1126	49	47	18	989
30-Aug-00	1118	57	146	-10	901
27-May-13	1117	132	49	-23	949
17-Apr-14	1116	123	258	5	716
18-Jun-11	1107	100	218	-24	803
11-Jul-07	1101	17	319	-3	720
11-Jun-14	1095	108	343	27	597

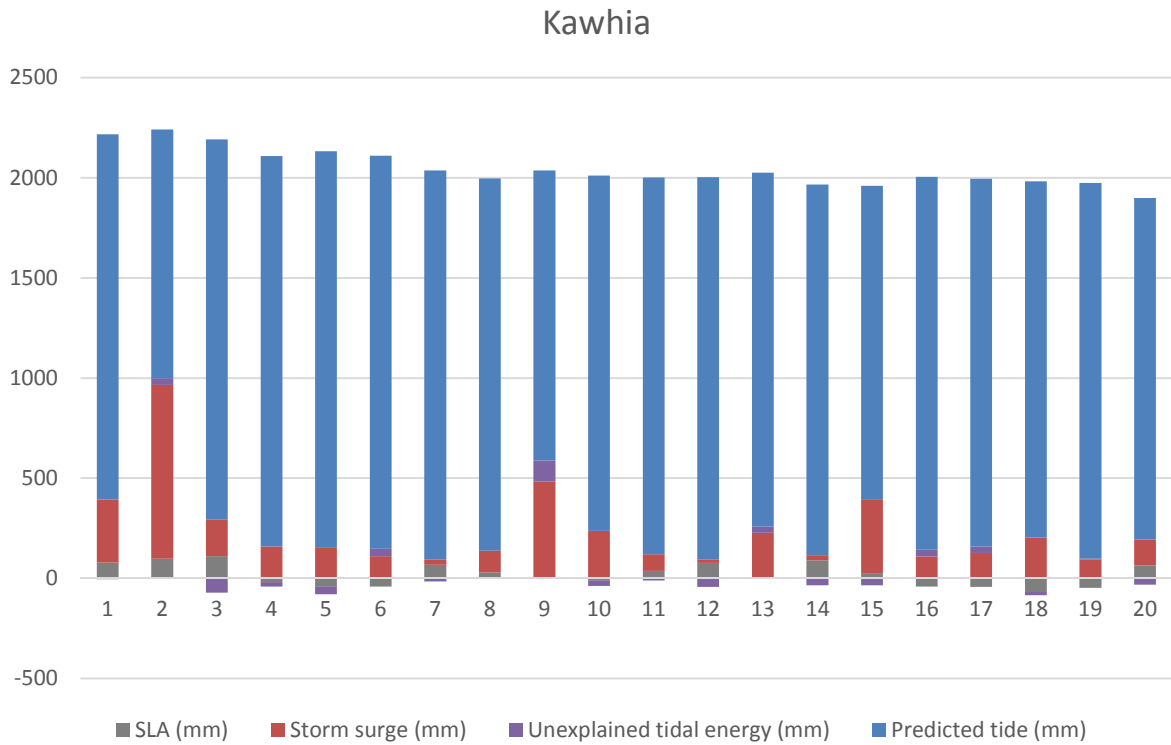


Figure 7-4: Breakdown of the sea-level components contributing to the largest 20 storm tides observed at Kawhia (2008-2014).

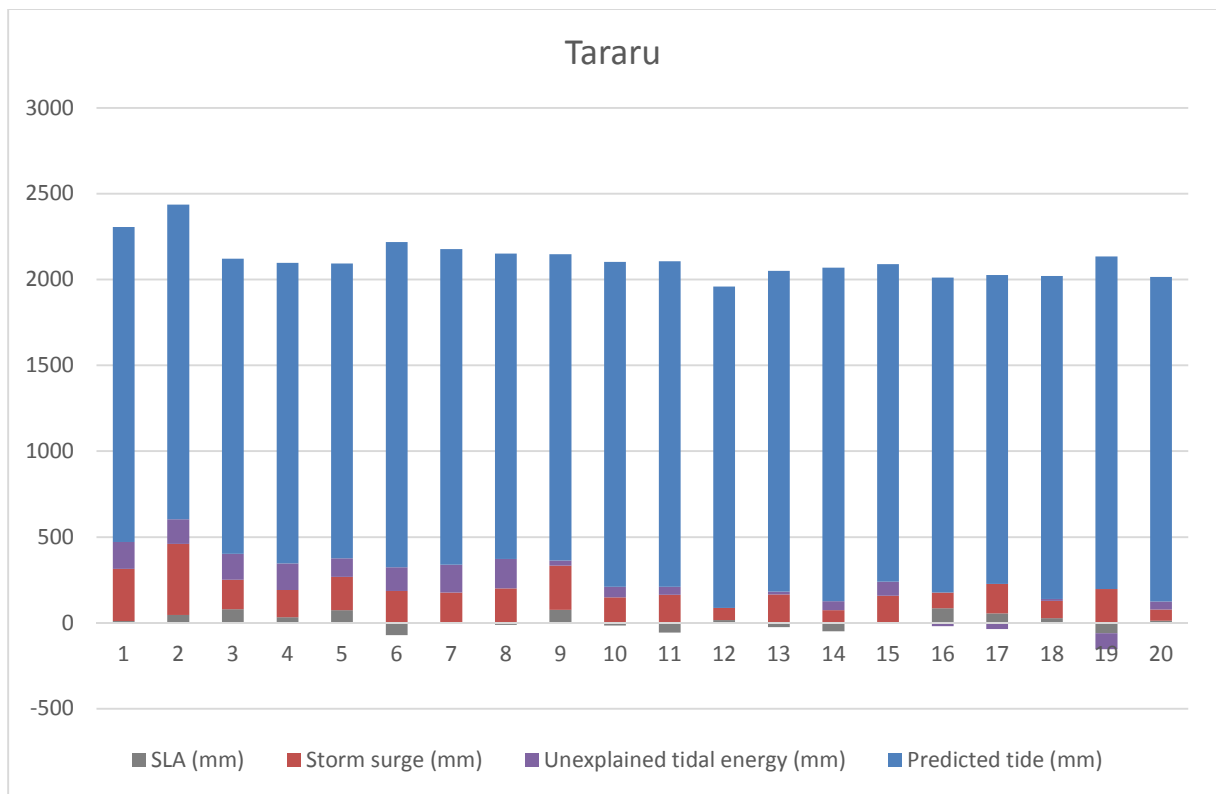


Figure 7-5: Breakdown of the sea-level components contributing to the largest 20 storm tides observed at Tararu (1990-2014).

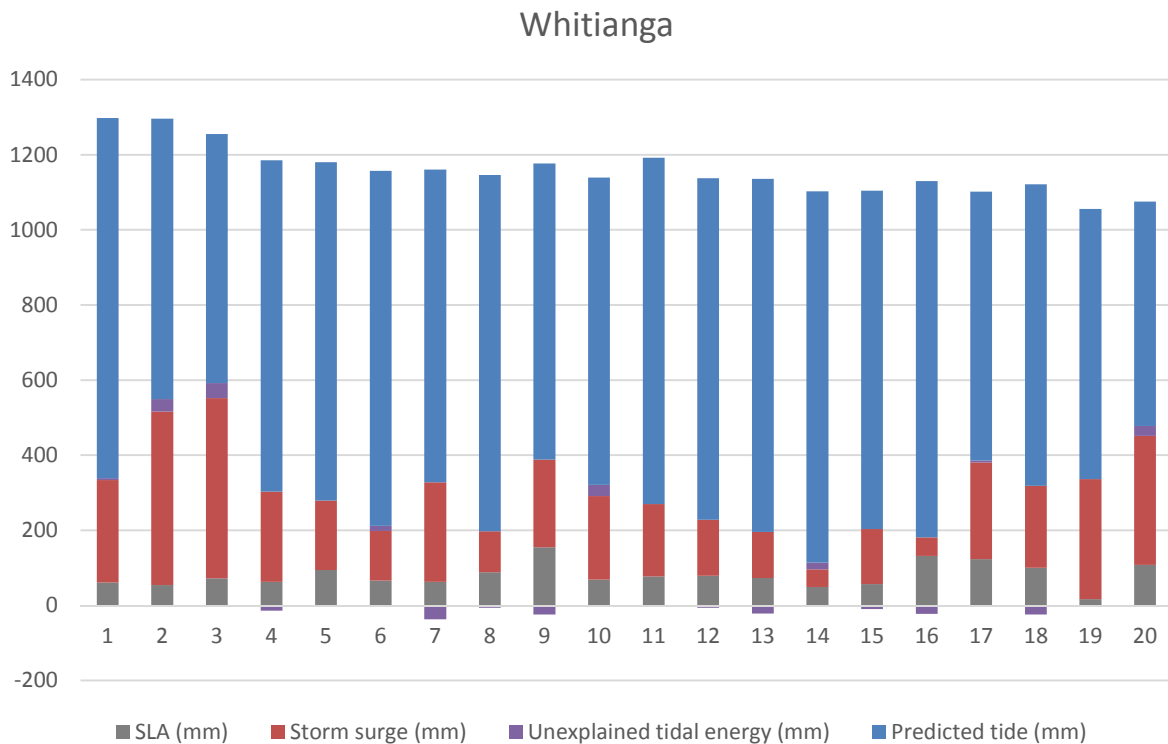


Figure 7-6: Breakdown of the sea-level components contributing to the largest 20 storm tides observed at Whitianga (1999-2014).

7.3 Seasonality of storm tides

For each site, a monthly boxplot was constructed of the 5 largest storm-tide events per year to highlight any seasonality in storm-tide hazard (created as a subset of the 20 largest storm-tide events). It is also useful to determine the months where the largest storm-tides occur most often, so a monthly bar chart was created of the largest 5 storm-tides per year.

7.3.1 Whitianga

At Whitianga there is no clear seasonal trend in the largest storm tides (Figure 7-7). However, there appears to be a higher propensity for large storm tides in winter, and also in January, with April/May and Oct/Nov/Dec being more quiescent, which is consistent with the seasonal distribution of storm surges (Figure 6-14). There is a seasonal trend in the *frequency* of storm tides, with more storm tides occurring during winter, and fewer occurring in late summer and early autumn (Figure 7-8).

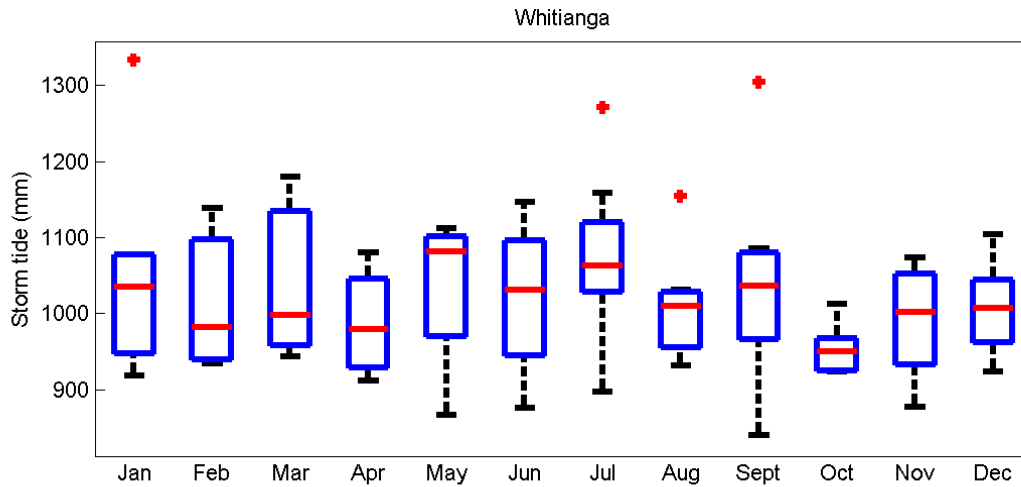


Figure 7-7: Monthly boxplot of the five largest storm tide events per year at Whitianga. The mean annual sea-level cycle has been removed. Median (red line), top and bottom of boxes represent 3rd and 1st quartiles respectively. Maximum and minimum (black lines), outliers (red dots) correspond to values greater than $Q3 + 1.5(Q3-Q1)$ or less than $Q1 - 1.5(Q3-Q1)$.

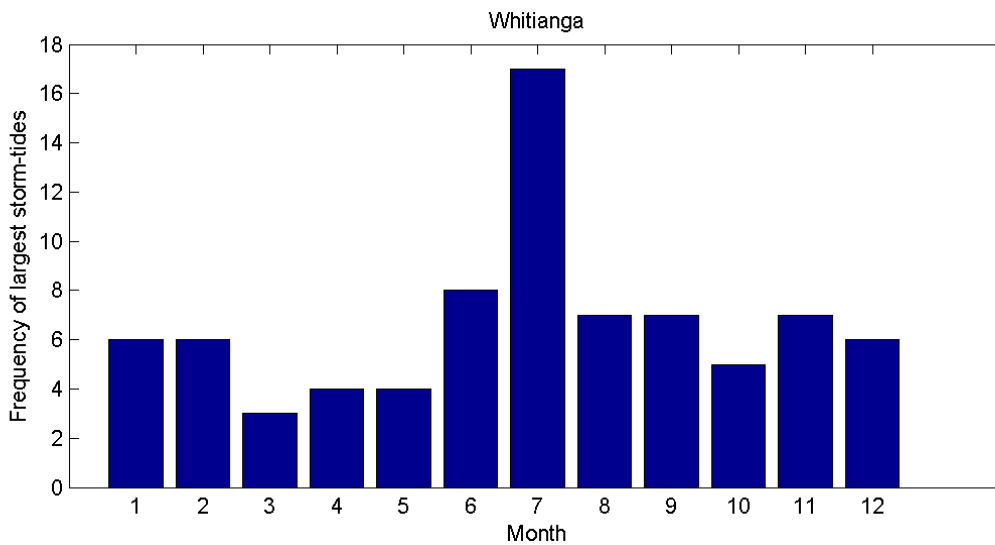


Figure 7-8: Frequency of the five largest storm-tides each year sorted by month at Whitianga. The mean annual sea-level cycle has been removed.

7.3.2 Tararu

There is no clear seasonal trend in the largest storm-tides at Tararu, although January and July to September contain the largest outliers (Figure 7-9). However, like Whitianga there appears to be a higher propensity for large storm tides in winter, and also in January, with April/May and Oct/Nov being more quiescent. The storm-tide frequency distribution shows a distinct quiescent period in April May when fewer storm tides occur (Figure 7-10).

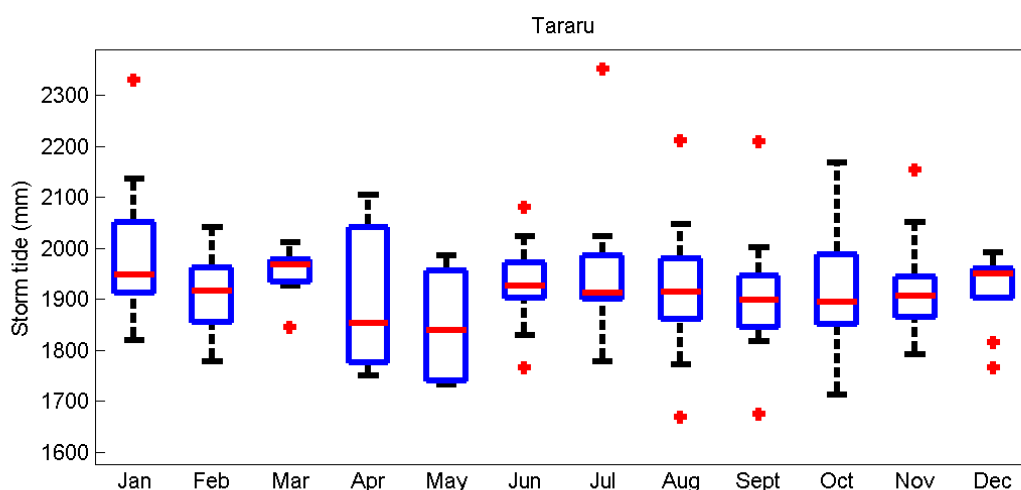


Figure 7-9: Monthly boxplot of the five largest storm tide events per year at Tararu. The mean annual sea-level cycle has been removed. Median (red line), top and bottom of boxes represent 3rd and 1st quartiles respectively. Maximum and minimum (excluding outliers) (black lines), outliers (red dots) correspond to values greater than $Q3 + 1.5(Q3-Q1)$ or less than $Q1 - 1.5(Q3-Q1)$.

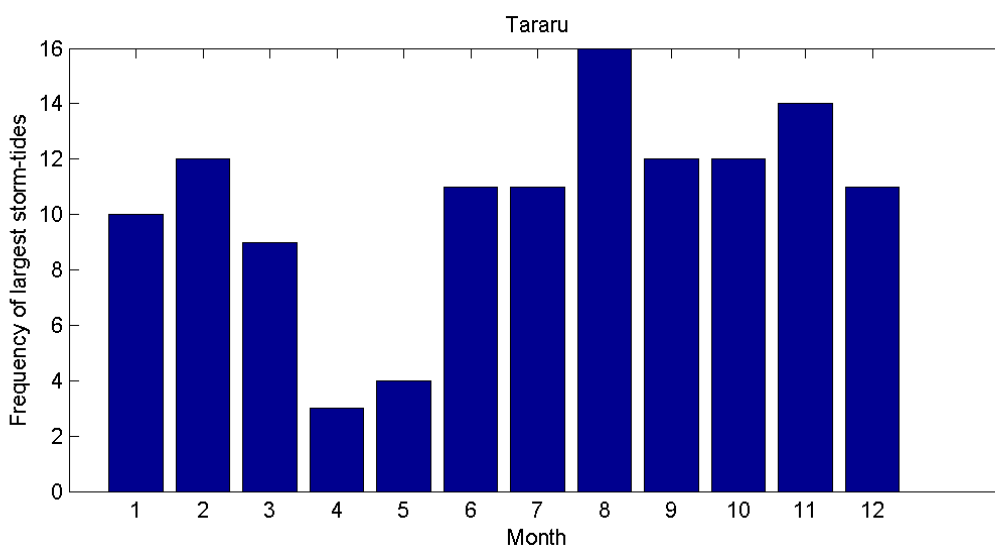


Figure 7-10: Frequency of the five largest storm-tides each year sorted by month at Tararu. The mean annual sea-level cycle has been removed.

7.3.3 Kawhia

The sea-level record at Kawhia is too short to meaningfully examine the seasonality of storm tides.

7.4 Maximum values of tide and surge

Table 7-7 shows the sum of the maximum tide, maximum storm surge and maximum sea-level anomaly, during the sea-level measurement periods. These maxima did *not* coincide, but occurred at different times. The summed maxima approach the maximum sea-level elevation we might expect if a very high tide combined with a very large storm surge and a very high sea-level anomaly, all at the same time. More extreme sea-level components are likely to be measured as the record lengths

increase. The probability of occurrence of the summed sea-level components is unknown, but is considerably less likely than the 0.5% AEP storm tide elevations shown in Table 7-1, Table 7-2 and Table 7-3.

Table 7-7: Maximum measured sea-level components. The elevation maxima presented here are given relative to a zero MSL. To calculate the elevations relative to MVD-53, add the present-day MSL datum offsets in Table 4-2.

	Tide	Storm surge	SLA	Sum
Whitianga	1053	631	175	1859
Tararu	1919	970	139	3028
Kawhia	1939	899	160	2998

8 Sea level anomaly

The sea level anomaly (SLA) is the variation of the non-tidal sea level about the longer term MSL on time scales ranging from a monthly basis to decades, due to climate variability. This includes ENSO and IPO patterns on sea level, winds and sea temperatures, and seasonal effects.

At each site, the mean, minimum and maximum SLA was calculated for each month of the year (Figure 8-1). A clear seasonal trend in the SLA is apparent, with mean SLA peaking in May and being at its lowest during October/November. The Kawhia SLA curve is less smooth, because the record is of short duration.

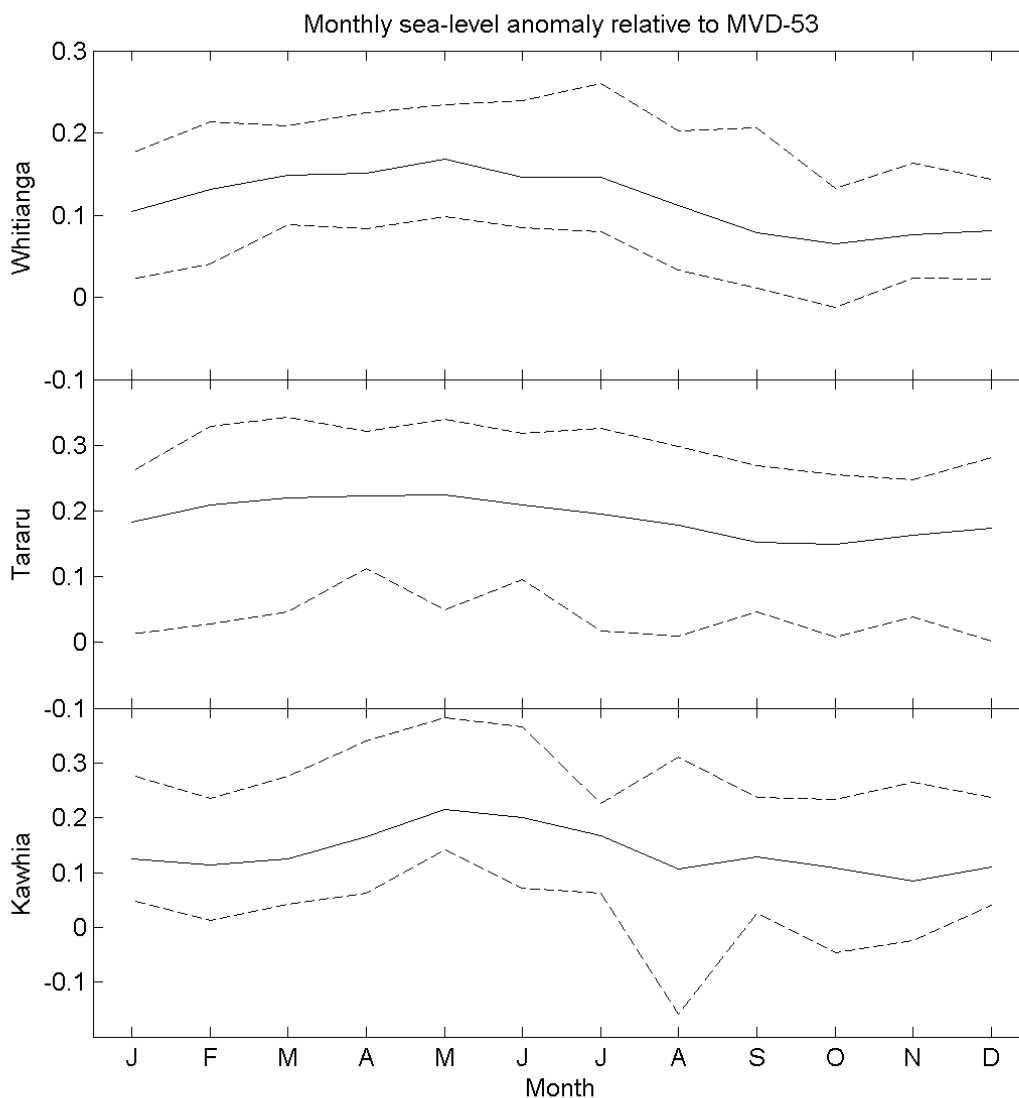


Figure 8-1: Mean, minimum and maximum monthly sea-level anomaly. The elevations are presented in metres relative to MVD-53.

Table 8-1: Mean, maximum and minimum SLA for each month of the year at Whitianga. The elevations are presented relative to MVD-53; they can be adjusted to zero MSL by subtracting the MSL offsets presented in Table 4-2.

Month	Mean SLA (mm)	Maximum SLA (mm)	Minimum SLA (mm)
Jan	104	175	22
Feb	132	213	41
Mar	149	209	88
Apr	150	224	83
May	169	235	98
Jun	146	239	85
Jul	145	260	80
Aug	112	202	33
Sep	78	206	12
Oct	65	132	-13
Nov	77	163	24
Dec	81	144	23

Table 8-2: Mean, maximum and minimum SLA for each month of the year at Tararu. The elevations are presented relative to MVD-53; they can be adjusted to zero MSL by subtracting the MSL offsets presented in Table 4-2.

Month	Mean SLA (mm)	Maximum SLA (mm)	Minimum SLA (mm)
Jan	184	260	12
Feb	210	328	27
Mar	221	343	47
Apr	223	321	112
May	225	340	49
Jun	210	319	96
Jul	196	326	17
Aug	180	298	9
Sep	153	270	46
Oct	150	256	8
Nov	163	247	39
Dec	175	282	1

Table 8-3: Mean, maximum and minimum SLA for each month of the year at Kawhia. The elevations are presented relative to MVD-53; they can be adjusted to zero MSL by subtracting the MSL offsets presented in Table 4-2.

Month	Mean SLA (mm)	Maximum SLA (mm)	Minimum SLA (mm)
Jan	125	278	49
Feb	113	235	13
Mar	124	275	42
Apr	165	341	62
May	215	383	142
Jun	201	365	72
Jul	168	226	62
Aug	106	311	-159
Sep	128	238	25
Oct	108	234	-45
Nov	85	264	-25
Dec	110	237	39

9 Wave measurements at Tararu

Surface gravity wave heights are measured by WRC at Tararu. The wave heights are calculated from surface elevation measurements collected every second, which are then averaged as follows:

- The average elevation is calculated over a specified averaging period.
- The minimum and maximum elevation in the averaging period is retained.
- The difference is calculated between the average elevation and both the minimum and maximum elevation.
- The wave amplitude is calculated as twice the smallest difference.

Before February 1998 the wave height data looks unreliably high, and we did not use that data. Between February 1998 and the end of June 2011 the wave data was collected at 5-minute intervals – an example is shown for a large wave event in August 2008 (Figure 9-1). The tide is seen to modulate the wave heights – at high tide the water depth and wind fetch increase, allowing large waves to approach the gauge. From July 2011 onward the wave data was collected at 1-minute intervals, and the 1-minute averages are highly variable with many spikes and many zero values. There is also a discrepancy between wave heights measured before (larger) and after (smaller) that date (Figure 9-2). We are unsure of the cause of this discrepancy. However, the smoothed wave height data does appear to contain useful information, and still shows the tidal modulation.

The wave height measurements require further quality control before being used. For example, a temporary wave gauge deployment could be made to calibrate the wave heights being recorded at the Tararu met-ocean recording site. Also, it would be useful to calculate wave period.

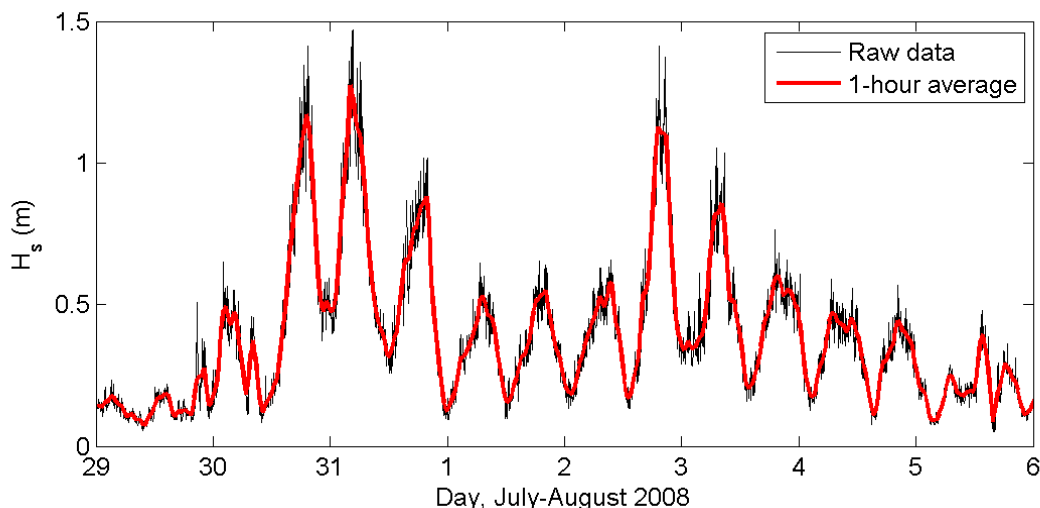


Figure 9-1: Wave height measured at Tararu in August 2008. Both the raw data and a 1-hour running average are plotted.

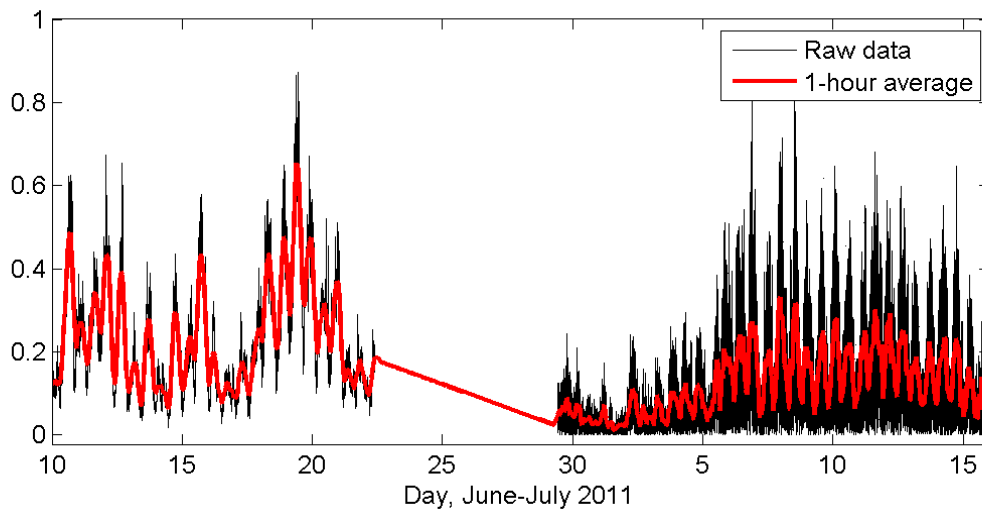


Figure 9-2: Thames wave data - change of sampling resolution in June 2011.

The largest smoothed wave heights in the record reached 1.3 m (Figure 9-1). Wind waves have a maximum fetch of about 45 km to Tararu. A wind of 20 m/s could produce waves with a significant height of about 1.8 m and a peak period of about 6 s (Young and Verhagen 1996). These could be expected to produce wave setup of about 0.1 m over a steep 1 in 10 gradient beach (Stockdon et al. 2006). Thus waves will not contribute much to storm-tide elevation in the southern Firth of Thames. Nevertheless, waves could contribute to relatively small overwash volumes right at the coast, or to coastal erosion.

After suitable quality control, the wave data has potential for joint-probability analysis between storm tide and wave height, which can be used for hazard assessments, see for example (Stephens et al. 2013).

10 Review of sea-level gauge network

As outlined in Section 1.1, sea-level records provide vital information for coastal management purposes. Important questions are:

- Q1: Does the existing WRC sea-level gauge network provide sufficient information to meet the Waikato Region's coastal management requirements now?
- Q2: Will the existing WRC sea-level gauge network provide sufficient information to meet the Waikato Region's coastal management requirements in future?
- Q3: How can the sea-level network be improved to meet those requirements?

A1: The existing sea-level gauges at Whitianga, Tararu and Kawhia appear to be collecting robust sea-level data. We note the following:

- The 1-minute sampling intervals are sufficient to measure the effects of tsunami and seiche.
- Tidal harmonic analysis enables future tides to be predicted at the gauge location. These can be used to calibrate tidal models.
- Sea-level gauges that are located in the surf zone will measure the effect of wave setup, as appears to be the case for Tararu. The Whitianga and Kawhia gauges are located in estuaries and are largely sheltered from waves.
- The gauges at Whitianga and Kawhia are located inside estuaries, which means that tidal and storm surge waves are affected by shoaling through the entrance and may not represent conditions outside the estuary well. For example the amplitude of the tidal wave is substantially attenuated inside Whitianga Harbour compared to outside (Section 5.1).
- Mean sea-level measurements can also be affected by morphological changes inside estuaries, such as siltation.
- The gauge records are not yet long enough to distinguish sea-level rise trends from the effects of climate variability.
- The gauge records at Tararu and Whitianga are only just long enough for reliable extreme sea-level analysis using joint-probability techniques, but the Kawhia record is still too short.
- Extreme storm surge modelling has high uncertainty because the record lengths are still short for this purpose.

A2: Important requirements for sea-level records in the future will include:

- The sea-level records will need to be accurate. This will require regular maintenance and calibration, and surveying checks on datum.
- Long records of annual MSL are needed to quantify changing exposure to SLR. Sea-level gauges by themselves measure relative SLR (SLR relative to the local landmass). However, tectonic uplift or subsidence of the landmass needs to be also accounted for

to enable absolute SLR to be calculated. Land uplift or subsidence rate measurements will be required to allow meaningful comparison of absolute SLR in future.

- Long records are required for accurate extreme sea-level modelling. To measure extreme events requires robust measurements during large “events”. This necessitates that the gauges are capable of surviving the extreme events and that their measurement range can capture extreme events. Records to date suggest that the gauges are fit for purpose in this regard. It is important that the gauges are in place and operating at the time that extreme events occur.
- The gauge network will ideally have sufficient spatial coverage to identify important geographical differences on sea level mean and variability.

A3: For the purpose of measuring tides and mean sea level, sea-level gauges would ideally be located in an open-water location where tidal amplitudes represent the adjacent coastline well, and outside of the wave breaking zone, since waves are known to degrade the quality of “still-water” sea level measurements.

The Tararu (25 years) and Whitianga (16 years) gauges are sufficiently established to provide valuable historical sea-level records that should be maintained and extended to improve extreme sea level estimates and measure changing MSL and rates of SLR.

The Kawhia gauge is still relatively short, and has less value for MSL or extreme sea-level analyses, compared with the other gauges, at this stage. Nevertheless, it has already measured three very large storm surges, with a frequency and magnitude distribution that is steeper than we have seen elsewhere. The tide and surge signals measured by the Kawhia gauge are likely to be modified by the harbour morphology relative to the open coast. In the long term the MSL record will prove valuable if this gauge is maintained.

Ideally, sea-level gauges would be added at open-coast locations on both the east and west coasts of the Waikato region to meet future sea-level record requirements. This is because gauges in open-coast locations measure tides before they have to pass through the narrow and shallow tidal inlet throat. Tides measured on the open coast are therefore representative of a longer coastline. Tidal measurements are important because tides are the largest component of sea-level variability.

Good locations would be on the lee side of small offshore islands, or on the lee side of a peninsula with relatively deep water adjacent, away from breaking waves and outside of estuaries. A good location on the east of the Coromandel Peninsula would be at or northward of Mercury Bay, as this is approximately halfway between the Tararu gauge and the Moturiki Island gauge operated by NIWA.

Land vertical tectonic movements should be recorded at all sea-level gauge locations to enable absolute MSL to be determined in future.

11 Conclusions

Waikato Regional Council (WRC) operates sea-level gauges at Tararu, Whitianga and Kawhia. Digital sea-level records at Tararu, Whitianga and Kawhia began in 1990, 1999 and 2008 respectively. WRC engaged NIWA to analyse the sea-level records. Of particular interest was the analysis of extremes in the sea-level records to understand the local anatomy of storm-tides in terms of sea-level response to tide, weather and wave action. This report presents a variety of sea-level analyses useful for coastal planning and regulation and hazard assessment, for the three gauge locations. The report accompanies electronic tables in excel format.

All three sea-level gauges appear to be collecting sound data. The gauges are delivering data of sufficient quality to confidently extract the various sea-level components, determine mean sea-level, and calculate extreme sea levels. Discrepancies with the Whitianga data reported by NIWA in 2012 and 2014 have been resolved. The discrepancies arose from datum offsets that were not being recorded in the data received by NIWA as part of the live data feed, and were not related to the sea-level gauge itself nor the quality of the data being collected by the gauge. In this study we used a high-quality sea-level record held by WRC, which included the correct datum offsets to the local vertical datum. The live feed that NIWA continues to receive now has the correct datum offset applied.

Mean sea levels of 0.16, 0.12, 0.14, 0.18 and 0.13 m relative to Moturiki vertical datum were calculated for Auckland, Moturiki, Whitianga, Tararu and Kawhia respectively, for the 2008–2014 period. Mean sea level is similar at all sites.

Mean high-water springs (MHWS) elevations were calculated from the three gauge records using several MHWS definitions. MHWS elevations are also presented at other locations around the coastline of the Waikato region. Considerable tidal dissipation occurs over the ebb-tidal delta of Whitianga Harbour, so MHWS elevations measured at the gauge location inside the harbour are about 10 cm lower than outside. It is likely that a similar effect occurs at the Kawhia gauge, which is also located inside a harbour. MHWS elevations measured by the gauge at Tararu are representative of MHWS along the nearby coastline. A substantial change in the tidal amplitudes was measured in the Whitianga estuary in February–March 2006, which is probably related to morphological change in the estuary entrance channel.

The frequency–magnitude distribution of storm surge was calculated at each gauge. 1% Annual Exceedance Probability (AEP) storm surges of 0.69, 0.97 and 1.36 m estimated for Whitianga, Tararu and Kawhia respectively. There is considerable uncertainty in these extreme storm surge estimates, particularly for the estimate at Kawhia which has higher uncertainty due to the short 6-year length record. We observed a different storm-surge climate between the east (Whitianga) and west (Kawhia) coasts of New Zealand. Storm surges at Whitianga were dominated by the drop in barometric pressure associated with tight, fast-moving, low-pressure weather systems. Onshore wind speeds are not sustained for long enough to produce surges much larger than 0.5 m at Whitianga. Conversely, storm surges at Kawhia were dominated by wind stress associated with persistently strong north-westerly winds from weather fronts blowing over several hours to days; they drive surges almost double those experienced at Whitianga with likely maximum storm surges of over 1 m. Likewise, wind fronts that align with the Firth of Thames are the dominant cause of the largest storm surges occurring at Tararu, and again these surges are larger than those experienced at Whitianga, and likely to reach over 1 m at times.

The frequency–magnitude distribution of storm tide was calculated at each gauge. 1% AEP storm tides of 1.46, 2.44 and 2.63 m estimated for Whitianga, Tararu and Kawhia respectively. The tide formed the dominant component of storm-tide in all cases. Large storm-tides occasionally consisted almost exclusively of tide, compounded by sea-level anomaly. However, the great majority of storm tides have some positive storm surge component, but often it is relatively small, especially at Tararu and Kawhia. Only one of the storm-surge annual maxima were observed in the top 20 storm-tides at Tararu and Kawhia; storm tides at these sites were generally dominated by the tide, despite large surges being observed. The large storm tides that did include an annual maximum storm surge were still not the largest storm tides at these sites, because peak storm-surge did not coincide with the peak of high-tide. Given the large size of some storm surge events at Tararu and Kawhia, there is potential for storm tides to occur that are very much larger than those observed in the existing gauge records, should they peak at the same time as a high spring tide. Four storm-surge annual maxima were observed in the top-20 storm tides at Whitianga. Whitianga is more storm dominated despite its smaller storm-surge climate, because it has a smaller tidal range.

A clear seasonal sea-level trend is apparent at all three gauge locations, with the sea-level anomaly peaking in May and being at its lowest during October/November. The seasonality of storm surges and storm tides was examined for Whitianga and Tararu, but not for Kawhia, which is too short to indicate patterns reliably. At both sites there were a greater number of large storm surges occurring in winter, but Whitianga also had a noticeable peak of large storm surges in summer due to its exposure to ex-tropical cyclones. There was no clear seasonal trend in the *magnitude* of storm tides, but *greater number* of large storm tides occurred in the winter months, reflecting the greater number of large storm surges occurring then.

There is a positive relationship between wave height and storm surge at Tararu because the same weather events that drive storm surge in the Firth of Thames also create sea waves, although there is considerable variability/scatter in the relationship. The wave data at Tararu could be used to undertake a joint-probability analysis between storm tide and wave height in future, which can be used for hazard assessments. Wave setup raises the sea level at the shore due to wave breaking, and could contribute up to about 0.1 m to the elevation of storm surge measured at Tararu.

Overall, the tidal gauges are collecting sound data and with continued gauge maintenance the records will be suitable for future analysis of sea-level trends, storm-surge and storm-tide anomalies. The sea-level records at Tararu (25 years long) and Whitianga (16 years long) are valuable historical sea-level records that should be maintained and extended to improve extreme sea level estimates and measure changing mean sea level and rates of sea-level rise. The Kawhia gauge record is still relatively short, and has less value for mean sea level or extreme sea-level analyses at this stage, but will prove valuable in the long term if maintained.

The sea-level network could be improved by adding gauges at open-coast locations on both the east and west coasts of the Waikato region to meet future sea-level record requirements. This is because small estuaries can be prone to large morphological changes that affect the tides within them. For example, the aforementioned change in tidal amplitude at Whitianga, which was probably related to a morphological change in the estuary. It was also shown that sea level in Kawhia Harbour is responding strongly to seasonal wind setup, which is causing higher annual mean sea level variability than is usually observed in New Zealand gauge records. For the purpose of measuring tides and mean sea level, sea-level gauges would ideally be located in an open-water location where tidal and storm surge amplitudes represent the adjacent coastline well, and outside of the wave breaking zone, since waves are known to degrade the quality of “still-water” sea level measurements. Good locations

would be on the lee side of small offshore islands, or on the lee side of a peninsula with relatively deep water adjacent, away from breaking waves and outside of estuaries. A good location on the east of the Coromandel Peninsula would be at or northward of Mercury Bay, as this is approximately halfway between the Tararu gauge and the Moturiki Island gauge operated by NIWA.

- Land vertical tectonic movements should be recorded at all sea-level gauge locations to enable absolute MSL to be determined in future.

12 Acknowledgements

WRC supplied sea-level data for completion of the work, including quality analysis of the Whitianga dataset. Auckland sea-level data was supplied by Auckland Council.

13 Glossary of abbreviations and terms

AEP	Annual exceedance probability – The probability of a given (usually high) sea level or wave height being equalled or exceeded in elevation, in any given calendar year. AEP can be specified as a fraction (e.g., 0.01) or a percentage (e.g., 1%).
ARI	Average recurrence interval – The average time interval (averaged over a very long time period and many “events”) that is expected to elapse between recurrences of an infrequent event of a given large magnitude (or larger). A large infrequent event would be expected to be equalled or exceeded in elevation, once, on average, every “ARI” years, but with considerable variability.
ENSO	El Niño Southern Oscillation. A natural global climate phenomenon involving the interaction between the tropical Pacific and the atmosphere, but has far-reaching effects on the global climate, especially for countries in the Pacific rim. ENSO is the strongest climate signal on time scales of one to several years. The quasi-periodic cycle oscillates between El Niño (unusually warm ocean waters along the tropical South American coast) and La Niña (colder-than-normal ocean waters off South America).
Epoch	A particular period of history that is selected as a point of reference – used in connection with developing a baseline sea level.
Equilibrium Tide	The elevation of the sea surface that would be in equilibrium with the tidal forces if the earth were covered with water and the response of the water to the tidal forces were instantaneous.
HF	High-frequency sea-level component – a product of wavelet filtering of the non-tidal residual sea level.
IPO	Interdecadal Pacific Oscillation – a long timescale oscillation in the ocean–atmosphere system that shifts climate in the Pacific region every one to three decades.
Joint probability	The probability of two separate processes occurring together (e.g., large waves and high storm-tide).
MCJP	Monte Carlo joint-probability technique. A technique to model extreme sea-level. Suitable for short data records, and provides the flexibility to mix measured and modelled sea-level components.
MHWPS	Mean high-water perigean springs – this occurs when MHWs coincides with the moon being closest to the Earth in its elliptical orbit (in perigee). MHWPS includes the sum of twice daily lunar M_2 tide, the twice daily solar S_2 tide, and the elliptic semi-diurnal N_2 tide: $MHWPS = M_2 + S_2 + N_2$.

MHWS	Mean high-water springs – The high tide height associated with higher than normal high tides that result from the beat of various tidal harmonic constituents. The high tide exceeds the mean high water springs elevation every 2 weeks approximately, at both new and full moon, when the gravitational forces of the Sun and the Earth’s moon align to produce higher than normal tides. Thus the nautical definition of MHWS (MHWSn) includes the sum of twice daily lunar M_2 tide and the twice daily solar S_2 tide: $MHWSn = M_2 + S_2$. MHWS can be defined in various ways, and the MHWS elevation varies according to definition.
MHWS-10	the elevation equalled or exceeded by the largest 10% of all high tides.
MSL	Mean sea level – obtained by averaging the sea level, relative to a local vertical datum, over a defined epoch.
NTR	Non-tidal residual – obtained by subtracting the predicted tide from the raw sea-level record.
SLA	Sea-level anomaly – the variation of the non-tidal sea level about the longer term MSL on time scales ranging from a monthly basis to decades, due to climate variability. This includes ENSO and IPO patterns on sea level, winds and sea temperatures, and seasonal effects.
SS	Storm surge – The rise in sea level due to storm meteorological effects. Low-atmospheric pressure relaxes the pressure on the ocean surface causing the sea-level to rise, and wind stress on the ocean surface pushes water down-wind (onshore winds) and to the left up against any adjacent coast (alongshore winds). Storm surge has timescales of sea-level response that coincide with typical synoptic weather motions; typically 1–3 days.
Storm surge	The rise in sea level due to storm meteorological effects. Low-atmospheric pressure relaxes the pressure on the ocean surface causing the sea-level to rise, and wind stress on the ocean surface pushes water down-wind (onshore winds) and to the left up against any adjacent coast (alongshore winds). Storm surge has timescales of sea-level response that coincide with typical synoptic weather motions; typically 1–3 days.
Storm tide	The sea-level peak around high tide reached during a storm event, resulting from a combination of SLA + tide + storm surge.
tide	The tides are caused by the gravitational attraction of solar-system bodies, primarily the Sun and the Earth’s moon, which then propagate as forced long waves in the ocean interacting in a complex way with continental shelves. In New Zealand the astronomical tides have by far the largest influence on sea level, followed by storm surge (in most locations).
Wave runup	The maximum vertical extent of wave “up-rush” on a beach or structure above the still water level, and thus constitutes only a short-term upper-bound fluctuation in water level relative to wave setup.

Wave setup

The average temporary increase in mean still-water sea level at the coast, resulting from the release of wave energy in the surf zone as waves break.

14 References

- Bell, R.G. (2010) Tidal exceedances, storm tides and the effect of sea-level rise. *Proceedings of the 17th Congress of the Asia and Pacific division of the IAHR*, Auckland, New Zealand, 10
- Bell, R.G., Dumnov, S.V., Williams, B.L., Greig, M.J.N. (1998) Hydrodynamics of Manukau Harbour, New Zealand. *New Zealand Journal of Marine and Freshwater Research*, 32: 81-100.
- Boon, J.D. (2013) *Secrets of the tide: tide and tidal current analysis and predictions, storm surges and sea level trends*. Elsevier.
- Denys, P. (2014) *Firth of Thames SET profile GNSS data analysis*. University of Otago memo to Waikato Regional Council
- Foreman, M.G.G., Cherniawsky, J.Y., Ballantyne, V.A. (2009) Versatile Harmonic Tidal Analysis: Improvements and Applications. *Journal of Atmospheric and Oceanic Technology*, 26: 806-817.
- Goodhue, N.G. (2012) Tide marks and mean sea-level for Whitianga and Tararu. *NIWA Client Report to Waikato Regional Council HAM2012-060*.
- Goring, D.G. (1999) Whitianga sea-level recorder: Preliminary analysis. *NIWA Client Report prepared for Environment Waikato, CHC99/87*.
- Goring, D.G. (2008) Extracting long waves from tide-gauge records. *Journal of Waterway Port Coastal and Ocean Engineering-ASCE*, 134: 306-312.
- Haigh, I.D., Nicholls, R., Wells, N. (2010) A comparison of the main methods for estimating probabilities of extreme still water levels. *Coastal Engineering*, 57: 838-849.
- Hannah, J., Bell, R.G. (2012) Regional sea level trends in New Zealand. *Journal of Geophysical Research-Oceans*, 117: C01004.
- MfE (2008) *Coastal Hazards and Climate Change: A Guidance Manual for Local Government in New Zealand 2nd edition*. Revised by Ramsay, D. and Bell, R. (NIWA). Ministry for the Environment. Wellington.
- Mullan, B., Carey-Smith, T., Griffiths, G., Sood, A. (2011) Scenarios of storminess and regional wind extremes under climate change. *NIWA Client Report to Ministry of Agriculture and Forestry, WLG2010-031*.
- Pugh, D.T. (1987) *Tides, surges and mean sea-level*. John Wiley & Sons Ltd.
- Pugh, D.T. (2004) *Changing sea levels. Effects of Tides, Weather and Climate*. Cambridge University Press. New York.
- Stephens, S.A., Bell, R.G., Ramsay, D., Goodhue, N. (2014) High-Water Alerts from Coinciding High Astronomical Tide and High Mean Sea Level Anomaly in the Pacific Islands Region. *Journal of Atmospheric and Oceanic Technology*, 31: 2829-2843.

- Stephens, S.A., Wadhwa, S., Bell, R., Speed, S., McNeil, M. (2012) Development of an updated Coastal Marine Area boundary for the Auckland region. Making Waves - 20 years and beyond. *New Zealand Coastal Society 20th Annual Conference*, 13-16 November 2012. Auckland,
- Stephens, S.A., Wadhwa, S., Gorman, R., Goodhue, N., Pritchard, M., Oviden, R., Reeve, G. (2013) Coastal inundation by storm-tides and waves in the Auckland Region. *NIWA Client Report to Auckland Council*, HAM2013-059: 138.
- Stockdon, H.F., Holman, R.A., Howd, P.A., Sallenger, A.H. (2006) Empirical parameterization of setup, swash, and runup. *Coastal Engineering*, 53: 573-588.
- Tonkin & Taylor Ltd (1986) *Manukau Harbour resources study*. Consulting report on behalf of Manukau Harbour Maritime Planning Authority
- Walters, R.A., Goring, D.G., Bell, R.G. (2001) Ocean tides around New Zealand. *New Zealand Journal of Marine and Freshwater Research*, 35: 567-579.
- Young, I.R., Verhagen, L.A. (1996) The growth of fetch limited waves in water of finite depth .2. Spectral evolution. *Coastal Engineering*, 29: 79-99.

Appendix A Quality assurance of tide-gauge data

Whitianga

The quality-assured data supplied by WRC, described in Section 3, was used for all analyses.

Kawhia

Erroneous spikes were removed from the Kawhia sea level gauge, in particular a large spike on 10th June 2014. Spikes were removed by linear interpolation between the nearest non-spiked values. Due to faulty recordings, sea level data from 18th May to 21st June 2012 was removed. Data was interpolated to hourly intervals as follows:

1. For each point, apply a running average of 15 minutes either side was applied.
2. Decimate this smoothed timeseries by taking a point every hour.

This method works provided that the data has a constant sampling interval beforehand. For Kawhia, the raw data is sampled every 2 minutes before 6 June 2012, and every 1 minute afterwards. Steps 1 to 3 were used on the 1 minute and 2 minute datasets separately, and then both data sets were merged together.

Figure 14-1 shows the raw and quality assured Kawhia sea level used in this project.

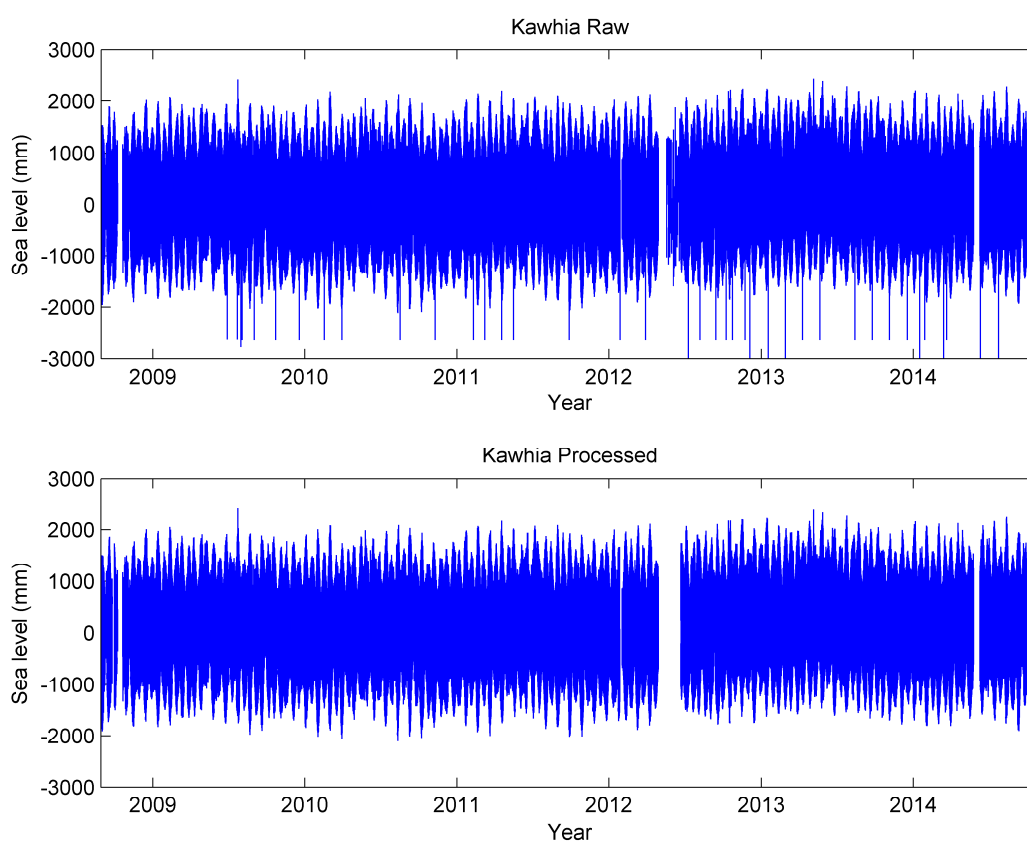


Figure 14-1: Raw and quality assured Kawhia sea level data. Sea level is relative to gauge zero.

Tararu

The Tararu gauge (Figure 14-2) didn't appear to have any errors in the measured sea level itself, but the sampling interval is irregular, often missing recordings at expected times. An irregular sampling interval creates problems when trying to interpolate to a common time step, which is often required when forecasting tides, and analysing the non-tidal residual. The following method was used to interpolate the sea level to a common hourly time step at Tararu:

1. Where there are missing times, fill these with place-holders (NaN using Matlab processing software).
2. Apply linear interpolation over the missing data, then apply a 30 minute window and smooth the time series. After smoothing, put the gaps back in the same places.
3. Decimate the time series to hourly. Where there is a place-holder value, take the average of the un-decimated data 30 minutes either side of the place-holder value. If less than 25% of the averaged data contains gaps, then replace the place-holder value in the decimated time series with the average value of the un-decimated data, otherwise the place-holder remains in.

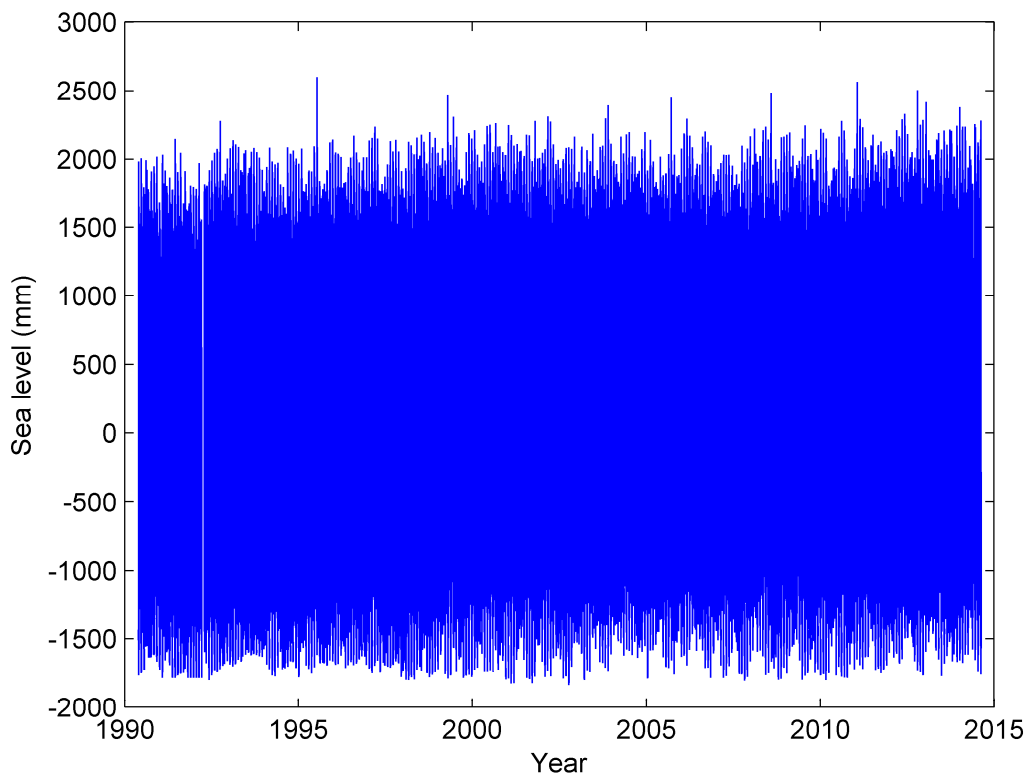


Figure 14-2: Tararu sea level data. Sea level is relative to Moturiki Vertical Datum 1953.

Appendix B MHWs elevations

Mean high-water springs elevations in the Waikato region are presented in Table B-1.

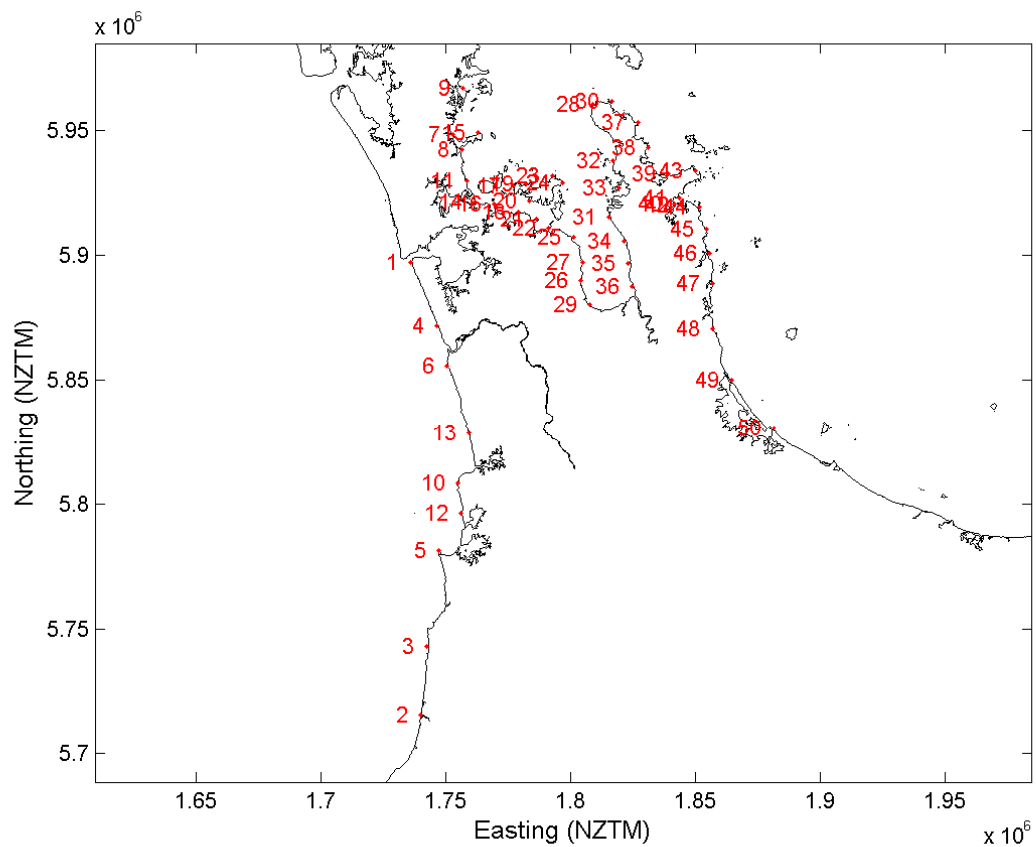


Figure B-1: Locations for MHWs elevations shown in Table B-1.

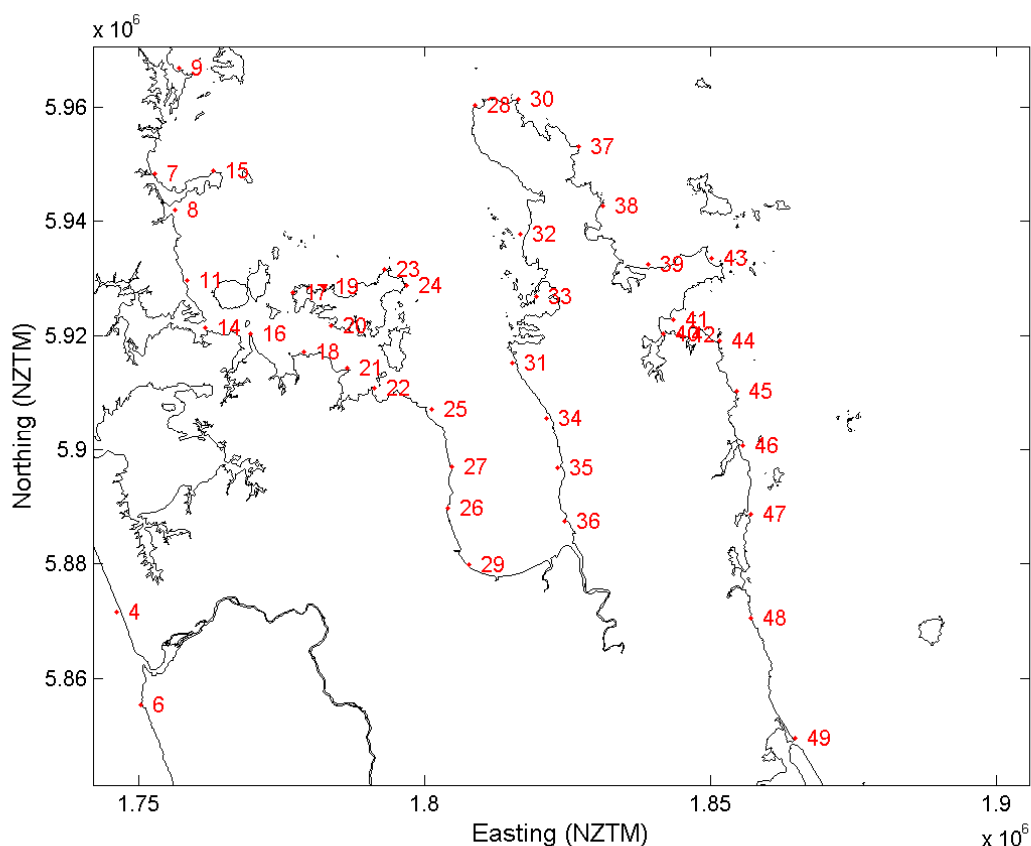


Figure B-2: Close-up view of locations for MHWS elevations shown in Table B-1.

Table B-1: Mean high-water springs elevations around the Waikato region. MHWS-10 and MHWPS values have been locally adjusted where needed from the EEZ tide model output. Vertical "datum" is MSL=0, i.e., relative to still water level locally.

Site	NZTM_easting	NZTM_northing	MHWS10 Adj	MHWPS Adj
1	1736036	5896835	1.53	1.62
2	1739880	5715676	1.69	1.79
3	1742437	5742856	1.65	1.75
4	1746202	5871714	1.55	1.64
5	1747000	5781341	1.61	1.71
6	1750438	5855383	1.56	1.66
7	1752951	5948294	1.33	1.37
8	1756317	5942007	1.37	1.41
9	1757008	5966784	1.30	1.35
10	1754683	5808423	1.59	1.69
11	1758461	5929712	1.39	1.44
12	1756250	5796293	1.60	1.70
13	1759265	5828375	1.59	1.68

Site	NZTM_easting	NZTM_northing	MHWS10 Adj	MHWPS Adj
14	1761739	5921374	1.50	1.55
15	1763084	5948905	1.32	1.37
16	1769530	5920425	1.47	1.52
17	1776936	5927599	1.41	1.46
18	1778882	5917209	1.49	1.54
19	1782252	5928586	1.37	1.42
20	1783649	5921763	1.50	1.55
21	1786415	5914401	1.51	1.56
22	1791195	5910891	1.52	1.58
23	1792913	5931706	1.38	1.42
24	1796833	5928873	1.41	1.46
25	1801222	5907155	1.53	1.58
26	1804043	5889793	1.59	1.66
27	1804823	5896959	1.55	1.61
28	1808793	5960394	1.23	1.27
29	1807735	5879870	1.62	1.69
30	1816452	5961340	1.15	1.18
31	1815416	5915278	1.48	1.53
32	1816776	5937885	1.37	1.42
33	1819538	5926847	1.42	1.47
34	1821238	5905591	1.53	1.59
35	1823189	5896801	1.57	1.63
36	1824437	5887507	1.61	1.68
37	1826926	5953129	1.05	1.08
38	1831226	5942802	1.03	1.06
39	1839047	5932503	1.02	1.05
40	1841698	5920369	0.84	0.87
41	1843460	5922793	0.96	0.99
42	1844557	5920153	0.96	0.99
43	1850153	5933518	0.97	1.00
44	1851566	5919153	0.94	0.97
45	1854647	5910360	0.94	0.96
46	1855601	5900603	0.94	0.96
47	1857027	5888722	0.93	0.96
48	1857077	5870559	0.93	0.96
49	1864726	5849733	0.94	0.97
50	1881304	5830611	0.95	0.98